

**AN ANALYSIS OF STIFFENED PLATING
SUBJECT TO EXTREME ICE LOADS**

CENTRE FOR NEWFOUNDLAND STUDIES

**TOTAL OF 10 PAGES ONLY
MAY BE XEROXED**

(Without Author's Permission)

TREVOR ROY BUTLER





National Library
of Canada

Bibliothèque nationale
du Canada

Acquisitions and
Bibliographic Services

Acquisitions et
services bibliographiques

395 Wellington Street
Ottawa ON K1A 0N4
Canada

395, rue Wellington
Ottawa ON K1A 0N4
Canada

Your file *Votre référence*

ISBN: 0-612-89616-1

Our file *Notre référence*

ISBN: 0-612-89616-1

The author has granted a non-exclusive licence allowing the National Library of Canada to reproduce, loan, distribute or sell copies of this thesis in microform, paper or electronic formats.

L'auteur a accordé une licence non exclusive permettant à la Bibliothèque nationale du Canada de reproduire, prêter, distribuer ou vendre des copies de cette thèse sous la forme de microfiche/film, de reproduction sur papier ou sur format électronique.

The author retains ownership of the copyright in this thesis. Neither the thesis nor substantial extracts from it may be printed or otherwise reproduced without the author's permission.

L'auteur conserve la propriété du droit d'auteur qui protège cette thèse. Ni la thèse ni des extraits substantiels de celle-ci ne doivent être imprimés ou autrement reproduits sans son autorisation.

In compliance with the Canadian Privacy Act some supporting forms may have been removed from this dissertation.

Conformément à la loi canadienne sur la protection de la vie privée, quelques formulaires secondaires ont été enlevés de ce manuscrit.

While these forms may be included in the document page count, their removal does not represent any loss of content from the dissertation.

Bien que ces formulaires aient inclus dans la pagination, il n'y aura aucun contenu manquant.

Canada

AN ANALYSIS OF STIFFENED PLATING SUBJECT TO EXTREME ICE LOADS

BY

©TREVOR ROY BUTLER, B. ENG

A Thesis Submitted to the School of Graduate Studies
in Partial Fulfillment of the Requirements for the Degree of
Master of Engineering

Faculty of Engineering and Applied Science
Memorial University of Newfoundland

December 2002

St. John's

Newfoundland

Canada

Abstract

Discovery of large oil and natural gas deposits in arctic and subarctic regions of Canada has led to vastly increased offshore activity in these areas. This activity has increased the exposure of marine structures to ice loads. The ability of designers to assess accurately the response to ice loading is essential for the efficient design of these structures. In arctic areas, structures regularly encounter various forms of ice such as level ice, pack ice and pressure ridges, which are composed of both first- and multi-year ice. In contrast, in subarctic regions (for example, off the coast of Newfoundland), structures have much less frequent encounters with first-year pack ice and icebergs. In these situations, inadequate consideration of ice loads could make the risk level of operations in ice unacceptably high.

This study is focussed on gaining an understanding of stiffened plating behaviour when subject to ice loads. Literature in three main areas was studied: ice failure processes during ice-structure interaction, definition of stiffened plate failure modes (or *limit states*) and reliability analysis, which incorporates these limit states into a probabilistic framework for design. The estimation of the response of a stiffened plate to extreme loads is greatly facilitated through an experimental analysis. To this end, a small-scale stiffened plate panel, subject to a lateral patch load, was tested to failure in the Structures Laboratory at Memorial University of Newfoundland. The patch loading is an idealisation of the two possible ice interaction scenarios in the waters off Newfoundland. The first is when level ice (or pack ice) acts upon, say, a ship's side shell. The second is the impact of a growler or bergy bit on a ship or platform leg. A detailed description of the physical model is given, along with results obtained. The use of finite element (FE) modelling techniques has greatly improved the study of complicated loading scenarios and structural response. A comparison of experimental results with those from a finite element analysis was carried out to assess the accuracy of the developed model. Once verified, the FE model is used in a sensitivity analysis of stiffener size to determine the effect size has on the ultimate strength of a stiffened plate. This will help understand the role the stiffeners play in structural design. Finally, a sample analysis is conducted to show how information regarding stiffened plate behaviour is implemented in reliability-based design.

Acknowledgements

I would first like to extend thanks to both my supervisors, Dr. Ian J. Jordaan and Dr. Mahmoud R. Haddara. The guidance and support provided over the years was greatly appreciated. Dr. Jordaan opened the door to an opportunity to apply my past education to the problem of ice loading, which I have found to be both quite challenging and especially rewarding. Dr. Haddara was the first to introduce me to the field of ship structures, a field I have grown to enjoy and, without this knowledge, would not have been able to pursue this study.

I also express my sincere thanks to Dr. Claude Daley for his assistance with the experimental work, and his time for answering my seemingly endless questions.

My thanks is also extended to several of my colleagues; Ms. Karen Muggeridge, Dr. Mark Fuglem, Dr. Dmitri Matskevitch, Mr. Paul Melanson, Dr. Irene Meglis, Dr. Bin Zou, Mr. Andrew Tomilson, Mr. Luksa Luznik, Mr. Rob Brown and Mr. Richard Hayward; for their help and encouragement along the way.

The assistance of Mr. Austin Bursey and Mr. Calvin Ward of the Structures Laboratory of Memorial University during the experimental work is gratefully acknowledged. The guidance and assistance provided by Mr. Paul Spencer of Sandwell, Inc. with the provision and calibration of the flatjack loading apparatus is also appreciated. In this regard, many thanks are extended to Drs. Stephen Jones and Bob Gagnon of the National Research Council's Institute for Marine Dynamics for providing valuable advice on the use of the above loading mechanism. Also, the excellent work of the Technical Services Department at Memorial, especially Mr. Jim Andrews and Mr. Mac Mercer, in construction of the test specimen is appreciated.

Without my wife Nicole, I would not have been able to complete this project. She was always there when I needed her support. My other family members are a large part of my life and their support is invaluable.

Contents

Abstract	ii
Acknowledgements	iii
Table of Contents	iv
List of Figures	vi
List of Tables	viii
Nomenclature	ix
1 Introduction	1
1.1 Background and Rationale	4
1.2 Focus and Scope	7
2 Designing Against Extreme Ice Loads: Current Practices	9
2.1 The Failure of Ice	10
2.2 Limit State Analysis for Stiffened Plates	16
2.3 Failure of Unsupported Plating	19
2.3.1 Yielding and Plastic Collapse	20
2.3.2 Rupture	21
2.4 Failure of Stiffened Plating	24

2.4.1	Yielding and Three-hinge Collapse	25
2.4.2	Rupture	27
2.5	Techniques for Reliability Analysis	27
3	Experimental Analysis of Stiffened Plating	32
3.1	Model Description	32
3.1.1	The Test Specimen	33
3.1.2	The Support Frame	35
3.2	Test Setup	37
3.2.1	The Loading Mechanism	37
3.2.2	Data Acquisition	38
3.3	Observations	40
3.4	Results	44
4	Numerical Analysis of Stiffened Plating	49
4.1	Model Description	49
4.1.1	Element Definition	50
4.1.2	Boundary Conditions	51
4.1.3	Material Model	52
4.1.4	Analysis Type	54
4.2	Results	56
5	Comparisons, Sensitivity and Design	59
5.1	Result Comparisons	59
5.1.1	FE and Experimental Results	59
5.1.2	FE and Experimental Results with Analytical Equations	62
5.2	Sensitivity	67
5.3	Reliability-based Design	69

6	Conclusions and Recommendations	73
	References	75
A	Experimental Design	81
B	Experimental Calibration	86
C	Finite Element Input Files	89
D	Analytical Calculations	122
E	Sample Reliability Analysis	124

List of Figures

2.1	Schematic of an interaction event (after Jordaan et al. 1997)	11
2.2	Nominal contact area at ice-structure interface	13
2.3	Variation in interaction areas	14
2.4	Typical structural arrangement of an icegoing vessel	18
2.5	Schematic of plating membrane action (after Zou, 1996)	22
2.6	The design point and safety index for Level 3 reliability	29
3.1	The test specimen and support frame	33
3.2	Picture of the test specimen and support frame prior to testing	36
3.3	Picture of the test apparatus	37
3.4	Location of strain gauges on the plate (4,5) and stiffeners (1,2,3) . . .	39
3.5	Key points from the loading time history	41
3.6	Loading ram/flatjack interaction and resulting flatjack indentations (inset)	42
3.7	View of deformed test specimen showing plate bending between stiff- eners (top) and buckled stiffeners (bottom)	43
3.8	Picture of tear at upper left corner of the model	43
3.9	Experimental load-deflection curve	45
3.10	Picture of deformed flatjack	46
3.11	Strain time histories for all gauges	47
3.12	Stiffener strain-deflection curve (0 to 15 mm)	48

4.1	Case A mesh (for clarity, only the plate elements are shown.)	50
4.2	Case B mesh (for clarity, the mid-side nodes are omitted and only the plate elements are shown.)	51
4.3	Material model used in FE analysis	54
4.4	FE load-deflection curves for Cases A and B	57
4.5	FE load-deflection curves for Cases A and B, showing the elastic-plastic transition	58
5.1	Comparison of Cases A and B with experimental results	60
5.2	Comparison of FE Case B and experiment with analytical results . . .	63
5.3	Elastic portion of response curves, showing shift in experimental response	64
5.4	Elastic portion of response curves, showing change in FE response . .	65
5.5	The complete load-deflection response curves, including modified results	66
5.6	Changes in the load-deflection response for varying stiffener sizes . . .	68
5.7	Deformed shape of stiffened plate: Cases 2x and 3x	68

List of Tables

2.1	Definitions of response categories	17
2.2	Seriousness of structural failure	19
3.1	Estimated failure pressures for test specimen	34
3.2	Comparison of full scale and model dimensions	35
3.3	Strain gauge parameters	39
3.4	Final calibration factors	40
3.5	Deflection and load at the key points	44
4.1	Material properties used in FE analysis	54
5.1	Structural particulars of sample design	72

Nomenclature

Abbreviations

FORM	First Order Reliability Method
SORM	Second Order Reliability Method
ASPPR	Arctic Shipping Pollution Prevention Regulations
LVDT	linear variable displacement transducer
SG	strain gauge
$\mu\epsilon$	microstrain (10^{-6} m/m)
FE	finite element(s)
MPC	multi-point constraint

Symbols

V	impacting velocity of ice feature
A_H	area of high pressure region of ice/structure interaction
A_B	area of damaged ice layer, or area of background pressure
A_S	spalled area, or area of zero pressure
n	number of critical zones within overall ice/structure contact area
L	web frame spacing longitudinal and transverse stiffener span
s	longitudinal and transverse stiffener spacing
P	ice load
b	ice load breadth
$M_{Y,P}$	yield, full plastic moment
$\sigma_{Y,ult,M}$	material yield, tensile, effective stress
t	plate thickness
ν, ν_P	elastic, plastic Poisson's ratio
$P_{Y,2h,3h,ult}$	pressure at first yield, 2-hinge, 3-hinge, ultimate collapse
$\delta_{Y,2h,3h,ult}$	deflection at first yield, 2-hinge, 3-hinge, ultimate collapse
E	Young's Modulus
F, F_H	fully plastic axial force, horizontal component of F
δ_{max}	maximum midspan deflection
θ	angle of line of action of the axial force with the horizontal

ϵ_{nom}	nominal material strain at ultimate collapse
I	moment of inertia of cross-section
Z, Z_P	elastic and plastic section modulus
P_F	probability of failure
Φ	standard normal distribution function
β	safety index
τ_Y	yield stress in shear
A	cross-sectional area
A_{shear}	total shear area of stiffened plate
F_{shear}	total shear force at the supports
Q_{design}	design torque of the support frame
t_{SF}	plate thickness of the support frame
W	width of the support frame
H	height of the support frame
$u_{x,y,z}$	translational boundary conditions in the x,y,z directions
$\phi_{x,y,z}$	rotational boundary conditions in the x,y,z directions

Chapter 1

Introduction

Discovery of large oil and natural gas deposits in arctic and subarctic regions of Canada has led to vastly increased offshore activity in these areas. This activity has increased the exposure of marine structures to ice loads. The ability of designers to assess accurately the response to ice loading is essential for the efficient design of these structures. In arctic areas, structures regularly encounter various forms of ice, such as level ice, pack ice and pressure ridges, composed of both first- and multi-year ice. In contrast, in subarctic regions (for example, off the coast of Newfoundland), structures have much less frequent encounters with first-year pack ice and icebergs. This variety has a huge effect on the material properties of the interacting ice as well as the nature of its interaction with the structure. Both of these factors contribute to the large variations in loads experienced by structures operating in ice environments. As such, the potential risk of these operations could become dangerously high if proper measures are not taken at the design stage.

A useful method of describing any type of structural problem is the concept of load vs. resistance. The *load* is the magnitude of the force, or forces, acting on the structure. These can be anything from a point load acting on a beam to a complex combination of environmental loads acting on a ship's side shell or platform leg. The structure's *resistance*, or strength, is its ability to withstand the loads acting on it. To

counteract the point load above, simple beam theory is used to calculate the maximum force a beam can withstand based on its material and sectional properties, as well as the type and nature of its supports. For a more complex situation, the overall strength is determined from a combination of calculated resistances to individual load components. Thus, an ideal structure would be one where the resistance and load were equal. In reality, they are dependant on a variety of parameters, each of which has some uncertainty in its assigned value. The result is an overall uncertainty in the exact values of both load and resistance.

In order to ensure that the load does not exceed the resistance, safety must be incorporated into the design. Traditionally, this was accomplished by separating these calculated values by a factor of safety. The concept of allowable stresses is a manifestation of this approach, where safety is achieved by reducing the yield stress by some amount, depending on the criticality of the component or variability in the load. This approach does not lend itself to efficient design as no effort is made to quantify the degree to which the individual uncertainty in each parameter affects the overall design. To optimise the design of such structures, and quantify the level of risk, designers must make use of reliability analysis. The random nature of both the structural particulars and load parameters is taken into consideration by assigning each a probability distribution. The resulting distribution of all variables can then be determined. The probability of failure is assessed by calculating the area under this joint distribution that falls outside a pre-defined boundary. Such a boundary, labelled a *limit state*, is derived from consideration of all possible failure modes of the structure in question. Each limit state equation is then tested to find the likelihood of it being exceeded. This is the probability of structural failure. The above analysis is repeated until this probability reaches an acceptable level.

Data from laboratory and field experiments has shown that marine structures can absorb quite large loads, much higher than the limits considered in traditional design practices. These extreme loads were found to be very localised, surrounded by areas of low background pressure. Resistance to this type of loading comes from the local structure, the plate panels between stiffening elements. Observations gathered from ice operations and field tests show that the plating undergoes considerable stretching and bending, much beyond the elastic limits of the structure. Further research has determined that the main mechanism behind the increased capacity is *membrane action*. This is a process by which, under the influence of large lateral loads, yielding in the plate panel, coupled with the resistance of the supports, cause axial forces to develop within the plate. These forces cause significant deflections of the plate, which allows the absorption of very large loads. A taut cable subject to out-of-plane loads behaves in a similar fashion. These experiences have translated into updated regulations, where the plastic capacity of plated structures has been utilised to reduce steel weight and cost for new designs. Reductions in required shell plate thicknesses have contributed the majority of these savings. An example of this is the acceptance of minor denting in the plating between stiffeners (or unsupported plating) in current icebreaker designs. This allows designers to specify reduced thicknesses to meet prescribed safety levels.

Similar changes to the design of the shell plate support, the stiffeners, have not occurred. Uncertainties in stiffener response to plating membrane action has resulted in the requirements for these structures remaining the same or, in some cases, becoming more conservative. This is to ensure that the plating has the support necessary to allow axial forces to develop. In the present study, experimental and finite element analyses of stiffened plating is performed to better understand their behaviour at large

loads. Within a reliability-based design framework, the ultimate goal of such research would be revised limit state equations to give acceptable safety at lower costs.

1.1 Background and Rationale

The problem of navigating in ice is not a recent one. The first historical record of encountering ice-covered waters is from 320 B. C. when the Greek sailor Pytheas travelled from the Mediterranean to what is now Iceland and witnessed the frozen waters of the Arctic Ocean. About 870 A. D. the Vikings discovered Iceland when their chieftain was blown off course on a voyage to the Faroe Islands. After this discovery, the Vikings began sailing regularly through the hazardous Arctic waters. On one of these voyages, twelve of twenty-five ships sank due to the treacherous conditions. Many centuries afterwards, stories of the travels of Marco Polo prompted explorers to sail north, braving the dangers of the icy waters, to seek a shorter shipping route to the riches of the Far East. In the nineteenth century, in conjunction with renewed interest in passage through the North, explorers began attempts at the North Pole. The Norwegian explorer Nansen built a vessel, *Fram*, specifically to resist ice loads. The main feature of the design was a more rounded shape to cause the ice pressure to push the ship upward, out of the ice, instead of it being crushed in the ice (Kirwan 1959). Probably, the most famous shipping encounter with the dangers of ice was in 1912, when the *Titanic* sunk southeast of Newfoundland after colliding with an iceberg.

With the advent of steam engines to provide more reliable power, vessels started to be designed specifically for operating in ice. In 1836, the vessel *Norwich* began icebreaking operations on New York's Hudson River, remaining in service for 87 years. As time progressed, variations in bow geometry and vast increases in horsepower caused great strides in icebreaker capability. In 1969, upon discovering oil in the

Beaufort Sea, the tanker *SS Manhattan* was fitted with additional strength members and thicker hull plating, as well as instrumented with strain gauges and pressure sensors, for the purposes of travelling through the Northwest Passage to seek out and ram large ice features. This effort was carried out to determine the ice forces to expect for vessels operating in the Arctic (Johansson et al. 1994). Since then, many vessels have been designed and operated successfully in ice environments. As more experience is gained, designs are becoming safer and more cost effective.

From the beginning, marine operations in ice had resulted in considerable damage. Initially, ships destined for service in ice were designed according to the “rulebook” approach, which treats both strength and applied loads as fixed, deterministic quantities, using a safety factor to allow for uncertainty in the design. These rules were empirical in nature, the equations used to calculate scantlings having been developed mainly from accumulated experience and vessel performance (Hughes 1988). Using the rules is ideal from a design perspective because of the ease of performing calculations to study the effects of changes on a particular design. Since there was very little data available for ice-going vessels, ice loads were accounted for by using a larger safety factor. It was soon realised that, even with apparently large safety margins, structural damage was considerable. Knowledge of the nature of ice loads, and structural response to them, was required to provide a more rational basis for design rules.

Hughes (1988) states that, as technology progresses, factors arise to precipitate changes in the means by which design objectives are met. They are:

- the need for adequate protection against pollution and for adequate safety for dangerous cargoes,

- new trade patterns, cargoes or tasks, which introduce special problems or lead to unusual ship geometries or proportions,
- the development of designs for standard ships which are to be produced in larger numbers and hence require greater cost efficiency, and
- the development of a wide variety of other types of floating structures for the extraction of ocean resources and for other uses of the sea.

The evolution of design for ice loads can be thought of along these lines as well. A resource, crude oil, was discovered in an area where special problems, ice loads, caused safety concerns regarding pollution. This led to new designs to combat ice loads, as well as the need for efficient construction to make extraction of the oil as economical as possible. These efforts are still ongoing.

Historically, rule changes only took place when they were deemed inadequate, usually when a serious failure occurred. This would lend itself to oversafe designs as safety factors would be greatly increased to prevent future mishaps. There are two scenarios that can result from this practice. One, the design becomes oversafe and uneconomical since too much steel is used in the construction. Two, a situation could arise where the design is only marginally safe, meaning that the probability of failure when the maximum design loading is encountered is unacceptably high. With new frontiers and unusual vessel types, the rules may be applied to meet design objectives which are outside the valid range on which they were based, more than likely causing a marginally safe design as described above. The damage mentioned earlier, in combination with the above factors, highlight the need for a better understanding of the uncertainties associated with ice loads and structural response to them.

A more rigorous approach, termed reliability analysis, is based on using statistical information to quantify the uncertainty about each of the parameters involved

in the design. The goal of this approach is to design a structure to meet a given probability of failure. The major advantage is that, instead of allowing for an overall uncertainty by using a safety factor, the variation in each design parameter can be analysed explicitly. Moreover, the capability exists to optimise a design for a pre-determined failure probability, or reliability level, which corresponds to an extreme design load. Designers are recognising these benefits as several regulations now use some form of reliability analysis to develop a better basis for prescribed safety factors (for example, Jordaan and Maes (1991)).

To use reliability techniques, limit state equations must be developed for all possible failure modes of the structure. The design of unsupported plating has benefitted greatly as research has discovered the enormous strength available when one considers membrane action. Stiffened plating design has lagged behind somewhat. This study is aimed toward gaining a greater understanding of stiffened plate response to ice loads as a first step towards a more efficient reliability-based design.

1.2 Focus and Scope

Within the above context, the aim of this study is to gain a better understanding of the response of stiffened plating to extreme ice loads. To this end, the main objectives of this thesis are to

1. Conduct a literature review of the state-of-the-art in:
 - ice behaviour during an interaction event,
 - stiffened plating design and analysis, and
 - techniques for conducting reliability analyses.

2. Describe experimental work, and associated finite element analyses, to understand how membrane behaviour develops in stiffened plates.
3. Compare and contrast results of above analyses with those given by available analytical equations.
4. Study the sensitivity of these findings and show how they fit into a reliability design framework.
5. Critically assess these results with reference to current knowledge and suggest possible courses of action for future research.

Chapter 2

Designing Against Extreme Ice Loads: Current Practices

To understand stiffened plating behaviour when subject to ice loads, three main areas, highlighted in Chapter 1, were studied: ice failure processes during ice-structure interaction, definition of stiffened plate failure modes (or *limit states*) and reliability analysis, which incorporates these limit states into a probabilistic framework for design. An ice-structure interaction event can induce many different ice failure modes, with the dominant process dependent on the type of structure and the properties of the ice itself. The loads produced are highly random, thus significant safety must be incorporated into the design calculations. The amount of uncertainty in these calculations can be assessed by using probabilistic techniques to determine the probability of occurrence of different load levels. These results are then easily incorporated into a reliability analysis. Descriptions of failure modes for a stiffened plate have been developed by some authors using beam theory, which neglects the effects of stiffener instability. Others have proposed that stiffeners contribute to structural strength until the point when they become unstable, for example when buckling or tripping occurs. Then, without the support of the stiffeners, the stiffened plate behaves as an unsupported plate. Consideration of plating ultimate strength equations may provide insight into possible extensions to stiffened plating analysis. There are many tech-

niques for conducting reliability analyses. These methods range from simply using a mean value with a variance measure, to a full probabilistic analysis in which various distributions are used to model each uncertain parameter, and the resulting combination determines the probability of failure. These ideas are discussed further in the following sections.

2.1 The Failure of Ice

Ice behaves in a random fashion where a variety of failure mechanisms could dominate depending on the physical conditions during an interaction event. When considering ice action on a ship or offshore structure, failure of the ice is compressive in nature. Even for sloped structures designed to promote ice failure in bending, compressive forces still exist near the ice-structure interface. These forces develop as the portion of the ice feature involved in the interaction is “squeezed” between the structure and remainder of the ice mass, either due to the momentum of the structure or of the ice feature, depending on the environment and structure type. Figure 2.1 depicts a typical ice-structure interaction event.

Within the interacting ice, there are at least two distinct failure phenomena happening. The first is the occurrence of fractures and spalls which act to reduce the contact area of the ice feature. As the overall compressive force builds during the impact, random flaws in the ice experience very high stresses, which cause cracks to propagate, resulting in the occurrence of a large fracture or spall. The other phenomenon taking place is the development of localised areas of extremely high pressure within a narrow layer of damaged ice at the ice-structure interface. Data from medium-scale indenter tests at Hobson’s Choice Ice Island (Frederking et al. 1990), as well as from ship ramming trials onboard CANMAR Kigoriak (Dome Petroleum Ltd. 1982) and CCGS Louis S. St. Laurent (Glen and Blount 1984), show that these

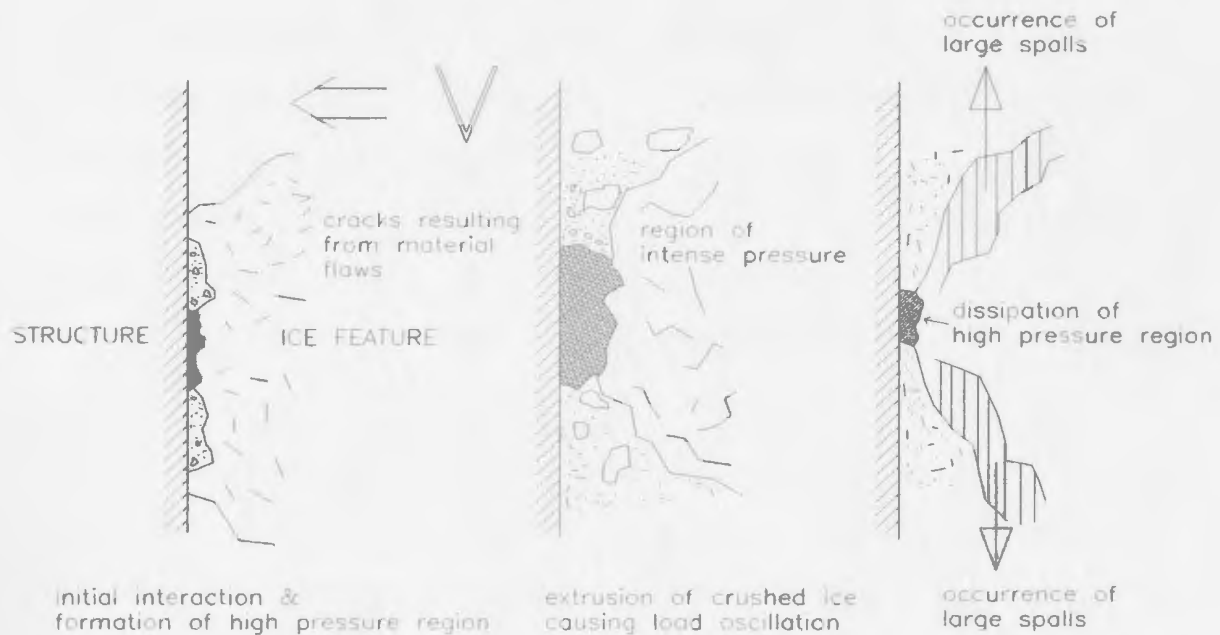


Figure 2.1: Schematic of an interaction event (after Jordaan et al. 1997)

high pressure areas occur randomly throughout the damaged layer, with varying size and intensity. Based on this data, these areas have been estimated to be on the order of 0.1 to 0.2 m², with an estimated density of one per square metre of contact area (Johnston 1994). Results from icebreaking trials in the Baltic Sea onboard the IB Sampo (Riska et al. 1990), and from laboratory testing (Daley 1991) show the development of a line-like area of high pressure within this layer of background pressure. Pressures reaching 70 MPa were recorded on individual sensors during the medium-scale indenter tests (Frederking et al. 1990), while sensor records show pressures of up to 51 MPa for ship ramming trials (Glen and Blount 1984). In the Baltic, the maximum recorded pressure from the trials of the IB Sampo (Riska et al. 1990) was approximately 54 MPa.

Observations from these tests suggest that the overall, or *nominal*, contact area of the ice has three distinct components, an outer band of zero pressure where spalling has occurred, an area where highly damaged ice creates a layer of background pressure,

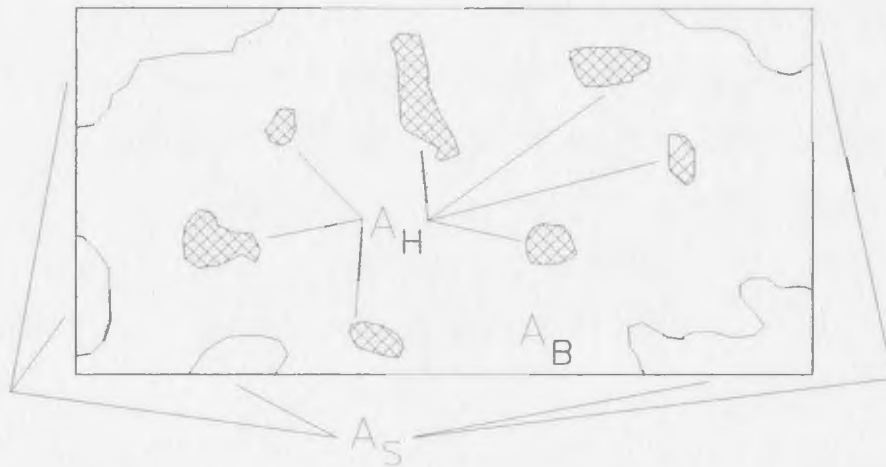
within which occur areas of intense pressure. Figure 2.2 shows this concept for both the randomly located areas, labelled “critical zones” (Jordaan et al. 1993) and the line-like zone (after Daley (1991)).

The behaviour of these regions of intense pressure is defined by two occurrences, one, stress concentrations arising from fracture and spalling action mentioned earlier, and two, extreme pressures within a region cause various microstructural changes in the ice (Jordaan et al. 1997). The following discussion is related to the concept of a critical zone (mentioned above), but is equally applicable to the line-like contact as well. In the initial stages of an interaction, microcracks form from flaws within the ice due to the buildup of compressive stresses. Near the edges of the interaction area, these microcracks could form larger cracks, which may result in spalling. Occurrence of fractures and spalls can be thought of as either a random process (Jordaan, Xiao, and Zou 1993), or a chaotic process (Daley 1991). Towards the centre of the interaction, crack growth is confined by the pressure in the surrounding ice. Pressures escalate within these confined regions, resulting in the formation of critical zones. Once formed, continued pressure from the surrounding ice mass causes microstructural change through the processes of pressure melting, microcracking and recrystallisation. The action of these processes tends to fail the critical zone, causing the extrusion of a “toothpaste-like” substance, which behaves as a viscoelastic solid (Johnston et al. 1995). The formation and disappearance of the high pressure areas likely causes the load oscillation seen in various field tests (for example, Frederking et al. (1990)). The majority of the load acting on the structure is transmitted through these high pressure regions.

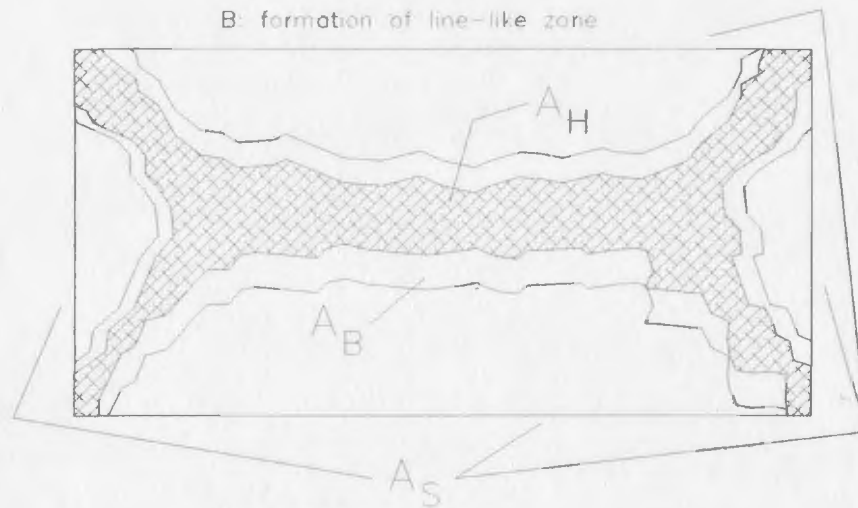
The next logical question to be raised is how do we extend the idea of high pressure areas to calculate global design pressures for a icegoing ship or offshore structure? General observations of pressure readings from all forms of ice testing (laboratory,

High Pressure Region Schematic:

A: randomly occurring critical zones



B: formation of line-like zone



- A_H - high pressure region
- A_B - damaged layer (background pressure)
- A_S - spalled areas (zero pressure)

Figure 2.2: Nominal contact area at ice-structure interface

medium-scale indentation and full-scale ship ramming) show that average pressures decrease as the scale of the interaction increases. Physically, a larger interaction will result in more spall events as more and more flaws are stressed and cracks propagated (Jordaan, Xiao, and Zou 1993). This idea is depicted as *overall areas* in Figure 2.3. But, even during ship ramming trials, individual sensors have recorded very high pressures while overall pressure was low (Glen and Blount (1984), for example). This would suggest that small subareas of high pressure exist within the larger contact area (shown as *local areas* in Figure 2.3). This second concept fits well with the design of stiffened plating for a ship or offshore structure as a stiffened plate is a small section of an overall hull or platform design.



Figure 2.3: Variation in interaction areas

Jordaan, Xiao, and Zou (1993) obtained a probability distribution for ice loads on large areas by considering these effects above as scale effects. Through analysis of high pressure zones, pressure was found to follow a gamma distribution. Using the information on size and density presented earlier, the force acting on a zone can be obtained. When considering a larger area, it is assumed that the number of critical

zones occurring within it increases. Obtaining the force acting on this larger area is achieved by a summation of the individual critical zonal forces. The distribution of this global force has the same mean value as the distribution for a single zone, but the variance is reduced by a factor $\frac{1}{\sqrt{n}}$, where n is the number of critical zones within the overall area. The global pressure is then found by considering the overall contact area on which the force is acting (Zou 1996). Thus, the decrease in pressure is quite pronounced as it is a result of two averages. The first, a force average, is obtained by dividing the total force by the number of zones over which it acts. The second, an area average, is a result of the variance reduction mentioned above. This has the effect of reducing the probability of an extreme load, which greatly reduces the chance of extreme pressures acting on large areas. This concept is borne out by Jordaan et al. (1993), who present a probabilistic ice load model which incorporates a decreasing pressure-area relationship.

The above model was used in a study of unsupported plating subject to random ice loads (Zou 1996). An “equivalent long plate” design model was proposed in which a dominant section through the overall plating area was assumed to behave as a fully fixed plate under uniform load. This section was selected by studying several cases of loading a plate with varying numbers of critical zones, and a section was taken where the majority of load was acting. The design model was composed of an “equivalent long plate” strength multiplied by a model uncertainty factor. This uncertainty was determined by comparison of the design equation result with Monte Carlo simulations of the plate subject to random loading. Good agreement was obtained in the above results, providing justification for the idealisation of random ice loads as uniform loads.

In the present study, a partial uniform loading, or *patch load*, is used to approximate the ice load on both a physical and numerical model of a stiffened plate. This

assumption is made for several reasons. Firstly, as mentioned above, pressure decreases with increasing area. At full scale, the area supported by a stiffened plate is on the order of several metres squared. This is quite a bit larger than the critical zonal area, thus the overall pressure is considerably less than that acting through a single critical zone. Also, since the stiffeners must support plating designed according to the above “equivalent long plate” model, it is reasonable to assume a partial uniform load on the stiffened plate corresponding to the location of the dominant section of plating. Finally, there is much uncertainty in how the critical zone pressures distribute over the larger area of a stiffened plate, so selecting a uniform loading is consistent with the unsupported plating design. Thus, a patch load was chosen as an appropriate loading mechanism for this study.

2.2 Limit State Analysis for Stiffened Plates

Design of stiffened plating is an integral part of an overall, rationally-based, ship design, as discussed in Chapter 1. To facilitate this type of design, the structural response of a ship or offshore structure is divided into three categories, primary, secondary and tertiary, which are defined in Table 2.1 (Paulling 1988). A typical structural arrangement of an icegoing vessel is shown in Figure 2.4. As can be seen, the structure located between stringers and bulkheads, or between web frames and decks, consists of shell plate supported by either transverse or longitudinal stiffeners. The response of this stiffened panel falls under the secondary category (see Table 2.1). Stiffened plating behaviour is also considered secondary response, since the panel is an assemblage of individual stiffened plates.

A schematic of an individual stiffened plate is also shown in Figure 2.4. The figure depicts two different loading scenarios: impact from a growler or bergy bit

Table 2.1: Definitions of response categories

Primary	the response of the entire ship hull, or platform leg to load by bending and twisting as a beam.
Secondary	the stresses and deflections of a stiffened panel, the structure supported between two bulkheads or web frames and two decks or stringers on ship or between two ring frames within a platform leg.
Tertiary	the deformation of a single panel of plating between two sets of longitudinal and transverse stiffeners, usually referred to as unsupported plating.

(shown acting on the longitudinal stiffeners) and interaction with level ice around the waterline (shown acting on the transverse stiffeners). Both situations produce loads over a portion of the stiffened plate span, or in other words, produce patch loads. Under this type of load, the stiffened plate will experience a variety of failure modes, which can be broken down into five groups: bending, shear, tripping, local buckling, and fracture (Melville Shipping Ltd. 1989). In the present study, effort is concentrated on bending deformation, which may include effects of membrane tension. Tripping and local buckling failures are treated indirectly via two approaches as outlined in Section 2.4. Other modes are outside the scope of the present investigation.

In design, there are two types of limit states for ships and offshore structures, serviceability and ultimate failure. Serviceability failures are those that cause minor inconveniences, but do not affect the main function of the structure. A typical example is minor denting in the side shell of an ice-going vessel. Ultimate failures are those that either result in complete loss of the structure, or demand immediate repair to resume its intended function. Loss of watertight integrity through hull rupture is an example of a complete loss. The consequences of exceeding these limit states are shown in Table 2.2 (Hughes 1988). Serviceability failures, such as minor denting of a ship's side shell, are usually considered to have only slight to moderate consequences.

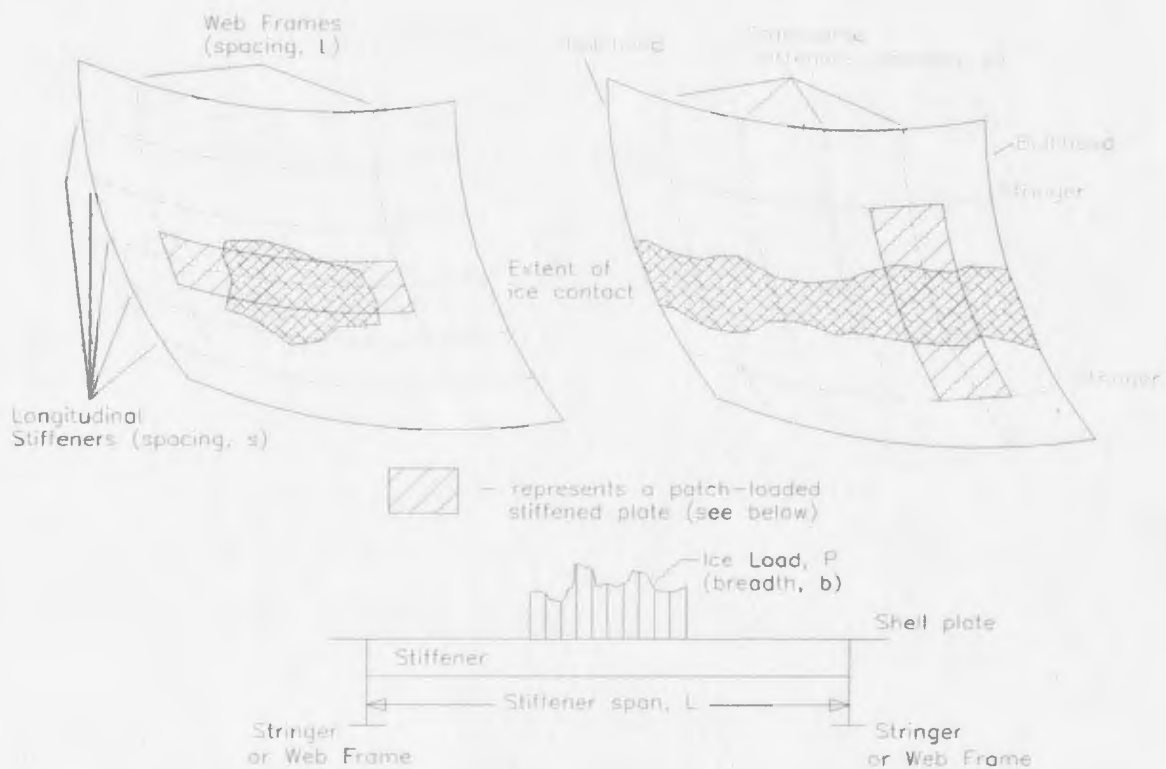


Figure 2.4: Typical structural arrangement of an icegoing vessel

Ultimate failures, such as hull rupture or large deformations that extend over a major portion of the vessel, are of a severe or extreme nature. This perceived risk level, as seen by the seriousness of consequences of structural failure, can be used in a reliability design to set appropriate probabilities of exceedance for the respective limit states equations.

For this study, serviceability will refer to three-hinge collapse, while ultimate failure is defined by rupture. Three-hinge failure occurs when material stresses exceed yield and plasticity spreads near each support and at midspan, forming three plastic “hinges”. Rupture is reached when the axial strain has attained a certain critical value. A value of 5% (Egge and Böckenbauer 1991) has been proposed based on collision studies and been used (Nessim et al. 1992) to derive an equation for ultimate failure.

Table 2.2: Seriousness of structural failure

Degree	Safety Consequences	Economic Consequences
Extreme	some fatalities likely, possible total loss.	complete loss, repair not economical.
Severe	small risk of fatalities.	partial loss, repair essential and costly.
Moderate	no appreciable risk of death, but subsequent failure would increase this risk.	structure operational but inefficient, repair as soon as possible.
Slight	no risk of death, but small risk of injury.	inconvenient, but no threat to main economic function.

2.3 Failure of Unsupported Plating

It was stated earlier that consideration of the ultimate limit state for unsupported plating would help in studying the ultimate behaviour of a stiffened plate. To this end, a long plate model (Zou 1996) is presented which describes serviceability limit states for two-hinge and three-hinge collapse, and a rupture ultimate limit state. For comparison purposes, the elastic solution proposed by Timoshenko and Woinowsky-Krieger (1959), valid until the onset of yielding, is also presented. Two-hinge collapse occurs when the applied loads result in the material stress exceeding yield and the spread of plasticity at the plate supports. This forms two plastic hinges, one at each support. When the load reaches a point where plasticity also occurs at midspan, the plating has suffered three-hinge collapse. Rupture is defined as the load at which the material strain reaches some pre-set, or design, value. Equations for these limit states are given in the following sections.

2.3.1 Yielding and Plastic Collapse

For a long plate clamped on all edges and subject to a uniform pressure P , the yield moment occurs first at the plate edges and is given by

$$M_Y = \frac{Ps^2}{12}, \quad (2.1)$$

where s is the stiffener spacing. The stress, σ , at this point is

$$\sigma = \frac{6M_Y}{t^2}, \quad (2.2)$$

where t is the plate thickness. For ductile materials, yielding begins for this moment when the strain energy of distortion reaches a certain value, where the stress is

$$\sigma_Y = \sigma \sqrt{1 - \nu + \nu^2}, \quad (2.3)$$

where ν is Poisson's ratio ($\nu = 0.3$ for steel). The resulting pressure, P_Y , is

$$P_Y = 2.25\sigma_Y \left(\frac{t}{s}\right)^2. \quad (2.4)$$

Timoshenko and Woinowsky-Krieger (1959) developed a closed form solution for the elastic deflection corresponding to this pressure as

$$\delta_Y = \frac{P_Y s^4 (1 - \nu^2)}{32Et^3}. \quad (2.5)$$

As yielding progresses, the moment capacity increases until plastic hinges are formed. This moment can be expressed in terms of material properties and plate geometry using the Hencky-von Mises yield criterion, which is

$$M_P = \frac{\sigma_Y}{\sqrt{1 - \nu_P + \nu_P^2}} \frac{t^2}{4}, \quad (2.6)$$

where ν_P is the plastic Poisson's ratio ($\nu_P = 0.5$ for steel). The pressure required to cause this moment, i. e. to form plastic hinges, at the plate supports, P_{2h} , is given by

$$P_{2h} = \frac{12M_P}{s^2}, \quad (2.7)$$

where s is the spacing between stiffeners. Substitution of Equation 2.6 in Equation 2.7 results in

$$P_{2h} = 3.464\sigma_Y \left(\frac{t}{s}\right)^2 . \quad (2.8)$$

The corresponding deflection, δ_{2h} , can be similarly described as in Equation 2.5, or

$$\delta_{2h} = \frac{P_{2h}s^4(1-\nu^2)}{32Et^3} \text{ (Zou 1996)}. \quad (2.9)$$

To form the additional plastic hinge at midspan, the pressure increases to the three-hinge pressure, P_{3h} , which is given by

$$P_{3h} = \frac{16M_P}{s^2} , \text{ or } 4.62\sigma_Y \left(\frac{t}{s}\right)^2 , \quad (2.10)$$

by using Equation 2.6. The failure of plating in this fashion results in denting as described in Section 2.2. The deflection, δ_{3h} , in this failure mode is based on the selection of a reasonable amount of permanent set. Ayyub et al. (1989) proposed a deflection of $\delta_{3h} = 2t$, while a deflection of $\delta_{3h} = 0.1s$ was suggested by Daley et al. (1991). Brown (1993) investigated these two criteria and determined that a permanent set of $2t$ resulted in thicknesses too thin for very stiff structures (high thickness to spacing ratio), while a permanent set of $0.1s$ gave thicknesses too thin for less stiff structures. For this study, the permanent set criterion of $\delta_{3h} = 2t$ was chosen as the test specimen described in Chapter 3 has a relatively low stiffness.

2.3.2 Rupture

As the pressure increases beyond three-hinge collapse, the plate deflections are governed by the development of axial, or membrane, forces. The degree to which the plate can withstand these pressures depends greatly on the restraint offered by the plate supports.

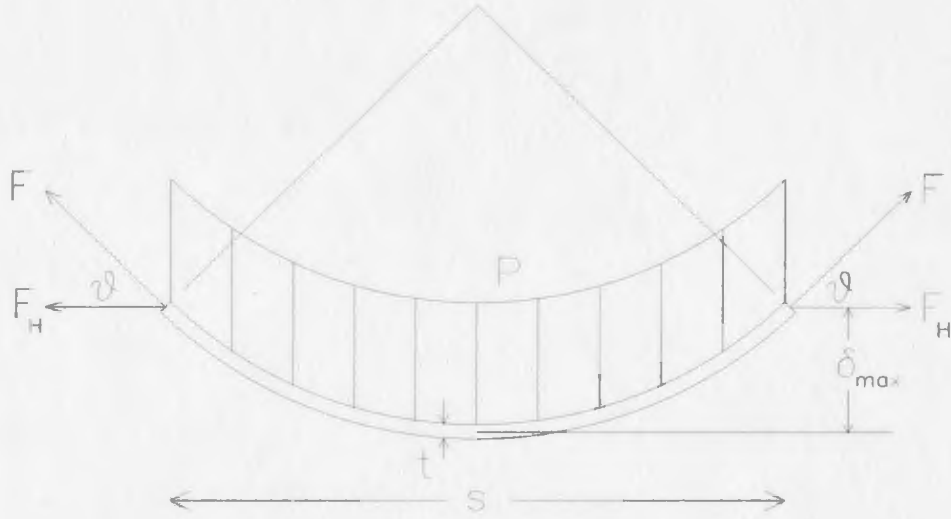


Figure 2.5: Schematic of plating membrane action (after Zou, 1996)

Figure 2.5 shows a diagram of the forces acting on the deflected plate. The maximum deflection occurs at midspan and is given by

$$\delta_{max} = \frac{Ps^2}{8F_H} \quad (2.11)$$

From this equation, the relationship between pressure and midspan deflection can be derived for elastic membrane action as (Ratzlaff and Kennedy 1985)

$$P = \frac{64}{3} \frac{Et\delta_{max}^2}{s^2(1-\nu^2)\sqrt{s^2 + (4\delta_{max})^2}} \quad (2.12)$$

where ν is the elastic Poisson's ratio. Once the material yields, this relationship can be re-written as

$$P = \frac{8\sigma_Y t}{\sqrt{1-\nu_P + \nu_P^2}} \frac{\delta_{max}}{s\sqrt{s^2 + (4\delta_{max})^2}} \quad (2.13)$$

Once the plate becomes fully plastic, it is assumed that the deflected shape resembles a circular arc. The angle, θ , that the membrane force makes with the horizontal can be defined in terms of the nominal material strain, ϵ_{nom} , as

$$\frac{\sin \theta}{\theta} = \frac{\pi}{180(1 + \epsilon_{nom})} \quad (2.14)$$

A suggested value for ϵ_{nom} is 5% (see Section 2.2), giving an angle of 31° . Equilibrium of the plate dictates that $2F \sin \theta = Ps$ or, using this value of θ and recognising this as the ultimate limit state,

$$P_{ult} = \frac{1.03F_{ult}}{s} . \quad (2.15)$$

The membrane force is given by

$$F_{ult} = \frac{1}{2} (\sigma_Y + \sigma_{ult}) t$$

(use of this average for stress is described in Section 4.1.3). Thus, the ultimate pressure for a long plate can be written as (Zou 1996)

$$P_{ult} = 0.515(\sigma_Y + \sigma_{ult}) \left(\frac{t}{s} \right) . \quad (2.16)$$

Substitution of Equation 2.15 into Equation 2.11 results in an ultimate deflection, δ_{ult} , of

$$\delta_{ult} = 0.1502s. \quad (2.17)$$

Ratzlaff and Kennedy (1986) present results of both numerical and experimental analyses to verify the above equations. The finite element analysis modelled the cross-section of a long, flat plate using several elements through the plate thickness. Two material models were used, a bilinear elastoplastic stress-strain curve and a curve which followed the shape of the stress-strain curve to failure. The experimental analysis consisted of a 152×456 mm flat plate, which was 1.47 mm thick, which was affixed to a support frame and loaded to failure via the application of fluid pressure. These analyses confirm the accuracy of the above equations throughout the entire range of behaviour.

Zou (1996) performed a numerical analysis of a long, flat plate subject to a patch load over a portion of the span. These results also matched closely to the ultimate load response described in Equation 2.16.

2.4 Failure of Stiffened Plating

Several authors have tackled the problem of determining limit loads for stiffened plates. All these approaches can fit into one of two categories. One, the stiffened plate is treated as a beam where bending and membrane tension occur simultaneously under lateral load. It is assumed that this membrane action discourages out-of-plane behaviour, e. g. buckling and tripping do not occur. The other category also considers the stiffened plate as a beam, but assumes that tripping and buckling failures occur prior to the development of axial tension in the cross-section. Thus, the stiffeners provide no stiffness when membrane action dominates the behaviour and the secondary structure, the entire stiffened panel, behaves somewhat like an unsupported plate due to the loss of its primary support mechanism. Study of membrane action in unsupported plating may help understand this idea.

Within the first category, Haythornthwaite (1957) presented an equation which defined the relationship between bending and axial tension for a fully fixed, rigid-plastic rectangular beam subject to a point load. Axial tension was calculated from the ratio of extension of the centroidal fibres to the rate of rotation of adjacent cross-sections within a plastic hinge. Using this, the author was able to define lateral load in terms of vertical deflection for axial tensions from zero to full yield. Experimental results were presented and showed reasonable agreement for the plastic range.

Campbell and Charlton (1973) extended this analysis for elastoplastic material behaviour assuming that elastic and plastic deformations could be linearly superimposed to obtain total deflection. The elastic solution was based on an assumed deflected shape. They then derived a differential equation which described the transition from elastic to plastic behaviour, from the point of initial plasticity to full plasticity of the section. After the section attained full plasticity, the rigid-plastic

solution again became valid. Comparison with experimental data showed excellent agreement throughout whole range of behaviour. Hodge (1974) extended this analysis by incorporating variable fixity at the beam supports. Ronalds and Dowling (1986) and Ronalds (1990) implemented these ideas to develop equations for the behaviour of unsymmetric T- and I-sections.

As stated earlier, the above analyses do not consider how instability affects stiffened plate response. Based on investigations of ship collisions, McDermott et al. (1974) state that the effects of membrane tension are significant only *after* stiffeners undergo tripping or local buckling. This idea was used in an analysis by Nessim et al. (1992), where limit state equations were developed for a patch loaded, fully fixed stiffened plate, as well as for unsupported plating. Serviceability limit states for three-hinge collapse and shear were derived without consideration of membrane action. Ultimate failure, or rupture, of the stiffened plate was defined in a similar fashion to rupture of unsupported plating (see Section 2.3). An empirical factor was used to arrive at a similar equation for the stiffened plate. These equations are described in the following section and will be used in subsequent chapters for comparisons with the experimental and finite element analysis conducted in this research effort.

2.4.1 Yielding and Three-hinge Collapse

To provide an analytical basis for the comparisons mentioned above, pressures for the three main failure modes, first yield, three-hinge and ultimate rupture, were defined. At first yield, the lateral pressure, P_Y , is obtained from elastic beam theory as (Blake 1990)

$$P_Y = \frac{-24M_Y L}{(b^2 - 3L^2)bs}, \quad (2.18)$$

where M_Y is the bending moment at the onset of yield, L the stiffened plate span, b the ice load breadth (width of patch load along the span) and s the stiffener spacing.

The corresponding midspan deflection is given by (Blake 1990)

$$\delta_Y = \frac{P_Y}{384EI} \left(\frac{b}{s} \right) (2b^2L - 2L^3 - b^3) . \quad (2.19)$$

As yielding progresses, plasticity occurs at the locations of highest stress - at the supports and at midspan - and hinges form at these locations. The lateral pressure, P_{3h} , required to form these hinges is derived as follows. Referring to Figure 2.4, consider half of the stiffened plate span from midspan to one of the supports. There is a reaction moment at the support due to the patch load. Taking moments about the fixed support gives

$$M_P - P_{3h} \frac{b}{2} s \left(\frac{L}{2} - \frac{b}{4} \right) = 0, \quad (2.20)$$

where M_P is the reaction moment at full plasticity. For the stiffened plate, $M_P = \sigma_Y Z_P$, where Z_P is the plastic section modulus of the stiffened plate cross-section. Substitution of this expression for bending moment into Equation 2.20 gives

$$P_{3h} = \frac{4\sigma_Y Z_P}{\left(L - \frac{b}{2}\right)bs}$$

for half of the span, or

$$P_{3h} = \frac{8\sigma_Y Z_P}{\left(L - \frac{b}{2}\right)bs}, \quad (2.21)$$

for the whole span (Nessim et al. 1992). Similarly to that shown for unsupported plating in Section 2.3.1, the deflection, δ_{3h} , can be taken as reasonable amount of permanent set. Thus, a deflection of

$$\delta_{3h} = 0.1s \quad (2.22)$$

is chosen as the relative stiffness of the stiffened plate is much greater than that of the unsupported plate.

2.4.2 Rupture

For ultimate failure, Nessim et al. (1992) gives a limit state equation that is similar in form to Equation 2.16, but incorporates an empirical factor to account for the differences between unsupported and stiffened plating. The ultimate failure limit state is written as

$$P_{ult} = (\sigma_Y + \sigma_{ult}) \frac{t}{b} \sin c,$$

where c is the solution of:

$$\frac{1 - \frac{b}{L}}{\cos c} + \frac{bc}{L \sin c} = 1.05. \quad (2.23)$$

Since the above equation assumes that the stiffeners have buckled, and are no longer contributing to the load bearing capacity of the section, the deflection, δ_{ult} , can be estimated from Equation 2.17, but instead of being proportional to stiffener spacing, the corresponding dimension for a stiffened plate, its length L , is used. The result is

$$\delta_{ult} = 0.1502L. \quad (2.24)$$

These equations are used for the experimental design in Chapter 3 and for comparisons with the experimental and finite element results in Chapter 5, where the validity of Equations 2.22 and 2.24 are investigated.

2.5 Techniques for Reliability Analysis

The use of reliability analysis stems from the need to better quantify the uncertainties that exist in both the loading and structural response. As stated in Section 2.1, the random nature of ice loading is due to complexities in adequately defining ice failure mechanisms. The response of the structure also has many uncertain parameters, such as variation in material properties, dimensions and quality of manufacture.

Also, there is uncertainty involved in using an idealised strength model. In terms of stiffened plates, plate theory uses certain assumptions that are but a representation of reality. Thus, by using this information, the likelihood of structural failure can be quantified.

There are four methods of performing reliability analysis that are in common practice, namely levels one through three and Monte Carlo simulations (Mansour 1990). Level three analysis, or the fully probabilistic approach, obtains failure probabilities through direct integration of a joint probability density function. This joint distribution is found through combination of the probability density functions of the individual variables. The unsafe ranges of all these variables are then used as integration limits on the joint distribution. This technique is extremely difficult to implement, even if the distributions for all variables are known, due to the complexities of performing the multiple integration. The only case where this integration can be performed in closed form is when a normal distribution can describe the joint distribution and when the surface defined by the limit state function is planar (Madsen et al. 1986). The probability of failure is then calculated by

$$P_F = \Phi(-\beta), \quad (2.25)$$

where β is the safety index, the minimum perpendicular distance from the origin to the failure surface, and $\Phi()$ is the standard normal distribution function (see Figure 2.6). In most cases, all variables will not be normally distributed and the failure surface will not be planar. But, these variables can be transformed to standard normal variates and the failure surface can be linearised at the point of minimum distance, or design point, to obtain an estimate of P_F . This procedure is referred to as the first order reliability method, or FORM (Madsen et al. 1986). Second order reliability methods (SORM) use a quadratic approximation of the failure surface at the design point.

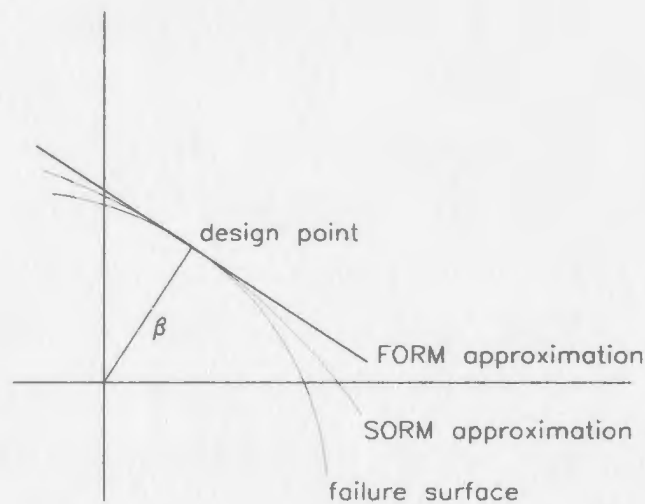


Figure 2.6: The design point and safety index for Level 3 reliability

The level two approach simplifies the above by approximating variables by their expected value, or mean, and a variance measure (Mansour 1990). A safety margin is then defined as the difference between strength and load. Correspondingly, the ratio of the mean and standard deviation of the safety margin provides an estimate of the safety index, β . If the variables are independent and normally distributed, this estimate will be the same as calculated above. Otherwise, a transformation of these variables into standard normal variates (Mansour 1990) can be performed. Also, if the safety margin equation is not linear, a Taylor Series expansion is used and all terms higher than first order are removed. These two points show the approximate nature of this method as compared to the above. Solutions are easier to obtain than for level 3 methods, but performing the distribution transformations is difficult.

Another approach, labelled level one, is the most common for its ease of use. Most reliability-based design codes use this method. The general idea is that level two analyses are performed where each parameter has an associated partial safety factor. Given the distribution information for each parameter (as above), the safety margin equation can be re-written to solve for these factors for a given safety index.

Once they are determined, the partial safety factors can be used in an otherwise deterministic design to factor the calculated load and structural resistance, thus giving the design approximately the same level of safety as if level two methods were used with the same safety index (Mansour 1990). This approach is used extensively by code writers so that the end user can simply pick appropriate partial safety factors and achieve a certain level of safety. This approach may seem no different from a totally deterministic design where an overall safety factor is used. But, by using level two methods, there is input of distribution information, which is a better uncertainty measure. Also, by using several partial safety factors, uncertainty in each parameter is accounted for with more adequacy.

Monte Carlo simulations (Melchers 1987) offer an alternative to the rigors of direct integration of the level three joint distribution. Statistical sampling techniques are used to obtain random samples from the distributions of all variables present in the problem. This data is then used to determine a sample solution, say to a previously defined limit state equation. If enough of these sample solutions are found, a statistical analysis of these solutions can be used to assess subsequent behaviour. For example, a probability distribution for ice loads (Jordaan et al. 1993) and associated distributions in the strength model, such as material property variation, can be sampled to arrive at a sample solution for the limiting load. Once many samples are obtained, an estimate of the failure probability can be made. One drawback to this approach is the extremely large number of samples needed to ensure validity of the statistical predictions. Importance sampling techniques (Melchers 1987) can be used to overcome this problem by adjusting the sampling point so that samples are taken from a region close to the failure surface. This greatly reduces the number of samples required for the accuracy of failure estimates.

Nessim et al. (1992) presents a reliability analysis of a stiffened plate using FORM techniques. This analysis is studied in detail in Chapter 5. Discussion of the experimental and numerical investigation carried out in the present study in conjunction with the reliability analysis may help eliminate some of the uncertainty associated with the ultimate failure of stiffened plates.

Chapter 3

Experimental Analysis of Stiffened Plating

As stated in Section 1.2, understanding the response of a stiffened plate to extreme loads would be greatly facilitated through an experimental analysis. To this end, a small-scale stiffened plate panel, subject to a lateral patch load, was tested to failure in the Structures Laboratory at Memorial University of Newfoundland. The patch loading is an idealisation of the two possible ice interaction scenarios in the waters off Newfoundland: one, level ice (or pack ice) acting upon, say, a ship's side shell, and two, impact of a growler or bergy bit on a ship or platform leg. Justification of the use of a patch load for stiffened plating was given in Section 2.1.

3.1 Model Description

The physical model consists of the test specimen, a small-scale stiffened plate panel, and a rigid support frame. The experimental model was constructed from 3.175 mm thick mild steel plating, measuring 500 mm in length and 150 mm wide, with three 50.8×3.175 mm stiffeners welded lengthwise. Support was provided by a rigid frame constructed using 12.7 mm mild steel plate and a hollow structural steel (HSS) section $51 \times 51 \times 6.4$ mm. Figure 3.1 shows details of both the test

specimen and support frame. Once constructed, the model was painted so that any small deformations would be easily seen from the flaking and tearing of the paint.

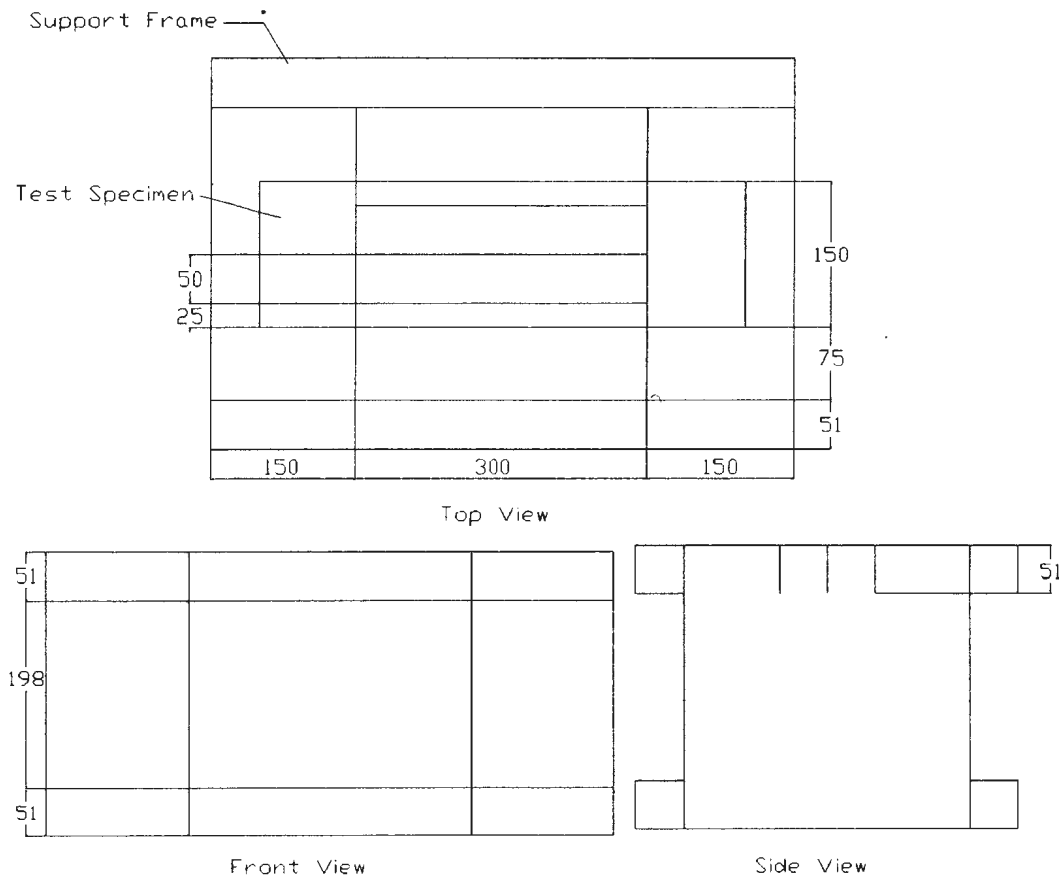


Figure 3.1: The test specimen and support frame

3.1.1 The Test Specimen

To design the physical model, initial dimensions were scaled linearly from full scale scantlings of an ice-transiting vessel (Nessim et al. 1992). The main objective of this experiment was to ensure that the full response of the structure could be observed. There are two factors which could have resulted in this objective not being met. One, if the specimen was overly stiff, there would have been insufficient load capacity from

the Laboratory’s hydraulic ram to cause failure. This was alleviated by considering the maximum load capacity of the ram (668 kN) when the estimated loads for different failure modes was calculated. Two, premature tripping or local buckling of ill-designed stiffeners would have allowed unrealistic structural response. The test specimen dimensions were checked against the stiffener tripping and local buckling criteria of the Arctic Shipping Pollution Prevention Regulations, or ASPPR (Transport Canada, Ship Safety 1995) to avoid this concern. Implementation of these ideas is described in the following paragraph.

An Excel spreadsheet (see Appendix A) was developed to determine the adequacy of the initial scantlings to meet the above objective. Estimates of critical patch loads were calculated for three conditions: first yield, three-hinge collapse and ultimate rupture using Equations 2.18, 2.21 and 2.23 respectively. The equations for three-hinge collapse and rupture were derived based on the second of the two approaches presented in Section 2.4, namely that no membrane behaviour occurs until after the stiffeners have tripped or buckled. Table 3.1 shows the calculated failure pressures for these three modes.

Table 3.1: Estimated failure pressures for test specimen

Failure Mode	Pressure [MPa]
first yield	2.73
three-hinge	5.87
ultimate rupture	9.73

To ensure that the specimen was not overly stiff, a fourth failure mode was considered: shear at the supports. This mode of failure would happen if the test specimen failed in shear at the welded supports before any other mode, such as bending, occurred. This mode provided a means of ensuring the test specimen was not so stiff

as to cause damage to the loading mechanism. The force required to cause shearing failure at both supports was calculated as

$$F_{shear} = 2\tau_Y A \quad (3.1)$$

where τ_Y is the yield stress in shear (usually $0.7\sigma_Y$) and A is the total cross-sectional area of the test specimen. These pressures were then multiplied by the overall patch area used to determine the load needed from the hydraulic ram. Test specimen dimensions could then be altered until appropriate critical loads were obtained. Table 3.2 shows the model dimensions arrived at using the above criteria, along with the corresponding full-scale dimensions.

Table 3.2: Comparison of full scale and model dimensions

Dimension [mm]:	Full-Scale	Model
plate thickness	50	3.175
stiffener thickness	29	3.175
stiffener spacing	760	50
stiffener depth	760	50.8
stiffener span	4920	300

3.1.2 The Support Frame

Also incorporated in the spreadsheet (see Appendix A) was a calculation of support frame dimensions. From Figure 3.1, it is seen that, if membrane behaviour of the stiffened plate is to be studied, the support frame must resist the developed axial force with negligible deflection. The maximum axial force in the specimen cross-section, labelled the fully plastic axial force F , is given by

$$F = \sigma_Y A. \quad (3.2)$$

Due to the position of the test specimen (see Figure 3.1), this axial force will cause torsion in the support frame. Since the loads must be transferred through the support

base, the torque has a lever arm that is the full height of the support frame. Thus, the maximum applied torque is equal to the above axial force multiplied by the height of the support frame. The overall width and height of the support frame were chosen for practical purposes. To determine the appropriate plate thickness, an initial value is assumed and a design torque, Q_{design} , is calculated from (Ross 1987)

$$Q_{design} = 2\tau_Y t_{SF}(W - t_{SF})(H - t_{SF}), \quad (3.3)$$

where t_{SF} is the plate thickness, W the width and H the height of the support frame. The plate thickness was considered appropriate when the ratio of design to maximum torque met or exceeded unity. For the chosen thickness of 12.7 mm, this ratio was approximately 2.4, which not only allowed the full response to be seen, but also provided a sufficient safety margin in the event that the estimated loads were inaccurate. Finally, HSS sections were welded lengthwise to hold the ends of the support frame rigidly apart. Figure 3.2 shows the completed test specimen.



Figure 3.2: Picture of the test specimen and support frame prior to testing

Designing a support frame in this fashion ensured that there was more than adequate support to allow the full structural response of the test specimen to be observed.

3.2 Test Setup

The experimental apparatus consists of four components (depicted in Figure 3.3): the model, its support, the loading mechanism and the data acquisition system. The model and support frame were described in the previous section. The loading mechanism and data acquisition system details are described here.



Figure 3.3: Picture of the test apparatus

3.2.1 The Loading Mechanism

The load was applied using a hydraulic ram acting on a 150×150 mm flatjack. The flatjack was constructed from two sheets of 1.2 mm stainless steel welded together, with an inlet and outlet tube attached along one side (labelled A in Figure 3.3). To prevent the ram from damaging the flatjack inlet and outlet tubes, a 25 mm thick steel block was placed between the ram and flatjack (labelled B in Figure 3.3). Prior to testing, the flatjack was filled with oil using a small hand pump, the outlet tube

was plugged and it was placed on the test specimen, centred at midspan. The plug was used to prevent air from entering, or oil leaking out of, the flatjack. This method of load application differs considerably from the typical methods of applying patch loads via wooden or metal blocks. The advantage of this method is that the flatjack does not have sharp edges, reducing the shear stresses occurring at the edges of the patch. Wooden or metal blocks tend to punch through the structure as a result of these high shear stresses.

To control the motion of the ram during the experiment, a function generator was used. This unit allows the user to define a path and total time period for the variation of load (load control) or displacement (stroke control). If load control was used, the ram could begin to move very rapidly as the structure failed in an attempt to maintain the pre-set load path. This could cause considerable damage to the laboratory equipment. Thus, the displacement of the ram was defined by a ramp function, varying linearly from zero to full stroke over a given time period.

3.2.2 Data Acquisition

Experimental measurements were recorded for applied load, displacement and axial strain. A load cell incorporated into the hydraulic ram provided the loading information. Output from the function generator used to control ram motion was recorded by a linear variable displacement transducer (LVDT) to get midspan deflection. To measure axial strain, five strain gauges were attached to the specimen at the locations shown in Figure 3.4. The properties of these gauges are shown in Table 3.3.

To complete the apparatus, a data acquisition system was used to record and convert the analog voltage readings from the load cell, LVDT and strain gauges into digital output. In all, seven channels were used for recording the load, displacement and axial strain from the five gauges. The system required a set of calibration factors

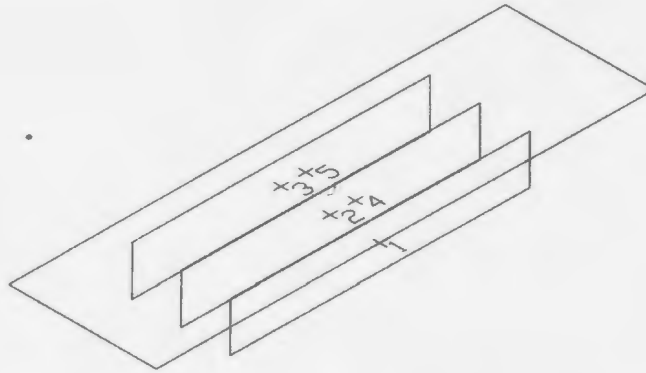


Figure 3.4: Location of strain gauges on the plate (4,5) and stiffeners (1,2,3)

Table 3.3: Strain gauge parameters

Gauge Description	EA Series Student Gauge
Gauge Type	EA-06-240LZ-120
Resistance	$120 \pm 0.3\%$ at 24°C
Gauge Factor	$2.070 \pm 0.5\%$ at 24°C
Gauge Length	6 mm
Strain Limits	5%

(one per channel) to allow interpretation of the experimental results in appropriate engineering units. To obtain these factors, a known quantity (eg. load, displacement or strain) was applied to each channel and the change in voltage it produced was recorded. These results were used to determine a conversion factor, in units per volt, for input into the system. For the strain gauges, a known strain of $1000\mu\epsilon$ was applied by connecting an appropriate amount of electrical resistance in parallel across each gauge and recording the voltage. The calibration of the LVDT was accomplished by fully retracting, then extending, the hydraulic ram, and then dividing the distance moved (stroke) by the voltage change. The load cell was calibrated by recording the voltage change produced by applying a known force to a rigid object.

The only remaining factor to consider is how the applied load from the ram is transmitted through the flatjack — how much of the flatjack is actually contacting

the test specimen? In order to determine this, the flatjack was placed between a rigid steel block and the ram, whose position was fixed. The jack was then pressurised while measuring the resulting load on the fixed ram. To pressurise the flatjack, a small hand pump, fitted with a pressure dial gauge, was used. This pressure gauge was also calibrated using a deadweight tester, a device where known pressures were applied to the gauge and compared with gauge readings. These results were then plotted to determine a correction factor to apply to the gauge readings during the flatjack calibration. The load measured on the fixed ram was compared with the load calculated assuming the entire cross-sectional area of the flatjack (150×150 mm) was in contact. From this, a ratio of measured load to calculated load was found which, when multiplied by the overall dimensions, gives the actual contact area of the flatjack. The result of this calibration was that the flatjack had a contact area of 15236 mm^2 , or 123.43×123.43 mm.

The final calibration data used in the experiment is given in Table 3.4. All calibration data and plots can be found in Appendix B.

Table 3.4: Final calibration factors

Channel	Units/Volt	Description
0	7.60859	LVDT (mm)
1	67413.9	Load (N)
3	201735	Strain Gauge 1 ($\mu\epsilon$)
4	201045	Strain Gauge 2 ($\mu\epsilon$)
5	200642	Strain Gauge 3 ($\mu\epsilon$)
6	200844	Strain Gauge 4 ($\mu\epsilon$)
7	200884	Strain Gauge 5 ($\mu\epsilon$)

3.3 Observations

During the experiment, the data acquisition system collected information from seven sources: the load cell, LVDT and strain gauges 1 through 5. This information

was stored in ASCII format, one row of data recorded every ten seconds. In all, about 800 data points were collected. Of these data points, certain “key” points were related to significant events in the progression of failure of the test specimen. Figure 3.5 shows these points as plotted on the applied load time history.

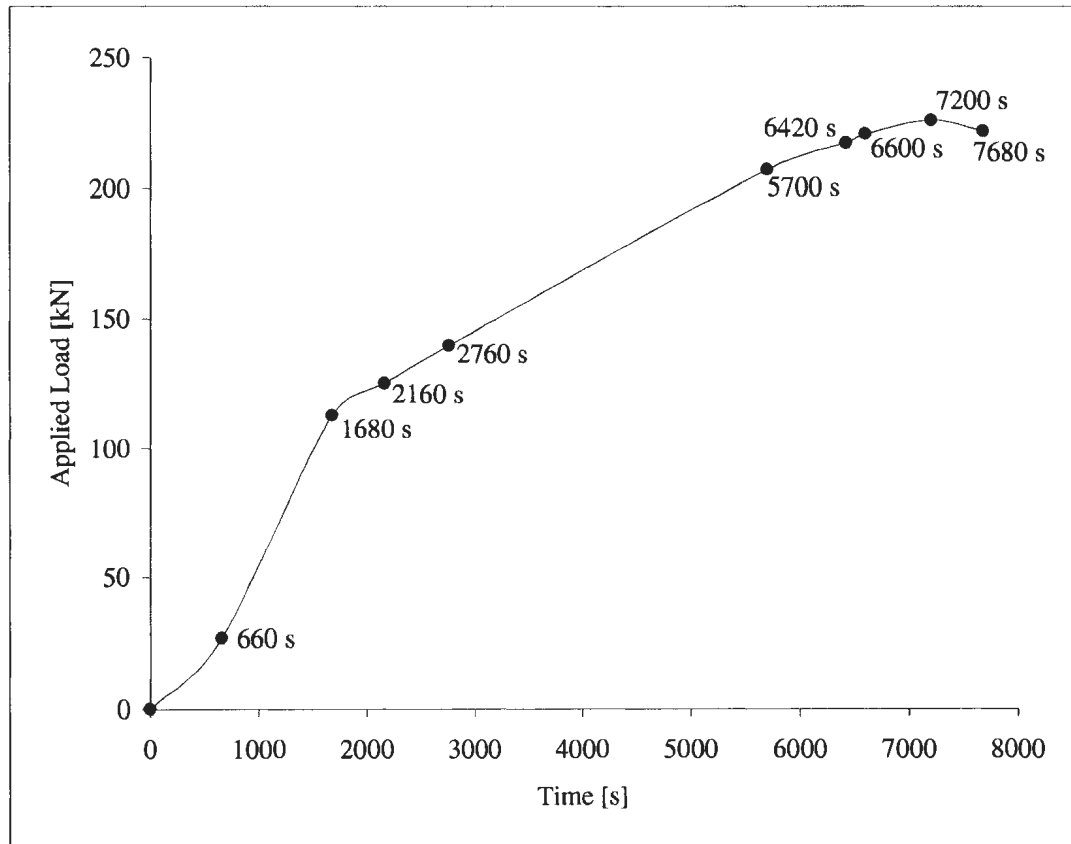


Figure 3.5: Key points from the loading time history

The experiment was started with a stroke rate of 15 mm/hr. This slow rate was used for the initial part of the experiment to ensure everything was in working order. At 660 s, the stroke rate was increased to 25 mm/hr. Also at this time, the edges of the steel block, used to separate the ram and flatjack, came into contact with the flatjack. Evidence of this is seen in Figure 3.6, which depicts the post-experiment view of flatjack and block, along with a close-up of loading ram side of the deformed



Figure 3.6: Loading ram/flatjack interaction and resulting flatjack indentations (inset)

flatjack. At 1680 s, the rate of increase in load dropped off considerably as compared to the increase in deflection. At 2160 s, tripping of the stiffeners was noticed. This caused the stiffener strain gauges to move out-of-plane from the load, and the strain, being measured. At 2760 s, transverse bending of the plating between stiffeners was noticed, giving the test specimen a “hungry horse” look. These observations can clearly be seen in Figure 3.7, which shows the test setup after completion of the experiment. Subsequently, the flatjack edges moved closer to touching the model. A tear was initiated at the upper left corner of the model (see Figure 3.8) at 5700 s. This tearing continued (6420 s) and additional stretching was noticed as paint flaking occurred at the upper right and lower left corners (6600 s). At 7200 s, the upper left



Figure 3.7: View of deformed test specimen showing plate bending between stiffeners (top) and buckled stiffeners (bottom)

tear crossed the end of the stiffener. The load capacity began to diminish soon after (7320 s) as deflection increased with a drop in applied load. This trend continued



Figure 3.8: Picture of tear at upper left corner of the model

and at 7680 s, the experiment was halted. The maximum load was approximately 226 kN.

Some additional comments can be made concerning the experiment. All three stiffeners experienced tripping, two to one side, one to the other. This lateral buckling

caused all stiffeners to bend out-of-plane to the extent that the gauge locations were almost horizontal at the end of the test. This buckling mode was preceded by local buckling at the supports to accommodate stiffened plate bending. The paint proved useful to indicate where tension and compression forces were acting. For example, there was considerable flaking at the stiffener supports due to the high compressive forces induced by the patch load while on the plating, the paint tore apart, revealing the action of high tensile forces.

3.4 Results

Recall that the driving force behind these experiments was to gain a better understanding of stiffened plating failure modes and to obtain results for comparisons with the finite element results of Chapter 4 and analytical equations given in Chapter 2. A study of the load-deflection response would be most appropriate to support this comparison.

The load-deflection curve for the stiffened plate model is given in Figure 3.9. Superimposed on this figure are the key points described in Section 3.3, with the load and deflection recorded at each of these points given in Table 3.5. The first item of

Table 3.5: Deflection and load at the key points

Time [s]	Deflection [mm]	Applied Load [kN]
660	2.69	26.82
1680	9.60	112.8
2160	12.9	125.2
2760	17.0	139.5
5700	37.2	207.0
6420	42.2	217.1
6600	43.4	220.5
7200	47.5	225.8
7680	50.9	221.7

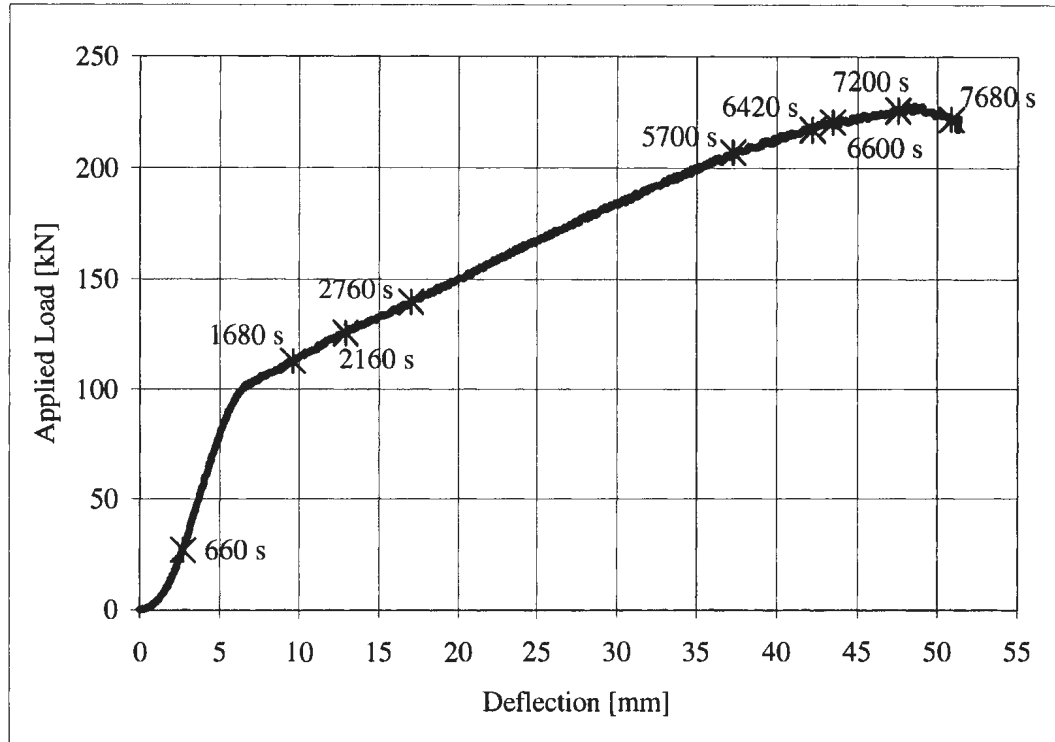


Figure 3.9: Experimental load-deflection curve

note from this curve is the distinct “knuckle”, or change of slope, at a deflection of approximately 6 mm which may indicate the failure of the model in 3-hinge collapse - the serviceability limit state defined in Chapter 2. From Section 3.3, the observation at 1680 s of a decrease in loading rate, coupled with an increase in deflection rate, supports the above conclusion. The ultimate load point is also evident at a deflection of about 48 mm, which is supported by the observations made at 7200 and 7680 s. A final point about the load-deflection response is that the slope for the elastic portion of the curve is quite gradual. Investigation of the flatjack after the test showed that it had undergone massive deformations, but did not rupture (see Figure 3.10). This deformation allowed the flatjack to maintain contact with the deflected plating and damaged structure, which increased the overall contact area. Observations at 660 and 2760 s, which indicated the movement of the flatjack edges, provide evidence of this



Figure 3.10: Picture of deformed flatjack

contact area increase. Post-experimental measurements confirmed these observations as the final contact area was estimated to be 16900mm^2 , or 130×130 mm. Due to its change of shape, use of the flatjack also prevented punch-through failure as described in Section 3.2. In order for these deformations to occur, the flatjack absorbed a significant portion of the initial energy supplied by the load ram. This indicates a “cushioning” effect which altered the model response as the load imparted by the ram did not transmit directly to the model, which is depicted by the response curve up to a deflection of 3 mm. Consideration was given to this “cushioning” in the comparisons with both the FE and analytical results in Chapter 5.

Additionally, the strain data gathered may be compared with the FE results as a further validation. Figure 3.11 shows the strain time histories for gauges 1 to 5 (see Figure 3.4 for gauge locations). As seen from these time histories, there was an increase in strain (rapidly for the stiffeners and more gradual for the plating), followed by a sharp drop - 2400-2600 s for the stiffeners, 4100-5700 s for the plating. There are two reasons for this behaviour. One, as stated in Section 3.3, the stiffeners experienced tripping and local buckling. This caused the strain gauges to move out-of-plane, thus unable to record accurate measurements. Two, the strain limit for the gauges used was 5% (Table 3.3), above which they are prone to de-bonding from the structure. Upon completion of the experiment, the gauges were checked and the stiffener gauges were found to have de-bonded. Similar checks of the plating gauges

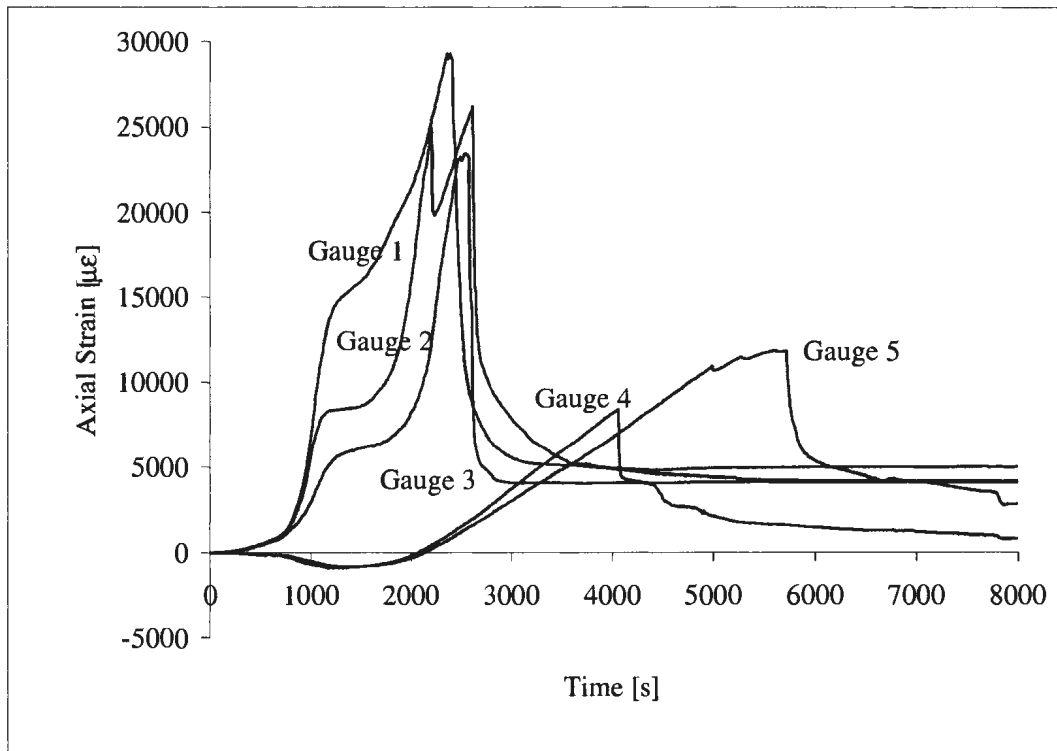


Figure 3.11: Strain time histories for all gauges

were inconclusive, but there were also sharp drops in these curves that would indicate the same behaviour, although the maximum strain recorded was considerably less. Thus, the strain results are unreliable for overall comparison to the FE results and will not be used.

Prior to their de-bonding, the stiffener gauge time histories show a knuckle at about 1200 s, which is approximately the same point where the applied load time history in Figure 3.5 changed slope. As reported in Section 3.3, this change of slope was associated with the observation of stiffener tripping at 2160 s. Figure 3.12 re-plots the stiffener strain against deflection for the initial portion of the experiment. This clearly shows the knuckle in the response at a deflection of approximately 6 mm - the same point where the load-deflection curve knuckles (see Figure 3.9). This provides

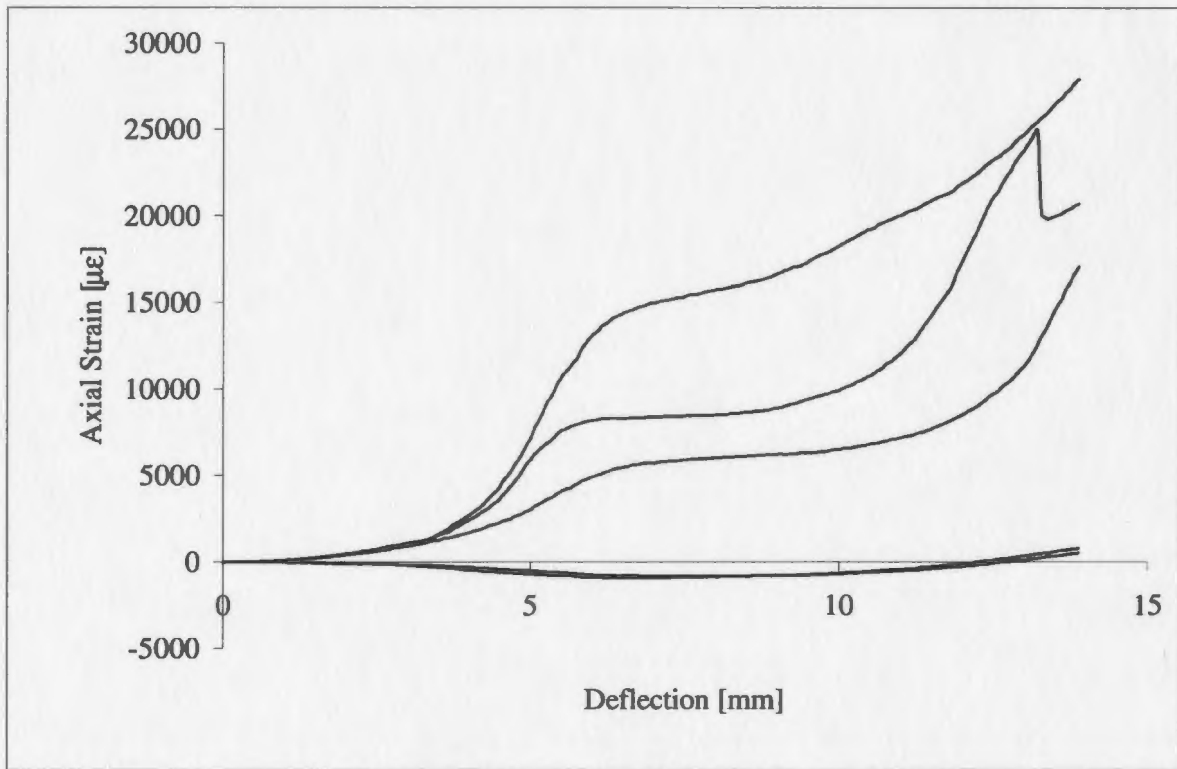


Figure 3.12: Stiffener strain-deflection curve (0 to 15 mm)

further confirmation of the conclusion drawn earlier in Section 3.4, namely that the 3-hinge collapse failure mode occurred at this point.

Chapter 4

Numerical Analysis of Stiffened Plating

While the experimental model described in Chapter 3 was designed to represent an ice-structure interaction, the complexities of such an event are quite difficult to replicate in a physical experiment. The use of finite element (FE) modelling techniques to study these loading scenarios and structural responses allows one to handle these complexities in a more direct fashion. Here, the finite element analysis of the physical model studied in Chapter 3 is described. These models were developed using the commercial finite element software ABAQUS (Hibbitt, Karlsson and Sorenson Inc. 1995a).

4.1 Model Description

There are four main components to a finite element model - element definition, boundary conditions, material model, and analysis type. To ensure accurate results, the user must make appropriate choices for these components. Two different element types were defined, Cases A and B, to determine whether or not elastic bending deflections were important in modelling the overall response of the stiffened plate. A set of boundary conditions, material model and analysis type that were common to

both cases are also defined. The resulting input files for these cases can be found in Appendix C.

4.1.1 Element Definition

As mentioned above, two different cases were studied - a mesh of 4-noded shell elements for both the plating and the stiffeners (Case A), and a refined mesh of 8-noded shell elements for both plating and stiffeners (Case B). For Case A, the 4-noded, isoparametric shell element S4R was used in a 6.25×12.5 mm mesh (see Figure 4.1). The main feature of this element is its finite (large) strain capability. Finite strain

vi

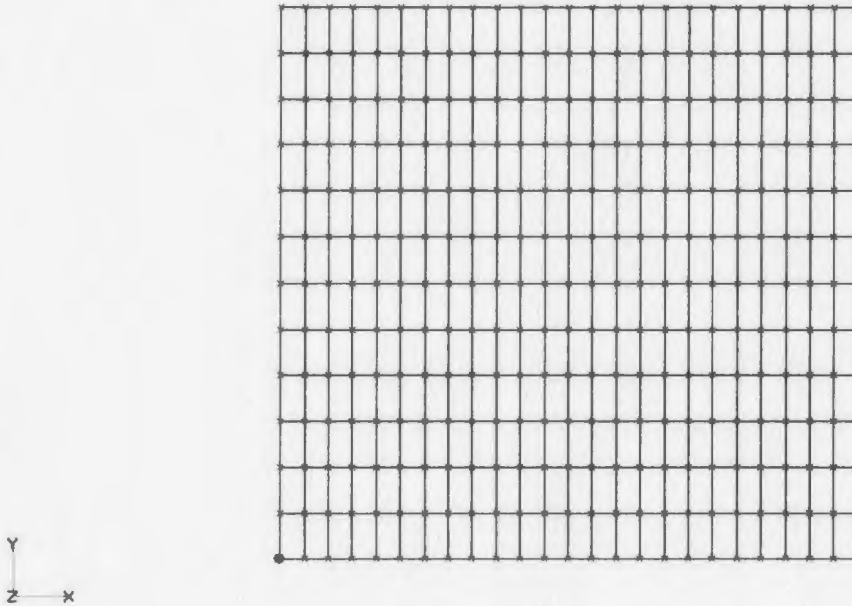


Figure 4.1: Case A mesh (for clarity, only the plate elements are shown.)

implies that the material strain induced within the element by the applied load is not small compared to the shell thickness. To ease calculations, the element behaviour is divided into two regimes, bending and membrane deformation. Since use of finite strain capability is reserved mainly for large displacement analyses, it is assumed

that the bending deflections are negligible compared to the membrane response (Hibbitt, Karlsson and Sorenson Inc. 1995a). This assumption could lead to over-stiff behaviour if the elastic portion of the load-deflection response is, in fact, important. Thus, the 8-noded isoparametric element S8R, which includes bending response and quadratic interpolation (Case B), was used for comparisons. This element type was implemented in a 10×5 mm mesh, as seen in Figure 4.2.

vi

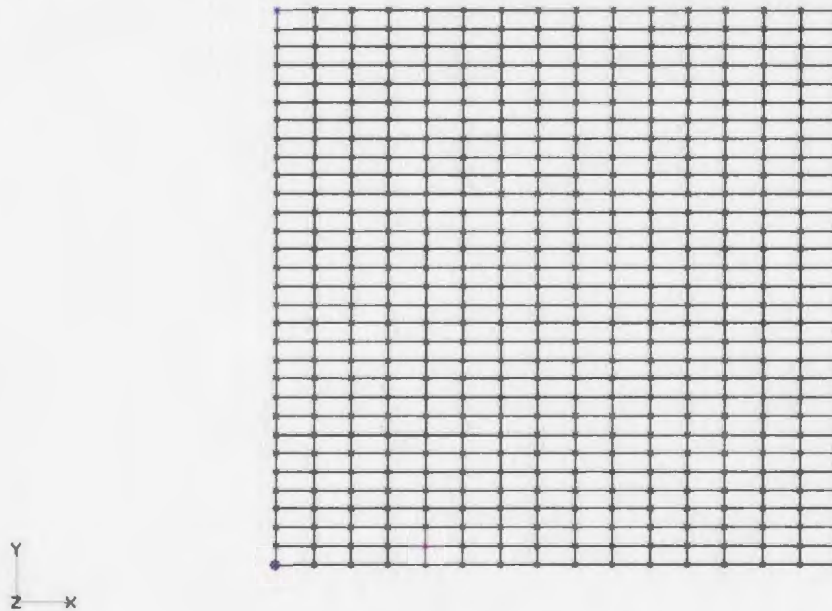


Figure 4.2: Case B mesh (for clarity, the mid-side nodes are omitted and only the plate elements are shown.)

4.1.2 Boundary Conditions

In finite element analysis, an accurate representation of an experimental model cannot be complete without consideration of its physical constraints. These constraints, called boundary conditions, allow an analyst to greatly simplify a numerical model so that it can be studied efficiently. Care must be taken to ensure that the FE model does not become an oversimplification of the experiment, since incorrect deci-

sions concerning the boundary conditions can render the analysis useless. Boundary conditions are applied by confining nodal degrees of freedom such that the desired behaviour is achieved. The degrees of freedom available for constraint depend on what element type is associated with the particular node. For the elements mentioned above, there are six active degrees of freedom: translation in the x, y and z directions (u_x, u_y, u_z) and rotation about the x, y and z axes (ϕ_x, ϕ_y, ϕ_z).

In the present study, the boundary conditions used are global constraints, that is they are applicable to all models tested. There were two global constraints used, one dealt with model symmetry, the other described the support conditions. Since the physical model was symmetric about midspan, only half of the span needed to be modelled. This global constraint was implemented by restricting the midspan nodes to only move in the x-z plane, meaning that u_x, ϕ_y and ϕ_z are equal to zero. Modelling the support condition involved restricting all movement at these nodes, a fully fixed boundary condition. This was used because the plating on the physical model overlaps the support frame and was welded on three sides, in addition to each stiffener being welded on both sides to the support. While a true fully fixed end restraint cannot be attained, the hefty construction of the model should allow use of this condition without introducing significant error.

4.1.3 Material Model

To ease comparisons with experimental results, a common material model was used for all finite element models. Typically, the material behaviour of steel can be idealised as one of four types of behaviour (Skrzypek 1993):

A: rigid, perfectly plastic,

B: elastic, perfectly plastic,

C: rigid, linear strain hardening, and

D: elastic, linear strain hardening.

A rigid, perfectly plastic material will not begin to deform until stress reaches yield. Once deformation begins, stress remains constant as the only mechanism available to resist load is deformation. In contrast, an elastic, perfectly plastic material takes into account the initial deflections experienced as the stress level rises to yield, which gives larger deflections under a given load as compared to the rigid model. Since typical code designs limit deflections to certain permissible values, considering elasticity will result in a more conservative design. The third and fourth approaches account for material hardening by assuming stress increases linearly during plastic deformation. This effectively gives the material more stiffness and, thus, a greater load capacity and results in a more optimistic design strategy.

McDermott et al. (1974) suggest using an elastic, perfectly plastic material model, with the elastic-plastic transition defined by an *effective* strength σ_M , which is given by

$$\sigma_M = \frac{1}{2}(\sigma_Y + \sigma_{ult}) , \quad (4.1)$$

where σ_Y and σ_{ult} are defined in Chapter 3. This material model is shown in Figure 4.3. This model has the benefit of accounting for some strain hardening through its definition of the transition and being computationally more efficient than those that consider strain hardening more directly. Good correlation with collision studies carried out by the above authors, as well as providing good results for analyses of both unsupported plating (Nessim et al. (1992), Brown (1993), and Zou (1996)) and for stiffened plates (Nessim et al. 1992). The material properties used in the FE analysis of the test specimen are given in Table 4.1.

Table 4.1: Material properties used in FE analysis

Symbol	Description	Value(Range)
σ_Y	yield strength [MPa]	248
σ_{ult}	ultimate strength [MPa]	400–552
σ_M	effective strength [MPa]	324 ¹
E	Young's Modulus [GPa]	207
ν	Poisson's ratio (elastic)	0.3
ν_P	Poisson's ratio (plastic)	0.5

¹ Only one effective strength value is given as this is a more conservative estimate of the material strength.

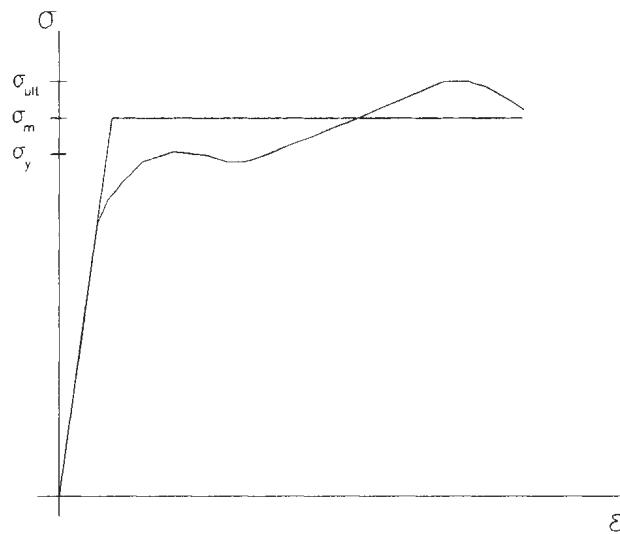


Figure 4.3: Material model used in FE analysis

4.1.4 Analysis Type

The final component of the FE model is determination of the analysis type. To make this choice, it is essential to picture the physical processes being studied. As stated in Chapter 1, there are two interaction phenomena which induce load on a stiffened plate structure, an impact from growler or bergy bit, or the action of level ice. Because of the nature of ice failure during an interaction (see Section 2.1), structural loads can be highly variable. This is mainly due to the rapid appearance

and disappearance of critical zones within the damaged layer. In designing for extreme loads, the usual practice is for the ultimate limit state for the strength of the structure to be a condition that has a set probability of occurrence, above which the structure fails. In the case of a stiffened plate subject to ice loads, the design can be done statically where a design ice load will be found that has a specified probability of exceedance. Therefore, the FE analysis of this case treats the load as a single event in a static manner. Repeated load events, which can be studied in terms of fatigue, are outside the scope of the present research.

Although the type of loading can be studied statically, the extreme loads associated with the ultimate limit state will induce nonlinear structural response. This nonlinearity is caused by a number of factors. Geometric imperfections in the scantlings and residual stresses due to welded construction cause the material to differ from its elastic properties. Strain hardening during plastification can also cause some material nonlinearities. This behaviour can cause unstable structural response, for example buckling or tripping. Using normal static analysis procedures, structural instabilities will result in numerical errors, terminating the analysis. Accurate prediction of unstable response at these loads is facilitated in ABAQUS through the use of an alternate iteration scheme, called the *modified Riks* method (Hibbitt, Karlsson and Sorenson Inc. 1995b).

The Riks method (Ramm 1981) is well suited to the analysis of unstable response since, at the beginning of each iteration, load and deflection are treated as unknowns. These unknowns are found by a path search from the solution point of the previous iteration. In this way, a particular load can occur at more than one deflection, which is essential if instabilities are to be modelled. The analysis is then terminated when one of two criteria are met: a specified load proportionality factor (a multiple of the initial load value given), or a specified displacement. The key input to this method

is an imperfect FE model. An imperfection is necessary as a perfectly symmetrical model will not become unstable as there exists no catalyst to initiate this behaviour. Introducing this imperfection can be done in one of two ways, either by applying a small disturbing force at the tip of the stiffeners or by directly altering the model geometry a certain amount. The magnitude and direction of these disturbing forces are determined from an eigenvalue analysis. But, since an eigenvalue analysis produces a deformed model shape, a more direct approach would be to change the model itself. ABAQUS provides a method of re-calculating all nodal co-ordinates so that the maximum imperfection would be some scale factor of a typical material dimension. In the present study, model imperfections were achieved via the second approach and the maximum imperfection was set to 50% of the plate thickness. By using this scheme, changes in the cross-sectional geometry as it undergoes plastic deformations are considered in the analysis. This is a much more accurate representation of material behaviour in the plastic range as high stresses will cause stretching, which tends to reduce section thickness.

4.2 Results

The two models, Case A and Case B, were subjected to a patch load similar to that used in Chapter 3. As described in the previous section, the analysis method is iterative and treats both the deflection and load as unknowns for each iteration. To begin the analysis, a nominal load of 1 MPa was placed on the patch area. This area was sized based on the calibration results from Section 3.2, but in order to create a reasonable mesh to suit the analysis, the exact area could not be replicated. Thus, a patch area of 125 mm² was used. Records of lateral pressure within the patch area and deflection were kept during the analyses. From these, the load-deflection relationship can be plotted similar to that plotted for the experimental analysis in

Section 3.4. The analyses were terminated once a deflection of 52 mm was reached (the second of two termination criteria given in Section 4.1.4). This deflection was chosen as it was the deflection at which the experiment was halted.

Figure 4.4 gives the load-deflection response of both FE models. Several observations are evident from this curve. In both cases, the transition from elastic to plastic behaviour is evident at a deflection of about 0.5 mm (which can be seen more

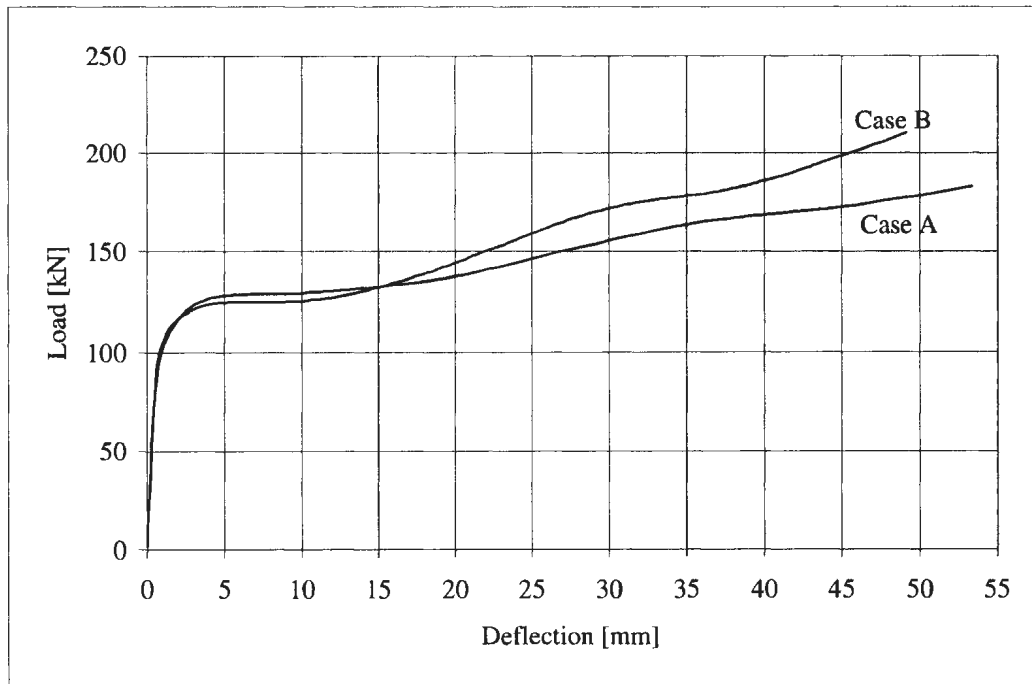


Figure 4.4: FE load-deflection curves for Cases A and B

clearly from Figure 4.5). In Section 4.1.1, it was stated that the difference between Cases A and B was the assumption of negligible bending deflections in Case A. This assumption should lead to differences in the initial portions of the load-deflection response. As can be seen from Figure 4.5, this is not the case as there is no discernible difference between the two curves. The variation in the load-deflection behaviour is significant only well into the plastic range, with Case B predicting a greater load-carrying capacity. This would seem to indicate that the quadratic interpolation

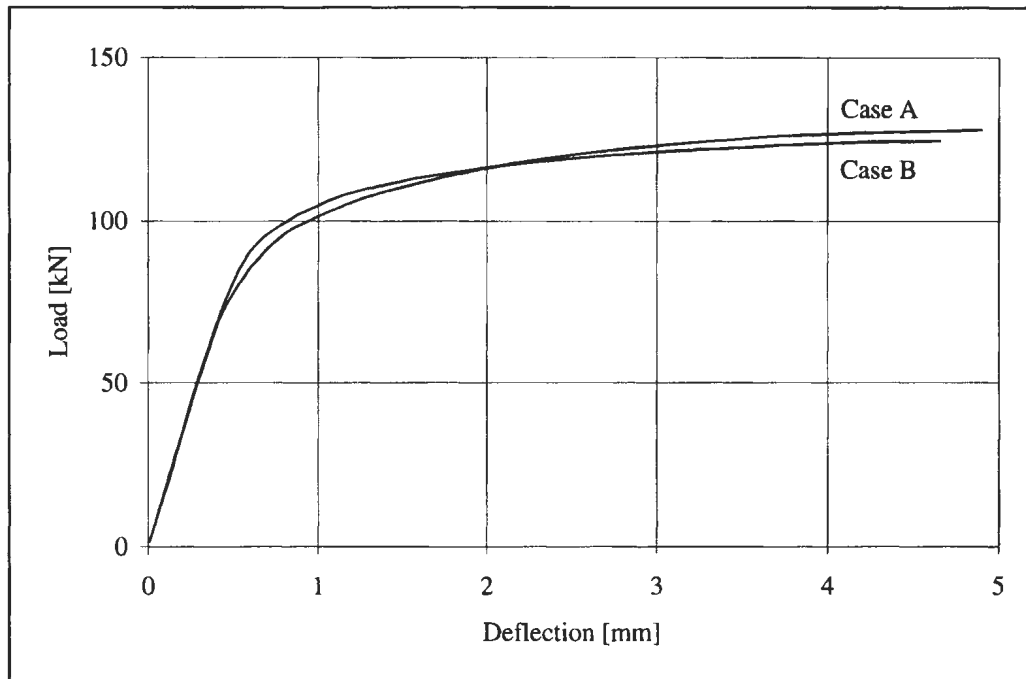


Figure 4.5: FE load-deflection curves for Cases A and B, showing the elastic-plastic transition

possible with the 8-noded element is the key feature, not the improved elastic bending response. An investigation of the difference in behaviour will be carried out in Chapter 5 when these curves are compared with the experimental results. Also, the load-deflection curve for Case B shows the termination of the response at a deflection less than 52 mm. The analysis method used has the additional feature of halting after a certain number of iterations with no change in the structural response. This prevents the analysis from cycling endlessly and is what caused the termination of the Case B response curve.

Chapter 5

Comparisons, Sensitivity and Design

To fulfill the scope of work described in Section 1.2, three tasks are undertaken here. First, the experimental results from Chapter 3 and finite element results from Chapter 4 are compared and contrasted, then both are compared to results from the analytical equations for stiffened plating presented in Chapter 2. Second, a sensitivity analysis of stiffener size using finite element techniques is carried out to determine the effects on the ultimate strength of the stiffened plate. This will help understand the role the stiffeners play in structural design. Third, a sample reliability analysis, based on previous work by Nessim et al. (1992), is conducted to show how information regarding stiffened plate behaviour is implemented in reliability-based design.

5.1 Result Comparisons

5.1.1 FE and Experimental Results

Load-deflection curves for both Case A and B are compared with experimental results in Figure 5.1. As can be seen, there are discrepancies in the response curves. In the initial portion of both curves, from the origin to where the curve changes slope, the slope of the experimental results is quite different from the FE results. The

general trend of the experimental results is matched to a certain degree by the FE model for the remaining portion, but there is an offset between them.

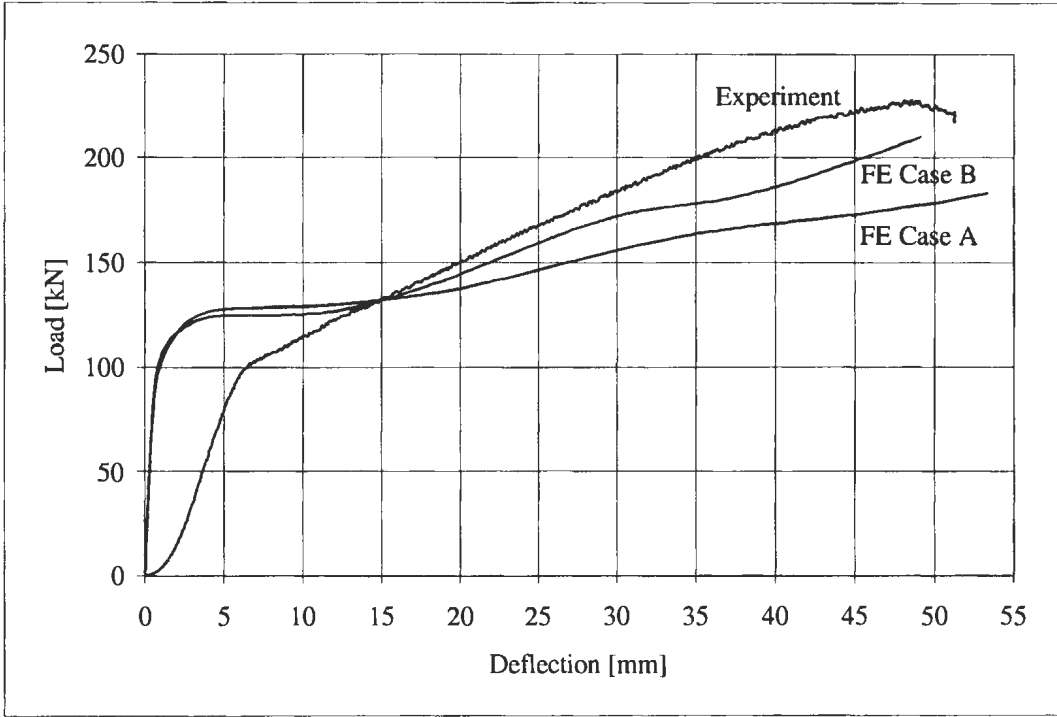


Figure 5.1: Comparison of Cases A and B with experimental results

Several reasons can be given for the differences in these curves. But, there is a common thread to all of these reasons and that is the errors involved in using an idealised model to study the behaviour of a physical system. First, during the experiment, the flatjack underwent severe deformations as it maintained contact with the structure. These deformations had the effect of altering the calibrated contact area of the flatjack from Section 3.2.2 as more of the flatjack came into contact with the structure. Also, these deformations were a result of energy absorption by the flatjack, thus the total energy imparted to the test setup by the hydraulic ram was not utilised to deform the test specimen. Second, since the deflection data recorded during the test was actually a record of the movement of the hydraulic ram, the deformation of

the flatjack led to errors in the deflection measurements, making the test specimen seem less stiff than its actual behaviour. Third, the support condition of the FE model was fully fixed, whereas in the physical model, it is impossible to construct a true fixed support. During the test, material tearing at the support, preceded by stretching, caused the test to end as the test specimen was no longer able to carry additional load. These deformations at the support also cause an apparent reduction in the test specimen stiffness, as compared with the FE model stiffness. The use of virtual very stiff springs to simulate the fixed welded edge and the use of very weak springs to simulate the left of the free edge may provide better agreement to the experimental results, but is beyond the scope of this effort. Fourth, the welds used in construction of the experimental model were of the same scale as those used on much larger structures. Thus, areas of residual welding stresses are a much larger percentage of the overall structure than at full-scale. Finally, as the stress in the material goes beyond yield, straining in the cross-section causes non-recoverable, plastic deformations of the structure. These deformations change the crystal structure of the material, making it more resistant to further deflections. The result is that the material can withstand stresses higher than yield, but at a loss of ductility. In the FE model, an ideal material model (see Section 4.1.3) is used in which the material is assumed to be elastic, perfectly plastic. This implies that once stress reaches yield, the material can only resist further increases in load through deformation. However, as seen in Section 4.1.3, an effective strength is used as the elastic-plastic transition point. Since this value is halfway between the yield and ultimate strengths of the material, the FE model is able to match the general trend of the experimental load-deflection curve, even though the slope was not matched.

All of these factors cause the physical model to have greater deflections at a given load value than the corresponding FE model, resulting in the slope discrepancies

between the FE and physical models. In contrast, a final visual comparison of the experimental test specimen and the FE model showed that the final deformed shape of both models was remarkably similar. This similarity validates the choice of the Riks method for the FE analysis.

Based on the discussions above and on the load-deflection curves plotted in Figure 5.1, Case B matches the experimental results much more closely, particularly in the plastic region. A finer mesh size for Case A may have matched the experimental behaviour more closely, but was considered unnecessary due to the results obtained from Case B. Thus, only the results for Case B will be used in the following comparisons and sensitivity analysis.

5.1.2 FE and Experimental Results with Analytical Equations

In addition to the above, a comparison was made with analytical loads and deflections calculated from the equations given for yield, three-hinge and rupture of stiffened plating in Chapter 2. These equations are repeated here for clarity.

$$\begin{aligned}
 \text{Yield} = P_Y &= \frac{-24M_Y L}{(b^2 - 3L^2)bs}, & \delta_Y &= \frac{P_Y}{384EI} \left(\frac{b}{s}\right) (2b^2L - 2L^3 - b^3) \\
 \text{Three-hinge} = P_{3h} &= \frac{8\sigma_Y Z_P}{(L - \frac{b}{2})bs}, & \delta_{3h} &= 0.1s \\
 \text{Rupture} = P_{ult} &= (\sigma_Y + \sigma_{ult}) \frac{t}{b} \sin c, & \delta_{ult} &= 0.1502L \\
 & & & \text{(where } c \text{ is the solution of: } \frac{1-\frac{b}{L}}{\cos c} + \frac{bc}{L \sin c} = 1.05)
 \end{aligned}$$

The pressures calculated from these equations are multiplied by the patch area to obtain the analytical load so that a direct comparison can be made to the experimental and FE results. Recall from Section 3.2 and 3.4 that the patch area for yielding and three-hinge collapse was 15236 mm² and for rupture was 16900 mm². Calculations of the analytical load-deflection response can be found in Appendix D.

Figure 5.2 shows the load-deflection curves for Case B, experiment and the above analytical equations. The elastic portion of the FE and analytical curves match

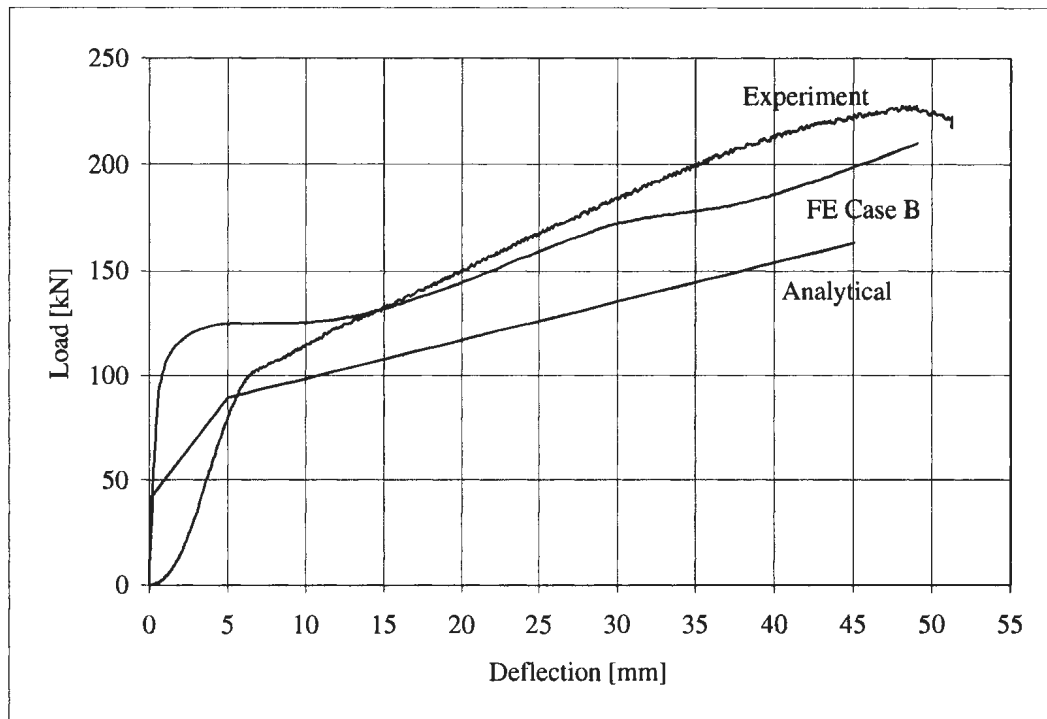


Figure 5.2: Comparison of FE Case B and experiment with analytical results

reasonably well. Looking at the initial portions of these curves more closely (curve (a) of Figure 5.3), the differences in the experimental response curve are obvious. But, to counteract the “cushioning” described in Section 3.4, the experimental curve can be shifted along the x-axis to the left by 2.5 mm. The magnitude of this shift is estimated as the deflection at which the experimental response curve first becomes linear. Curve (b) of Figure 5.3 shows the initial portions of the curves re-plotted. It is immediately evident that the elastic-plastic transition points now match more closely in terms of deflection.

Another point to consider is the magnitude of the elastic-plastic transition on the FE response curve. Recall from Section 4.1.3 that the yield point used in the FE

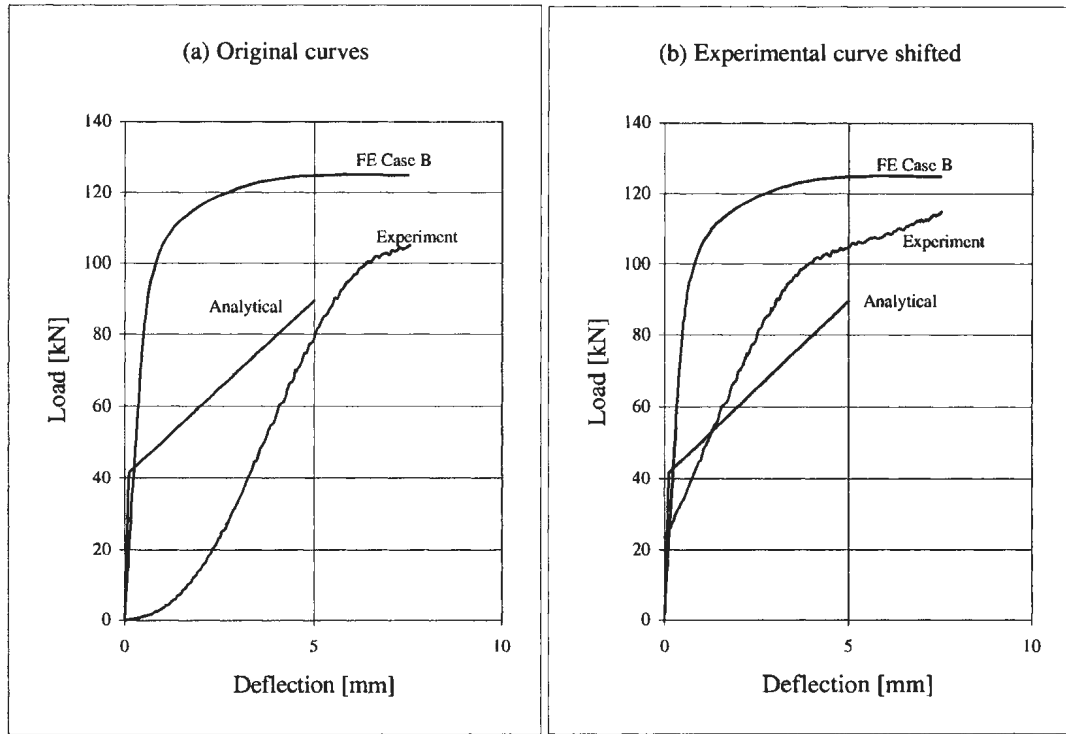


Figure 5.3: Elastic portion of response curves, showing shift in experimental response

analyses was an effective stress, σ_M , defined as $\frac{1}{2}(\sigma_Y + \sigma_{ult})$. This material definition was used to capture the effects of plastic strain hardening, without an attempt to explicitly define a strain hardening rate. In the analytical calculations, this effective stress concept is only considered in the calculation of the rupture load, not in the yield and three-hinge collapse loads. Also, the reality of the physical experiment is that the material will begin to yield at its yield point and undergo strain hardening during plastification. The increase in the predicted elastic-plastic transition load from the FE analyses can be attributed to the increased resistance to yielding of the FE material model from the use of the effective stress. As seen from the plastic portion of the response curve (Figure 5.2), the FE model does match the trend of the experimental

response quite well. Thus, we can modify the elastic response using

$$P'_{FE} = \frac{\sigma_Y}{\sigma_M} P_{FE}, \quad (5.1)$$

since the collapse load is directly proportional to the material stress. This load reduction is applied fully for deflections up to 2 mm, just beyond the pronounced change in curvature of the response, then its effectiveness is diminished linearly up to a deflection of 15 mm to obtain a smooth transition to the plastic portion of the response curve. Figure 5.4 shows the results of this modification.

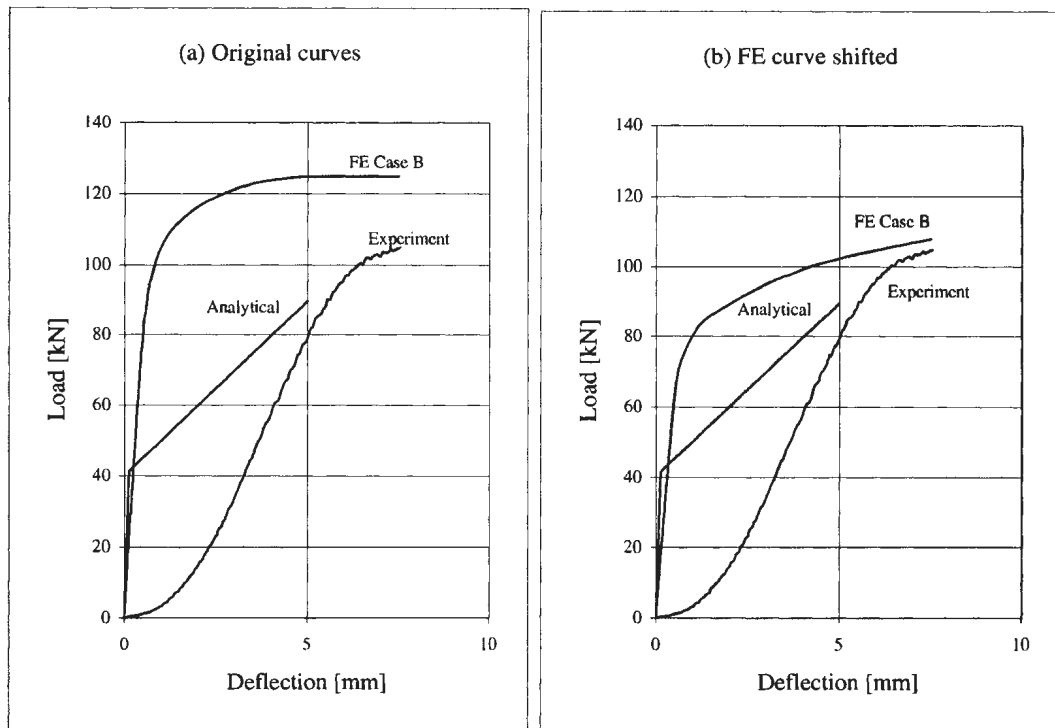


Figure 5.4: Elastic portion of response curves, showing change in FE response

These comparisons confirm the accuracy of the FE model and reinforce the explanations given for the discrepancies with the experimental results. Figure 5.5 shows the complete response curves of Figure 5.2 with the modified experimental and FE results.

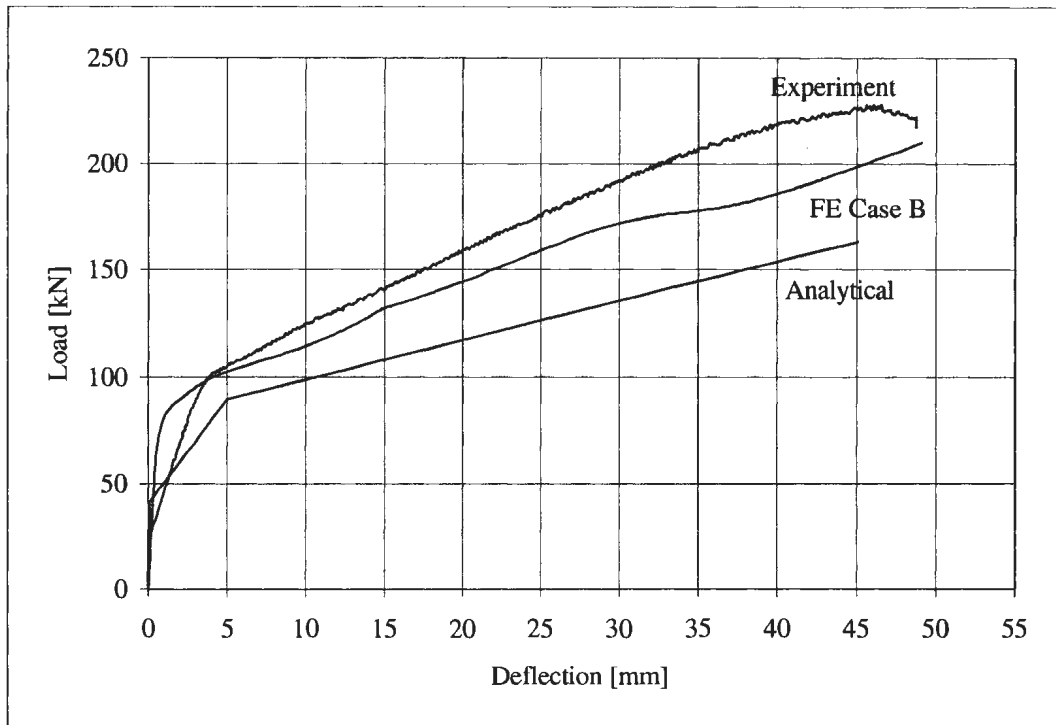


Figure 5.5: The complete load-deflection response curves, including modified results

A final comment on these response curves is that, while the elastic portion of the response seems to be modelled quite well, the FE and experimental results for the rupture load are significantly higher than that given by the analytical equations. The reason for this discrepancy is that the analytical equations assume the stiffeners make no contribution to the ultimate strength. Sidhu and Daley (1997) present a FE analysis of instability behaviour of various shapes of stiffeners, showing that there could be significant contributions to ultimate strength, depending on shape. This type of work would allow a greater load capacity for a given deflection. Thus, the analytical solution used here represents a lower bound to stiffened plate behaviour.

5.2 Sensitivity

From these comparisons, the underlying assumption made to derive the analytical equations of Chapter 2, may not be entirely accurate. An in-depth study to confirm this result is outside the scope of this research, but some preliminary indications of the role of stiffeners in the ultimate behaviour of these structures can be made. To this end, the sensitivity of the load-deflection response of a stiffened plate to the relative stiffness of the attached stiffeners was investigated numerically by changing the shell thickness of the stiffener elements given in Case B of the FE analysis presented in Chapter 4. Two additional models were analysed (input files for these cases can be found in Appendix C):

Case 2x the shell thickness for the stiffener elements was doubled from Case B, and

Case 3x the same thickness was tripled from Case B.

Figure 5.6 shows the load-deflection behaviour for Case B and the two sensitivity analyses. The most striking feature of these curves is the significant change in the elastic-plastic transition point. This shows the significant impact the stiffeners have on elastic strength. But, notice that in both Case 2x and 3x, the curve does not extend beyond a deflection of 15 mm. The FE analyses were terminated at these points due to numerical instabilities in the models. This is evident when considering the deflected shape of these two cases, as shown in Figure 5.7. Since the stiffeners have become so stiff elastically, the majority of the deformation has occurred in the plating. These large deformations have caused excessive membrane strains, much higher than the limiting value of 5% mentioned in Chapter 2. This is particularly true for Case 3x, where there was very little out-of-plane movement of the stiffeners.

From these results, we can conclude that the assumption stated in Section 2.4, namely that the stiffeners provide no stiffness for the development of plating mem-

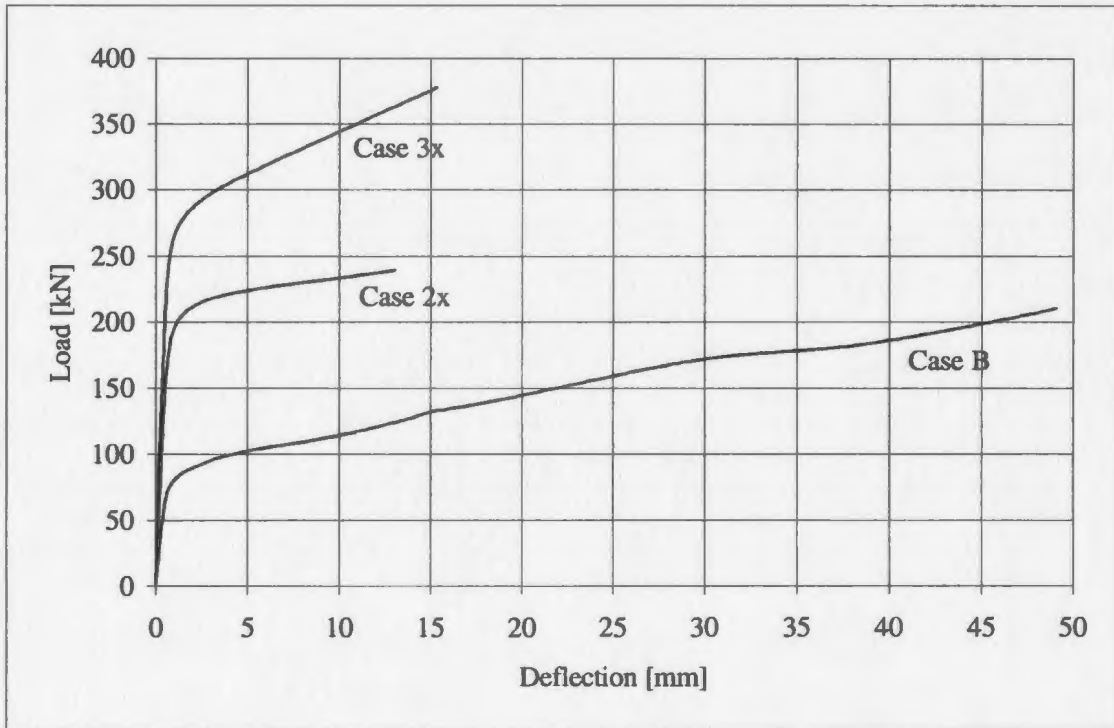


Figure 5.6: Changes in the load-deflection response for varying stiffener sizes

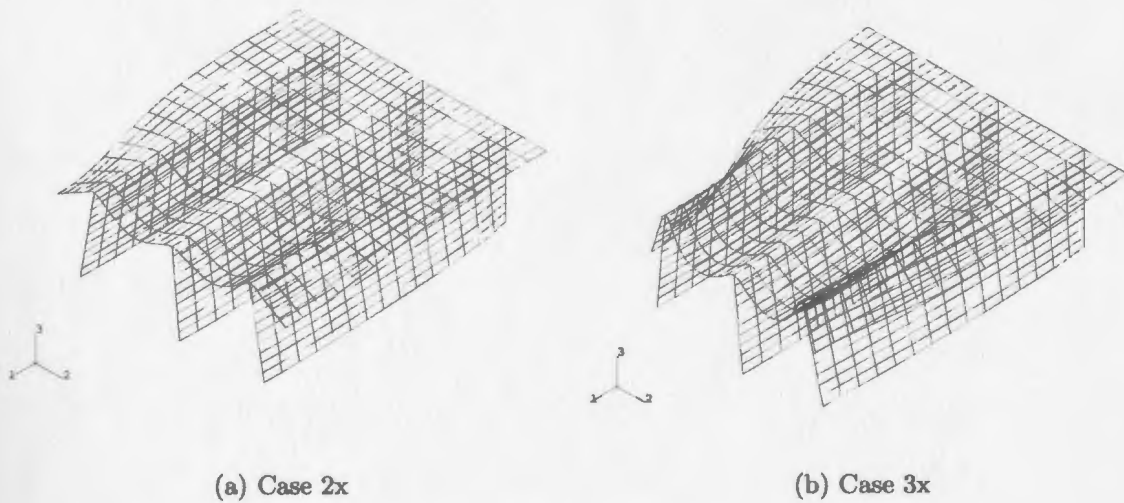


Figure 5.7: Deformed shape of stiffened plate: Cases 2x and 3x

brane action, breaks down when considering plating adjacent to very stiff structures, such as deep web frames or horizontal stringers. In addition, as seen from Figure 5.5, there is a marked reserve of strength seen from the experimental and FE response curves, as compared to the analytical response. This can be partially attributed to contributions to the ultimate strength from the stiffeners prior to their collapse. Observations from Section 3.3 support this conclusion as the stiffeners did not buckle until a deflection of approximately 12 mm was reached, which was well into the plastic portion of the response curve. This further supports the statement in the previous section that the analytical response represents a lower bound to stiffened plate behaviour.

5.3 Reliability-based Design

To show how the analysis of stiffened plating fits in a reliability-based design framework, an analysis was performed on a sample tanker design for offshore Newfoundland waters. In this region, the ice-structure interaction is defined by infrequent encounters with glacial ice features, such as growlers and bergy bits. A study by Fuglem et al. (1996) showed that vessels operating in this region typically have 0.1 to 4 impacts with glacial ice per year. For such a rare event, the appropriate design decision is to consider ice impact as an ultimate limit state. This choice guards against catastrophic failure from these loads, but does not cause over-design, from a serviceability standpoint, for an event that may only occur a handful of times during the service life of the vessel. To reflect this, Carter et al. (1996) suggest a target probability of failure for this ultimate limit state of 1×10^{-6} . This target will be used to determine the required thickness for the plating and the flatbar stiffener.

Performing a reliability calculation requires definition of both the structural resistance and the impinging load. Based on the discussions of the previous sections, it

is clear that, for resistance to ultimate failure, Equation 2.23 is a lower bound. The apparent contribution of the stiffener to the overall structural resistance seen in both the experimental and FE results is not considered. To address this, Equation 2.23 is modified to incorporate parameters of the supporting stiffeners to give

$$P'_{ult} = (\sigma_Y + \sigma_{ult}) \frac{t}{b} \frac{d}{t_w}^k \sin c,$$

where, as before, c is the solution of: (5.2)

$$\frac{1 - \frac{b}{L}}{\cos c} + \frac{bc}{L \sin c} = 1.05.$$

The term $\frac{d}{t_w}^k$ is the depth-to-thickness ratio of the stiffener, which is commonly used to as an indication of its rigidity, raised to the power of a constant, k . An initial estimate of this rigidity term can be obtained from the ratio of the experimental ultimate load and the previously calculated analytical load based on Equation 2.23, which is 1.387. Now, in order for P'_{ult} to be accurate, the term $\frac{d}{t_w}^k$ must equal this ratio. From the experimental geometry, k is determined to be 0.118.

In Section 2.1, the process by which ice-structure interaction imparts load onto the structure was described. The two main features defining this interaction were highlighted, namely

- the relationship between pressure and contact area, and
- how to describe the nature of the process.

As stated, Jordaan et al. (1993) presented a exponentially decreasing form for the pressure-area curve based on a wide range of experimental data ranging from small-scale laboratory tests to large-scale field experiments, incorporated with a probabilistic model for extreme load prediction based on the concept of critical zones. This

definition of ice loading is used here and is given by a Gumbel(max) distribution of the form

$$F_Z(z) = \exp\left\{-\exp\left\{\frac{-(z - x_0 - x_1)}{\alpha}\right\}\right\}, \quad (5.3)$$

where $\alpha = 1.25a^{-0.7}$ defines the pressure-area relationship, with a being the overall contact area with the ice feature, $x_0 = -0.03$ is the initial pressure before impact, and $x_1 = \alpha(\log \nu + \log r)$ is a coefficient representing both exposure of the vessel to ice features (ν) and the percentage that result in impacts (r). An assessment of the experimental data shows that r can be taken as 0.46 (Jordaan et al. 1993). To determine the exposure, the type of ice operations undertaken is considered. The operation of an arctic icebreaker requires frequent encounters with a variety of ice features, resulting in many interactions. On the other hand, a shuttle tanker operating offshore Newfoundland will have infrequent encounters with glacial ice (as stated above). To quantify these differences, Carter et al. (1992) specify the following categories of ice-going vessels in terms of the expected number of encounters:

CAC1 10,000,

CAC2 1,000,

CAC3 100, and

CAC4 10.

Based on the range of impacts of 0.1 to 4 per year, ν was taken as 5 for this analysis. A summary of these and other random variables and constants used are listed in Table 5.1.

The reliability analysis involved conducting iterative FORM calculations, altering the plate and flatbar thicknesses until the target probability of failure mentioned

Table 5.1: Structural particulars of sample design

Item	Description	Value
plate thickness, t [mm]	Normal	$\mu = 1.014t, \sigma = 0.01\mu$
flatbar thickness, w [mm]	Normal	$\mu = 1.014w, \sigma = 0.01\mu$
load [MPa]	Gumbel(max)	$\mu = x_0 + x_1 + 0.577\alpha, \sigma = 1.283\alpha$
yield strength, σ_Y [MPa]	Lognormal	$\mu = 315, \sigma = 15.75$
ultimate strength, σ_{ult} [MPa]	Lognormal	$\mu = 515, \sigma = 25.75$
stiffener depth, d [mm]	Constant	250
stiffener spacing, s [mm]	Constant	600
stiffener span, L [mm]	Constant	1490
ice load breadth, b [mm]	Constant	870

above was reached. The thicknesses obtained were 15.8 and 10 mm, respectively.

Input and output from these calculations are given in Appendix E.

Chapter 6

Conclusions and Recommendations

An in-depth analysis of stiffened plating behaviour has been presented in the preceding chapters. Several conclusions can be drawn from this effort, namely

1. A flatjack was used successfully to apply a partial uniform load to a small-scale stiffened plate.
2. Comparisons between finite element, experimental and analytical results showed good agreement, particularly after some modifications to the finite element and experimental results to address analysis observations.
3. The comparisons also indicated that the analytical ultimate limit state proposed by Nessim et al. (1992) to be lower bound to the stiffened plate behaviour.
4. A modified ultimate limit state was proposed, which incorporates stiffener rigidity.
5. Sensitivity analyses were conducted and showed that by increasing the stiffener size, major structural deflections were limited to the plating.
6. A sample reliability analysis was conducted, based on the proposed ultimate limit state, which resulted in plating and flatbar thicknesses 15.8 and 10 mm for a target probability of failure of 1×10^{-6} .

To further the understanding of the role of stiffened plating in membrane behaviour, several recommendations for future study can be made:

1. Studies into stiffener instability, such as the finite element work being carried out by Sidhu and Daley (1997), should be continued and verified with large scale experiments.
2. Further experiments should be conducted to determine the accuracy of the stiffener rigidity term, $\frac{d}{t_w}^k$, particularly the value of the exponent, k .
3. When using a flatjack loading mechanism, displacements of the test specimen could be measured from the side of the specimen opposite the applied load (perhaps with a spring-loaded dial gauge) to improve interpretation of results.
4. Future finite element analysis work could benefit from using springs in the definition of the support condition.

References

- Ayyub, B. M., G. J. White, and E. S. Purcell (1989). Estimation of structural service life of ships. *Naval Engineers Journal* 101(3), 156–166.
- Blake, A. (1990). *Practical Stress Analysis in Engineering Design* (Second ed.). New York, New York, USA: Marcel Dekker, Inc.
- Brown, P. W. (1993). Optimal design of bow plating for ships operating in ice. Master's thesis, Memorial University of Newfoundland.
- Campbell, T. I. and T. M. Charlton (1973). Finite deformation of a fully-fixed beam comprised of a non-linear material. *International Journal of Mechanical Sciences* 15, 415–428.
- Carter, J. E., C. Daley, M. Fuglem, I. J. Jordaan, A. Keinonen, C. Revill, T. R. Butler, K. Muggeridge, and B. Zou (1996). Maximum bow force for arctic shipping pollution prevention regulations (asppr) - phase ii. Technical Report TP12652, Ocean Engineering Research Centre, Memorial University of Newfoundland. prepared for Transport Canada, Ship Safety, Northern Region.
- Carter, J. E., R. M. W. Frederking, I. J. Jordaan, W. J. Milne, M. A. Nessim, and B. Zou (1992). Review and verification of proposals for the revision of the arctic shipping pollution prevention regulations. Technical Report TP11366E, Ocean Engineering Research Centre, Memorial University of Newfoundland. prepared for Transport Canada, Ship Safety, Northern Region.

- Daley, C. (1991). *Ice Edge Contact - A Brittle Failure Process Model*. Ph. D. thesis, Laboratory of Naval Architecture and Marine Engineering, Helsinki University of Technology. Published in Acta Polytechnica Scandinavica, Mechanical Engineering Series No. 100.
- Daley, C. G., C. Ferregut, and R. Brown (1991). Structural risk model of arctic shipping. In *IUTAM-IAHR Symposium on Ice-Structure Interaction, St. John's, Newfoundland, Canada*, pp. 507–540.
- Dome Petroleum Ltd. (1982). Report on full-scale measurements of ice impact loads and response of the 'CANMAR Kigoriak' - August and October 1981. Technical report, Dome Petroleum Ltd.
- EGGE, E. D. and M. Böckenbauer (1991). Calculation of the collision resistance of ships and its assessment for classification purposes. *Marine Structures* 4, 35–56.
- Frederking, R., I. J. Jordaan, and J. S. McCallum (1990). Field tests of ice indentation at medium scale: Hobson's choice ice island, 1989. In *Proceedings of the 10th International Symposium on Ice, IAHR '90, Espoo, Finland, Volume 2*, pp. 931–944.
- Fuglem, M. K., I. J. Jordaan, and G. Crocker (1996). Iceberg-structure interaction: Probabilities for design. Accepted for publication by the Canadian Journal of Civil Engineering.
- Glen, I. F. and H. Blount (1984). Measurements of ice impact pressures and loads onboard CCGS Louis S. St. Laurent. In *Proceedings of the 3rd International Conference on Offshore Mechanics and Arctic Engineering, New Orleans, Louisiana, USA, Volume 3*, pp. 246–252.
- Haythornthwaite, R. M. (1957). Beams with full end fixity: Axial forces may increase load capacity many times. *Engineering* 183, 110–112.

- Hibbitt, Karlsson and Sorenson Inc. (1995a). *ABAQUS Theory Manual, Version 5.5*. Pawtucket, Rhode Island, USA: Hibbitt, Karlsson and Sorenson Inc.
- Hibbitt, Karlsson and Sorenson Inc. (1995b). *ABAQUS/Standard User's Manual, Version 5.5, Volumes I and II*. Pawtucket, Rhode Island, USA: Hibbitt, Karlsson and Sorenson Inc.
- Hodge, Jr., P. G. (1974). Post yield behaviour of a beam with partial end fixity. *International Journal of Mechanical Sciences* 16, 385–388.
- Hughes, O. (1988). *Ship Structural Design: A Rationally-Based Computer-Aided Optimization Approach* (Second ed.). Jersey City, New Jersey, USA: Society of Naval Architects and Marine Engineers.
- Johansson, B. M., J. Ciring, W. Jolles, E. Stalder, and R. D. Rowe (1994, March). Revolutionary icebreaker design. In *Proceedings of Icetech '94, Fifth International Conference on Ships and Marine Structures in Cold Regions, Calgary, Alberta*, pp. O1–O34. Society of Naval Architects and Marine Engineers, Arctic Section.
- Johnston, M. (1994). Variation of local pressures during ice-structure interaction. Master's thesis, Memorial University of Newfoundland.
- Johnston, M., K. R. Croasdale, and I. J. Jordaan (1995). Localized pressures during ice-structure interaction: Relevance to design criteria. Submitted for publication.
- Jordaan, I. J. and M. A. Maes (1991). Rationale for load specifications and load factors in the new CSA code for fixed offshore structures. *Canadian Journal of Civil Engineering* 18(3), 454–464.
- Jordaan, I. J., M. A. Maes, P. W. Brown, and I. P. Hermans (1993, February). Probabilistic analysis of local ice pressures. *Journal of Offshore Mechanics and*

Arctic Engineering 115, 83–89.

Jordaan, I. J., D. G. Matskevitch, and I. L. Meglis (1997). Disintegration of ice under fast compressive loading. Submitted for publication to the *International Journal of Fracture*.

Jordaan, I. J., J. Xiao, and B. Zou (1993). Fracture and damage of ice: Towards practical implementation. In *Proceedings of Ice Mechanics '93, Charlottesville, Virginia*, pp. 251–260.

Kirwan, L. P. (1959). *The White Road: A Survey of Polar Exploration*. London, England: Hollis and Carter, Limited.

Madsen, H. O., S. Krenk, and N. C. Lind (1986). *Methods of Structural Safety*. Englewood Cliffs, N.J.: Prentice-Hall Inc.

Mansour, A. E. (1990). An introduction to structural reliability theory. Technical Report SSC–351, Ship Structure Committee, Washington, D.C.

McDermott, J. F., R. G. Kline, J. E. L. Jones, N. M. Maniar, and W. P. Chiang (1974). Tanker structural analysis for minor collisions. *SNAME Transactions* 82, 382–414.

Melchers, R. E. (1987). *Structural Reliability: Analysis and Prediction*. Chichester, West Sussex, England: Ellis Horwood Limited.

Melville Shipping Ltd. (1989). Proposal for the Revision of the Arctic Shipping Pollution Prevention Regulations: Volume 1 - Background. Technical Report TP9981, Canadian Coast Guard - Northern.

Nessim, M., H. P. Hong, and M. Stephens (1992). Risk-based assessment of hull response and brittle fracture of vessels designed to ASPPR. Technical Report 90–35, Centre for Frontier Engineering Research. Final Report to the Ocean

Engineering Research Centre, Memorial University of Newfoundland.

- Paulling, J. R. (1988). Strength of ships. In E. V. Lewis (Ed.), *Principles of Naval Architecture* (Second ed.), Volume I - Stability and Strength, Chapter 4, pp. 205–300. Society of Naval Architects and Marine Engineers.
- Ramm, E. (1981). Strategies for tracing the nonlinear response near limit points. In W. Wunderlich, E. Stein, and K. J. Bathe (Eds.), *Proceedings: Nonlinear Finite Element Analysis in Structural Mechanics Workshop*, Berlin, Germany, pp. 63–89. Ruhr-Universität Bochum: Springer-Verlag.
- Ratzlaff, K. P. and D. J. L. Kennedy (1985). Analysis of continuous steel plates subjected to uniform transverse loads. *Canadian Journal of Civil Engineering* 12, 685–699.
- Ratzlaff, K. P. and D. J. L. Kennedy (1986). Behaviour and ultimate strength of continuous steel plates subjected to uniform transverse loads. *Canadian Journal of Civil Engineering* 13, 76–85.
- Riska, K., H. Rantala, and A. Joensuu (1990). Full scale observations of ship-ice contact. Technical Report M-97, Ship Laboratory, Faculty of Mechanical Engineering, Helsinki University of Technology.
- Ronalds, B. F. (1990). Membrane action in the beam mechanism. *Journal of Strain Analysis* 25(4), 241–253.
- Ronalds, B. F. and P. J. Dowling (1986). Finite deformations of stringer stiffened plates and shells under knife edge loading. In *Proceedings: Fifth International Symposium on Offshore Mechanics and Arctic Engineering*, Volume 3, pp. 323–331.
- Ross, C. T. F. (1987). *Advanced Applied Stress Analysis*. Chichester, West Sussex, England: Ellis Horwood Ltd.

- Sidhu, H. and C. Daley (1997, January). Investigation of plastic instability in laterally loaded ship stiffeners. Technical Report LR OST 97001, Ocean Engineering Research Centre, Memorial University of Newfoundland.
- Skrzypek, J. J. (1993). *Plasticity and Creep*. Boca Raton, Florida, USA: Begell House, CRC Press. English edition editor: R. B. Hetnarski.
- Timoshenko, S. and S. Woinowsky-Krieger (1959). *Theory of Plates and Shells*. New York, N.Y.: McGraw-Hill Book Company.
- Transport Canada, Ship Safety (1995, December). *Arctic Shipping Pollution Prevention Regulations (ASPPR): Equivalent Standards for the Construction of Arctic Class Ships*. Transport Canada, Ship Safety. Rules updated based on ASPPR Proposals and Fmax project.
- Zou, B. (1996). *Ships in Ice: Principles in Design*. Ph. D. thesis, Memorial University of Newfoundland.

Appendix A

Experimental Design

DESIGN OF TEST SPECIMEN AND SUPPORT FRAME

Part A: Test Specimen Design

Test Specimen Particulars

t	3.175	plate thickness [mm]
s	50.00	stiffener spacing [mm]
d _w	50.80	web depth [mm]
t _w	3.175	web thickness [mm]
L	300.00	stiffener span [mm]
b	123.43	ice load breadth [mm]

Material Particulars (ASTM A36)

σ _y	248	yield stress [MPa]
σ _u	400	ultimate stress [MPa]
E	1.92E+05	Young's modulus [MPa]
ν	0.3	Poisson's ratio (elastic)
ν _p	0.5	Poisson's ratio (plastic)

The test specimen in question was subject to a patch load to represent ice impact. This patch load was applied using a flatjack arrangement (described in Chapter 3). The flatjack used in these tests was 150 x 150 mm, which produced an effective patch load area of 15236 mm², or 123.43 x 123.43 mm (see Appendix B).

Buckling Check on Specimen Dimensions

(from Transport Canada, Ship Safety (1995, December) *Arctic Shipping Pollution Prevention Regulations (ASPPR)*, Report No. TP12260)

a) The web thickness must be greater than, or equal to:

$$t_{w_min} = d_w(\sigma_y)^{1/2}/282 = 2.84 \text{ mm} \quad \text{Offered thickness?} \quad \text{OK}$$

b) The web depth to thickness ratio must also be less than, or equal to:

$$d_w/t_w \leq 168N/VV = 24.55 \quad \text{Offered } d_w/t_w? \quad \text{OK}$$

$$\text{where: } N = 1$$

$$VV = (\sigma_y Z_{PRD}/Z_{PAF})^{1/2} = 6.84$$

$$Z_{PAF} = d_w t_w (d_w + t)/2000 = 4.35$$

$$Z_{PRD} = 0.04167 s L A_F P_{AV} B B R_2 C C / \sigma_y = 0.82$$

$$B B = \nu_p (3 - \nu_p / L) / 1000 = 0.13$$

Constants:

A _F	0.50	CC	0.80
P _{AV}	7.66	ν _p	45
R ₂	0.83		

Since the requirements of a) and b) above are met, the specimen meets ASPPR buckling criteria.

Area & Elastic Section Modulus

A_p	158.8 plate area [mm ²]
A_w	161.3 web area [mm ²]
x_{bar}	15.19 location of elastic NA from top of plate [mm]
I	93089 moment of inertia about NA [mm ⁴]
$Z_{elastic}$	2400 elastic section modulus [mm ³]

Plastic Section Modulus

(after Ronalds, B.F. (1990) Membrane action in the beam mechanism. *Journal of Strain Analysis* 25 (4), 241-253.)

C_1	0.007874	} coefficients which determine relative contributions of plate and web to the total section modulus.
C_2	0.492	
g_1	0.400	
$Z_{plastic}$	4348 plastic section modulus [mm ³]	

Plating Failure Loads and Deflections (Section 2.3)

$$P_y = 2.25\sigma_y(t/s)^2 = 2.25 \text{ MPa, pressure to initiate yielding at the supports.}$$

$$\delta_y = (P_y s^4(1-\nu^2))/(32Et^3) = 0.07 \text{ mm, corresponding deflection.}$$

$$P_{2h} = 3.464\sigma_y(t/s)^2 = 3.46 \text{ MPa, pressure to cause yielding \& hinge formation at the supports.}$$

$$\delta_{2h} = (P_{2h} s^4(1-\nu^2))/(32Et^3) = 0.10 \text{ mm, corresponding deflection.}$$

$$P_{3h} = 4.62\sigma_y(t/s)^2 = 4.62 \text{ MPa, pressure to cause the formation of the third plastic hinge at midspan.}$$

$$\delta_{3h} = 2t = 6.35 \text{ mm, corresponding deflection.}$$

$$P_{ult} = 0.515(\sigma_y + \sigma_u)(t/s) = 21.19 \text{ MPa, pressure to cause rupture at 5\% strain.}$$

$$\delta_{ult} = 0.1502s = 7.51 \text{ mm, corresponding deflection.}$$

Stiffened Plating Failure Loads and Deflections (Section 2.4)

$$P_y = (-24\sigma_y Z_{elastic} L)/(bs(b^2 - 3L^2)) = 2.73 \text{ MPa, pressure to cause first yield.}$$

$$\delta_y = P_y bs(2b^2 L - 2L^3 - b^3)/384EI = 0.11 \text{ mm, corresponding deflection.}$$

Stiffened Plating Failure Loads and Deflections, con't (Section 2.4)

$$P_{3h} = (8\sigma_y Z_{plastic}) / (bs(L-b/2)) = 5.87 \text{ MPa, pressure to cause three-hinge formation.}$$

$$\delta_{3h} = 0.1s = 5.00 \text{ mm, corresponding deflection.}$$

$$c = 2.51825 \text{ The solution for } c \text{ from Equation 2.18.}$$

$$P_{ult} = (\sigma_y + \sigma_u)(t/b)\sin(c) = 9.73 \text{ MPa, pressure to cause rupture at 5\% strain.}$$

$$\delta_{ult} = 0.1502L = 45.06 \text{ mm, corresponding deflection.}$$

Fully Plastic Axial Force

$$F = \sigma_y(A_p + A_w)/1000 = 79.37 \text{ kN, for one (1) stiffened plate unit.}$$

$$F_{tot} = 3F = 238.11 \text{ kN, for test specimen w/3 stiffeners.}$$

As a final check of the test specimen design, the plastic capacity in shear was calculated and compared against the maximum possible force available from the loading ram, which was 150,000 lbs or 668 kN.

$$A_{tot} = 3(A_p + A_w) = 960 \text{ mm}^2, \text{ total area (w/3 stiffeners).}$$

$$\tau_y = 0.7\sigma_y = 174 \text{ MPa, yield stress in shear.}$$

$$F_{shear} = 2\tau_y A_{tot} / 1000 = 333 \text{ kN, shear load req'd to fail test specimen.}$$

Since F & F_{shear} are less than 668 kN, laboratory equipment is sufficient to fail specimen.

Part B: Support Frame Design

As can be seen from Figure 3.1, the above forces cause torsion in the support frame. Thus, the support frame was designed to resist this induced torque as follows:

H	300	support frame height [mm].	} These dimensions were chosen for simplicity.
W	150	support frame width (= H/2) [mm].	
LA	300	lever arm of load, F_{tot} [mm].	

$$Q_{max} = F_{tot}LA = 71433 \text{ kN-mm, maximum induced torque.}$$

Now, since the support frame thickness is the only unknown, a reasonable value was selected, the design torque calculated and compared against Q_{\max} .

$$\begin{aligned}t_{\text{SF}} &= 12.7 \text{ mm, support frame thickness.} \\ Q_{\text{design}} &= 2\tau_y t_{\text{SF}}(W-t_{\text{SF}})(H-t_{\text{SF}})/1000 = 173936 \text{ kN-mm, resulting torque capacity.} \\ \text{Safety Factor} &= Q_{\text{design}}/Q_{\max} = 2.435\end{aligned}$$

Since Q_{design} is greater than Q_{\max} , a support frame thickness of 12.7 mm is adequate and also provides sufficient safety should experimental loads exceed those calculated here.

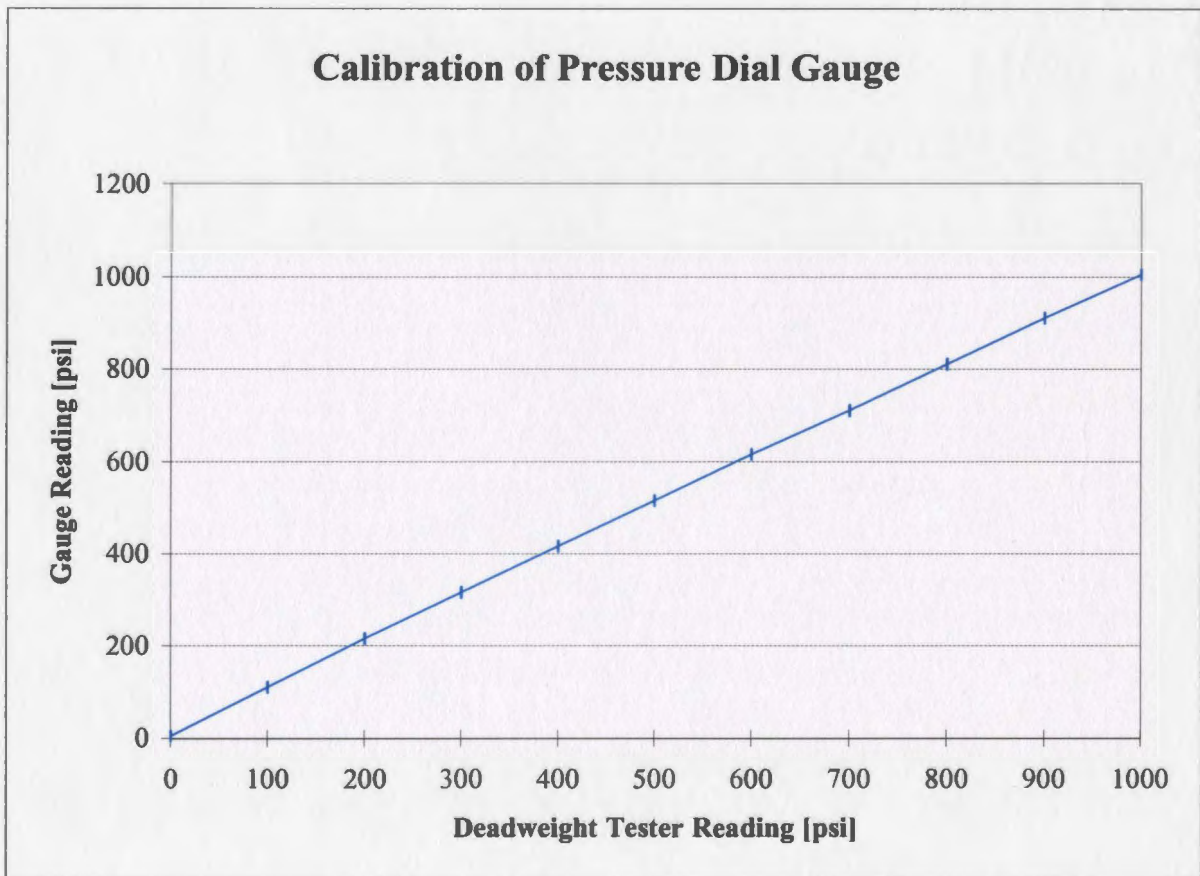
Appendix B

Experimental Calibration

Part A: Pressure Gauge Calibration

Used Deadweight Tester to check pressure gauge readings.

Deadweight	Gauge Reading [psi]	Slope
0	5	--
100	110	1.05
200	215	1.05
300	315	1.00
400	415	1.00
500	515	1.00
600	615	1.00
700	710	0.95
800	810	1.00
900	910	1.00
1000	1005	0.95
Average Slope =		1.0000



Part B: Flatjack Calibration

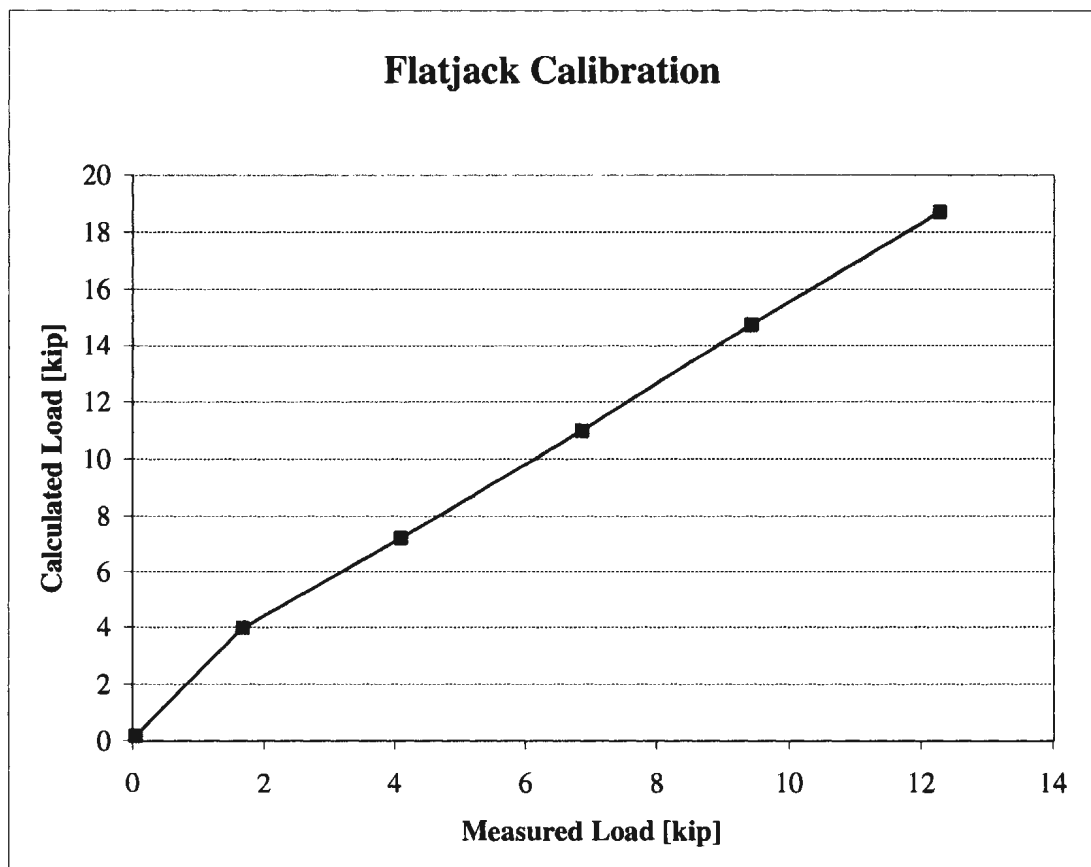
Held ram at a fixed gap of 10 mm then pressurized to ~ 500 psi as follows:

Measured Load [kip]	Pressure [psi]	Calculated Load [kip] ¹	Load Ratio	Area [in ²]	Area [mm ²]
0.04	5	0.18	4.50000	8.00000	5161
1.68	110	3.96	2.35714	15.27273	9853
4.09	200	7.20	1.76039	20.45000	13194
6.86	305	10.98	1.60058	22.49180	14511
9.43	410	14.76	1.56522	23.00000	14839
12.28	520	18.72	1.52443	23.61538	15236

(see Note 2)

Notes:

1. This is based on an area of the undeformed 150 x 150 mm flatjack, which is ~36 in².
2. This area of 15236 mm² results in an actual contact footprint of 123.43 x 123.43 mm.



Appendix C

Finite Element Input Files

CASE A: EIGENVALUE BUCKLING ANALYSIS

```
*HEADING
FE Model of Test Specimen
*PREPRINT,ECHO=YES,MODEL=NO,HISTORY=NO
*****
** This model represents the laboratory specimen, by using symmetry
** only half its length needs modelling.
**
** General Notes:
** 1. All dimensions and loads are in metric units.
** 2. Material is ASTM A36 steel.
** 3. Structure is modelled using S4R finite strain shell elements,
**    which are designed for use in large displacement analyses.
**
** Comments related to this particular input file:
** 1. modelling lab test number 1, with a 125 x 125 mm patch load.
** 2. fully fixed support condition.
** 3. eigenvalue buckling prediction.
** 4. distributed load applied.
*****
**
** Plating Nodal Definition
**
** *NODE
1,0,0,0
25,.15,0,0
601,0,.15,0
625,.15,.15,0
** Defines the corner nodes of the 150x150 mm shell plate.
** *NGEN, NSET=EDGE1
1,25,1
** *NGEN, NSET=EDGE2
601,625,1
** Generates two plate edges lengthwise.
** *NFILL, NSET=PNODES
EDGE1,EDGE2,12,50
** Fills nodes in between EDGE1 and EDGE2.
**
** Stiffener Nodal Definition
**
** *NODE
651,0,.025,-.012675
675,.15,.025,-.012675
801,0,.025,-.0507
825,.15,.025,-.0507
851,0,.075,-.012675
875,.15,.075,-.012675
1001,0,.075,-.0507
1025,.15,.075,-.0507
1051,0,.125,-.012675
1075,.15,.125,-.012675
```

```

1201,0,.125,-.0507
1225,.15,.125,-.0507
** Defines the corner nodes for each of the three stiffeners.
** Starts at an offset z-coordinate because the nodes on the
** line z=0 have already been generated with the plate nodes.
*NGEN, NSET=ALAYER
651,675,1
851,875,1
1051,1075,1
*NGEN, NSET=BLAYER
801,825,1
1001,1025,1
1201,1225,1
** Generates two lengthwise strings of nodes along each
** stiffener.
*NFILL, NSET=SNODES
ALAYER,BLAYER,3,50
** Fills nodes between ALAYER and BLAYER.
**
** Plating Element Definition
**
*ELEMENT, TYPE=S4R
1,1,2,52,51
** Defines element #1 with its 4 corner nodes.
*ELGEN, ELSET=PLATE
1,24,1,1,12,50,24
** Generates all plate elements as per the following
** sequence:
** master elem. #, # of elems in row, inc. in elem. #'s in row,
** inc. in node #'s between elems., # of rows, inc. in node #'s
** between rows, inc. in elem #'s between rows.
**
** Stiffener Element Definition
**
*ELEMENT, TYPE=S4R
301,651,652,102,101
325,701,702,652,651
401,851,852,302,301
425,901,902,852,851
501,1051,1052,502,501
525,1101,1102,1052,1051
** Defines the first two elements in each stiffener (This is done
** because of the different increments in node #'s for the
** stiffener elements attached to the plating.)
*ELGEN, ELSET=FRAMES
301,24,1,1
325,24,1,1,3,50,24
401,24,1,1
425,24,1,1,3,50,24
501,24,1,1
525,24,1,1,3,50,24

```

```

** Generates the stiffener elements as follows:
** - the line with 01 element #'s generates only 1 row of elements
**   (refer to plating element generation for explanation of each #).
** - the line with 25 element #'s generates the remaining 3 rows
**   necessary to fully define the stiffener.
**
** Node and Element Definition for Boundary Conditions
** and Load Application
**
*NGEN, NSET=FIXEDEND
1,601,50
651,801,50
851,1001,50
1051,1201,50
** Defines the end nodes which will have a fully fixed boundary
** condition.
*NGEN, NSET=SYMEND
25,625,50
675,825,50
875,1025,50
1075,1225,50
** Defines the nodes which will have a symmetric boundary condition.
*NGEN, NSET=NPATCH1
65,75,1
*NGEN, NSET=NPATCH2
565,575,1
** Generates the edge nodes of the elements making up the location
** of the 125 x 125 mm patch load application.
*NFILL, NSET=NPATCH
NPATCH1,NPATCH2,10,50
** Fills in the remaining nodes within the patch.
*ELGEN, ELSET=ELPATCH
39,10,1,1,10,50,24
** Defines the element set that to which the patch load will be
** applied.
**
** Material Definition
**
*MATERIAL, NAME=ASTMA36
*ELASTIC
192E3,.3
** Sets the Young's Modulus to be 192E3 MPa and Poisson's ratio to 0.3
*PLASTIC
324
** Defines perfect plastic behaviour beyond a stress level of
** 0.5*(yield + ultimate).
**
** Plate and Stiffener Section Definition
**
*SHELL SECTION, ELSET=PLATE, MATERIAL=ASTMA36, POISSON=0.5
.003175

```

```

*SHELL SECTION, ELSET=FRAMES, MATERIAL=ASTMA36, POISSON=0.5
.003175
** Defines the plate and stiffeners as having a shell thickness of
** 3.175 mm, or 1/8".
**
** Boundary Conditions (Global)
**
*BOUNDARY
FIXEDEND,1,6
** Sets all dof to zero (fully fixed end).
SYMEND,XSYMM
** Sets appropriate dof such that the nodes move in a plane
** z=constant.
**
** Loading Definition
**
*STEP
*BUCKLE
1,1
** Defines the # of eigenvalues estimated (1), the max.
** eigenvalue (1) and the # of iterations is 30 (default).
**
*DLOAD
ELPATCH,P,-1
** Defines 1 MPa pressure acting on element set ELPATCH.
**
*EL PRINT, FREQ=0
S, MISES
E
IE,PEMAG,CEMAG
** suppresses printed output to the .dat file in order to
** reduce file sizes.
*NODE PRINT, FREQ=0
U
V
A
RF
NT
** suppresses printed output to the .dat file in order to
** reduce file sizes.
*NODE FILE
U
** Outputs all displacements for all nodes to a file.
*RESTART,WRITE,OVERLAY
** Writes job info to a restart file for future processing.
*END STEP

```

CASE A: POSTBUCKLING ANALYSIS

```
*HEADING
FE Model of Test Specimen
*PREPRINT,ECHO=YES,MODEL=NO,HISTORY=NO
*****
** This model represents the laboratory specimen, by using symmetry
** only half its length needs modelling.
**
** General Notes:
** 1. All dimensions and loads are in metric units.
** 2. Material is ASTM A36 steel.
** 3. Structure is modelled using S4R finite strain shell elements,
**    which are designed for use in large displacement analyses.
**
** Comments related to this particular input file:
** 1. modelling lab test number 1, with a 125 x 125 mm patch load.
** 2. fully fixed support condition.
** 3. postbuckling analysis.
** 4. distributed load applied.
*****
**
** *NODE, INPUT=stfa3.cds
** inputs displaced (50% imperfection) nodal geometry
** from eigenvalue buckling prediction.
**
** Plating Nodal Defintion
**
** *NGEN, NSET=EDGE1
1,25,1
** *NGEN, NSET=EDGE2
601,625,1
** Generates two plate edges lengthwise.
** *NFILL, NSET=PNODES
EDGE1,EDGE2,12,50
** Fills nodes in between EDGE1 and EDGE2.
**
** Stiffener Nodal Definition
**
** *NGEN, NSET=ALAYER
651,675,1
851,875,1
1051,1075,1
** *NGEN, NSET=BLAYER
801,825,1
1001,1025,1
1201,1225,1
** Generates two lengthwise strings of nodes along each
** stiffener.
** *NFILL, NSET=SNODES
ALAYER,BLAYER,3,50
** Fills nodes between ALAYER and BLAYER.
```

```

**
** Plating Element Definition
**
**
**ELEMENT, TYPE=S4R
1,1,2,52,51
** Defines element #1 with its 4 corner nodes.
**
**ELGEN, ELSET=PLATE
1,24,1,1,12,50,24
** Generates all plate elements as per the following
** sequence:
** master elem. #, # of elems in row, inc. in elem. #'s in row,
** inc. in node #'s between elems., # of rows, inc. in node #'s
** between rows, inc. in elem #'s between rows.
**
** Stiffener Element Definition
**
**
**ELEMENT, TYPE=S4R
301,651,652,102,101
325,701,702,652,651
401,851,852,302,301
425,901,902,852,851
501,1051,1052,502,501
525,1101,1102,1052,1051
** Defines the first two elements in each stiffener (This is done
** because of the different increments in node #'s for the
** stiffener elements attached to the plating.)
**
**ELGEN, ELSET=FRAMES
301,24,1,1
325,24,1,1,3,50,24
401,24,1,1
425,24,1,1,3,50,24
501,24,1,1
525,24,1,1,3,50,24
** Generates the stiffener elements as follows:
** - the line with 01 element #'s generates only 1 row of elements
**   (refer to plating element generation for explanation of each #).
** - the line with 25 element #'s generates the remaining 3 rows
**   necessary to fully define the stiffener.
**
** Node and Element Definition for Boundary Conditions
** and Load Application
**
**
**NGEN, NSET=FIXEDEND
1,601,50
651,801,50
851,1001,50
1051,1201,50
** Defines the end nodes which will have a fully fixed boundary
** condition.
**
**NGEN, NSET=SYMEND
25,625,50

```

```

675,825,50
875,1025,50
1075,1225,50
** Defines the nodes which will have a symmetric boundary condition.
*NGEN, NSET=NPATCH1
65,75,1
*NGEN, NSET=NPATCH2
565,575,1
** Generates the edge nodes of the elements making up the location
** of the 125 x 125 mm patch load application.
*NFILL, NSET=NPATCH
NPATCH1,NPATCH2,10,50
** Fills in the remaining nodes within the patch.
*ELGEN, ELSET=ELPATCH
39,10,1,1,10,50,24
** Defines the element set that to which the patch load will be
** applied.
*ELSET,ELSET=ELSTRAIN
96,120,192,216,396,496,596
** Defines elements where axial strain is to be measured to compare with
** experimental data.
**
** Material Definition
**
*MATERIAL, NAME=ASTMA36
*ELASTIC
192E3,.3
** Sets the Young's Modulus to be 192E3 MPa and Poisson's ratio to 0.3
*PLASTIC
324
** Defines perfect plastic behaviour beyond a stress level of
** 0.5*(yield + ultimate).
**
** Plate and Stiffener Section Definition
**
*SHELL SECTION, ELSET=PLATE, MATERIAL=ASTMA36, POISSON=0.5
.003175
*SHELL SECTION, ELSET=FRAMES, MATERIAL=ASTMA36, POISSON=0.5
.003175
** Defines the plate and stiffeners as having a shell thickness of
** 3.175 mm, or 1/8".
**
** Boundary Conditions (Global)
**
*BOUNDARY
FIXEDEND,1,6
** Sets all dof to zero (fully fixed end).
SYMEND,XYMM
** Sets appropriate dof such that the nodes move in a plane
** z=constant.
**

```

```

** Loading Definition
**
*STEP,NLGEOM,INC=120
** Defines large displacement analysis and the max.
** # of iterations as 120.
*STATIC,RIKS
0.1,1.0,,,,325,3,-.052
** Defines a riks analysis (load-deflection curve).
** Parameters: time increment, total step time, min.
** time increment, max. increment, max. value of load
** proportionality factor, node # for displ. monitoring,
** dof being monitored, value of total displ. that ends
** step (here 52 mm, same as lab test).
*DLOAD
ELPATCH,P,-1
** Defines 1 MPa pressure acting on element set ELPATCH.
**
*EL PRINT, FREQ=0
S, MISES
E
IE,PEMAG,CEMAG
** suppresses printed output to the .dat file in order to
** reduce file sizes.
*NODE PRINT, FREQ=0
U
V
A
RF
NT
** suppresses printed output to the .dat file in order to
** reduce file sizes.
*NODE FILE,NSET=SYMEND
U
** outputs all displacement components for all nodes to
** the results file.
*EL FILE,ELSET=ELPATCH
LOADS
** outputs distributed loads
** to the results file for element set ELPATCH.
*EL FILE,ELSET=ELSTRAIN
S,E
** outputs stresses and strains for element set ELSTRAIN.
** These elements are located at the same positions as the
** strain gauges on the test specimen.
*RESTART,WRITE,OVERLAY
** Writes job info. to a restart file for future processing.
** The OVERLAY parameter indicates that only the info. from
** the last increment completed is retained in the restart
** file. This greatly reduces disk space required to analyse
** structure.
*END STEP

```

CASE B: EIGENVALUE BUCKLING ANALYSIS

```
*HEADING
FE model of test specimen with support frame.
*PREPRINT,ECHO=YES,MODEL=NO,HISTORY=NO
*****
** This model represents the laboratory specimen, by using symmetry
** only half its length needs modelling.
**
** General Notes:
** 1. All dimensions and loads are in metric units.
** 2. Material is ASTM A36 steel.
** 3. Structure is modelled using S8R thick shell elements.
** 4. Support frame is modelled with C3D8 solid elements.
**
** Comments related to this particular input file:
** 1. modelling lab test number 1, with a 125 x 125 mm patch load.
** 2. eigenvalue buckling analysis.
** 3. distributed load applied.
*****
**
** PART A: Stiffened Plate Modelling
**
** Plating Nodal Definition
**
**
** *NODE
1,0,0,0
31,.15,0,0
3001,0,.15,0
3031,.15,.15,0
** Defines the corner nodes of the 150x150 mm shell plate.
** *NGEN, NSET=EDGE1
1,31,1
** *NGEN, NSET=EDGE2
3001,3031,1
** Generates two plate edges lengthwise.
** *NFILL, NSET=PNODES
EDGE1,EDGE2,60,50
** Fills nodes in between EDGE1 and EDGE2.
**
**
** Plating Element Definition
**
** *ELEMENT, TYPE=S8R
1,1,3,103,101,2,53,102,51
** Defines element #1 with its 8 nodes.
** *ELGEN, ELSET=PLATE
1,15,2,1,30,100,50
** Generates all plate elements as per the following
** sequence:
** master elem. #, # of elems in row, inc. in node #'s between elems.,
** inc. in elem. #'s in row, # of rows, inc. in node #'s
** between rows, inc. in elem #'s between rows.
```

```

**
** Stiffener Nodal Definition
**
**
*NODE
3051,0,.025,-.0025
3081,.15,.025,-.0025
4001,0,.025,-.05
4031,.15,.025,-.05
4051,0,.075,-.0025
4081,.15,.075,-.0025
5001,0,.075,-.05
5031,.15,.075,-.05
5051,0,.125,-.0025
5081,.15,.125,-.0025
6001,0,.125,-.05
6031,.15,.125,-.05
** Defines the nodes for the first stiffener.
** Starts at an offset z-coordinate because the nodes on the
** line z=0 have already been generated with the plate nodes.
*NGEN, NSET=ALAYER
3051,3081,1
4051,4081,1
5051,5081,1
*NGEN, NSET=BLAYER
4001,4031,1
5001,5031,1
6001,6031,1
** Generates two lengthwise strings of nodes along top & bottom of
** first stiffener.
*NFILL, NSET=SNODES
ALAYER,BLAYER,19,50
** Fills nodes between LAYER's.
**
** Stiffener Element Definition
**
**
*ELEMENT, TYPE=S8R
1501,3101,3103,503,501,3102,3053,502,3051
1521,3201,3203,3103,3101,3202,3153,3102,3151
1701,4101,4103,1503,1501,4102,4053,1502,4051
1721,4201,4203,4103,4101,4202,4153,4102,4151
1901,5101,5103,2503,2501,5102,5053,2502,5051
1921,5201,5203,5103,5101,5202,5153,5102,5151
** Defines the first two elements in each stiffener (This is done
** because of the different increments in node #'s for the
** stiffener elements attached to the plating.)
*ELGEN, ELSET=FRAMES
1501,15,2,1
1521,15,2,1,9,100,20
1701,15,2,1
1721,15,2,1,9,100,20
1901,15,2,1

```

```

1921,15,2,1,9,100,20
** Generates the stiffener elements as follows:
** - the line with 01 element #'s generates only 1 row of elements
**   (refer to plating element generation for explanation of each #).
** - the line with 21 element #'s generates the remaining 3 rows
**   necessary to fully define the stiffener.
**
** PART B: Node and Element Definition for Boundary Conditions
**         and Load Application
**
*NGEN,NSET=FIXEDEND
1,3001,50
3051,4001,50
4051,5001,50
5051,6001,50
** Defines nodes as fully fixed.
*NGEN, NSET=SYMEND
31,3031,50
3081,4031,50
4081,5031,50
5081,6031,50
** Defines the nodes which will have a symmetric boundary condition.
*ELGEN, ELSET=ELPATCH
110,6,2,1,26,100,50
** Defines the element set that to which the patch load will be
** applied.
*ELSET,ELSET=ELSTRAIN
465,515,965,1015,1695,1895,2095
** Defines elements where axial strain is to be measured to compare with
** experimental data.
**
** Material Definition
**
*MATERIAL, NAME=ASTMA36
*ELASTIC
192E3,.3
** Sets the Young's Modulus to be 192E3 MPa and Poisson's ratio to 0.3
*PLASTIC
324
** Defines perfect plastic behaviour beyond a stress level of
** 0.5*(yield + ultimate).
**
** Plate and Stiffener Section Definition
**
*SHELL SECTION, ELSET=PLATE, MATERIAL=ASTMA36, POISSON=0.5
.003175
*SHELL SECTION, ELSET=FRAMES, MATERIAL=ASTMA36, POISSON=0.5
.003175
** Defines the plate and stiffeners as having a shell thickness of
** 3.175 mm, or 1/8".
**

```

```

** PART D: Boundary Conditions (Global)
**
*BOUNDARY
FIXEDEND,1,6
** Sets all dof at support end to zero (fully fixed).
SYMEND, XSYMM
** Sets appropriate dof such that the nodes move in a plane
** z=constant.
**
** Loading Definition
**
*STEP
*BUCKLE
1,1
** Defines the # of eigenvalues estimated (1), the max.
** eigenvalue (1) and the # of iterations is 30 (default).
**
*DLOAD
ELPATCH,P,-1
** Defines 1 MPa pressure acting on element set ELPATCH.
**
*EL PRINT, FREQ=0
S, MISES
E
IE,PEMAG,CEMAG
** suppresses printed output to the .dat file in order to
** reduce file sizes.
*NODE PRINT, FREQ=0
U
V
A
RF
NT
** suppresses printed output to the .dat file in order to
** reduce file sizes.
*NODE FILE
U
** Outputs all displacements for all nodes to a file.
*RESTART,WRITE,OVERLAY
** Writes job info to a restart file for future processing.
*END STEP

```

CASE B: POSTBUCKLING ANALYSIS

```
*HEADING
FE model of test specimen with support frame.
*PREPRINT,ECHO=YES,MODEL=NO,HISTORY=NO
*****
** This model represents the laboratory specimen, by using symmetry
** only half its length needs modelling.
**
** General Notes:
** 1. All dimensions and loads are in metric units.
** 2. Material is ASTM A36 steel.
** 3. Structure is modelled using S8R thick shell elements.
**
** Comments related to this particular input file:
** 1. modelling lab test number 1, with a 125 x 125 mm patch load.
** 2. postbuckling analysis.
** 3. distributed load applied.
*****
**
** *NODE,INPUT=stfm.cds
** input of nodal coordinates from eigenvalue analysis.
** (max. imperfection = 50% plate thickness)
**
** PART A: Stiffened Plate Modelling
**
** Plating Nodal Definition
**
** *NGEN, NSET=EDGE1
1,31,1
** *NGEN, NSET=EDGE2
3001,3031,1
** Generates two plate edges lengthwise.
** *NFILL, NSET=PNODES
EDGE1,EDGE2,60,50
** Fills nodes in between EDGE1 and EDGE2.
**
** Plating Element Definition
**
** *ELEMENT, TYPE=S8R
1,1,3,103,101,2,53,102,51
** Defines element #1 with its 8 nodes.
** *ELGEN, ELSET=PLATE
1,15,2,1,30,100,50
** Generates all plate elements as per the following
** sequence:
** master elem. #, # of elems in row, inc. in node #'s between elems.,
** inc. in elem. #'s in row, # of rows, inc. in node #'s
** between rows, inc. in elem #'s between rows.
**
** Stiffener Nodal Definition
**
```

```

*NGEN, NSET=ALAYER
3051,3081,1
4051,4081,1
5051,5081,1
*NGEN,NSET=BLAYER
4001,4031,1
5001,5031,1
6001,6031,1
** Generates two lengthwise strings of nodes along top & bottom of
** first stiffener.
*NFILL, NSET=SNODES
ALAYER,BLAYER,19,50
** Fills nodes between LAYER's.
**
** Stiffener Element Definition
**
*ELEMENT, TYPE=S8R
1501,3101,3103,503,501,3102,3053,502,3051
1521,3201,3203,3103,3101,3202,3153,3102,3151
1701,4101,4103,1503,1501,4102,4053,1502,4051
1721,4201,4203,4103,4101,4202,4153,4102,4151
1901,5101,5103,2503,2501,5102,5053,2502,5051
1921,5201,5203,5103,5101,5202,5153,5102,5151
** Defines the first two elements in each stiffener (This is done
** because of the different increments in node #'s for the
** stiffener elements attached to the plating.)
*ELGEN, ELSET=FRAMES
1501,15,2,1
1521,15,2,1,9,100,20
1701,15,2,1
1721,15,2,1,9,100,20
1901,15,2,1
1921,15,2,1,9,100,20
** Generates the stiffener elements as follows:
** - the line with 01 element #'s generates only 1 row of elements
**   (refer to plating element generation for explanation of each #).
** - the line with 21 element #'s generates the remaining 3 rows
**   necessary to fully define the stiffener.
**
** PART B: Node and Element Definition for Boundary Conditions
**         and Load Application
**
*NGEN,NSET=FIXEDEND
1,3001,50
3051,4001,50
4051,5001,50
5051,6001,50
** Defines nodes as fully fixed.
*NGEN, NSET=SYMEND
31,3031,50
3081,4031,50

```

```

4081,5031,50
5081,6031,50
** Defines the nodes which will have a symmetric boundary condition.
*ELGEN, ELSET=ELPATCH
110,6,2,1,26,100,50
** Defines the element set that to which the patch load will be
** applied.
*ELSET,ELSET=ELSTRAIN
465,515,965,1015,1695,1895,2095
** Defines elements where axial strain is to be measured to compare with
** experimental data.
**
** Material Definition
**
*MATERIAL, NAME=ASTMA36
*ELASTIC
192E3,.3
** Sets the Young's Modulus to be 192E3 MPa and Poisson's ratio to 0.3
*PLASTIC
324
** Defines perfect plastic behaviour beyond a stress level of
** 0.5*(yield + ultimate).
**
** Plate and Stiffener Section Definition
**
*SHELL SECTION, ELSET=PLATE, MATERIAL=ASTMA36, POISSON=0.5
.003175
*SHELL SECTION, ELSET=FRAMES, MATERIAL=ASTMA36, POISSON=0.5
.003175
** Defines the plate and stiffeners as having a shell thickness of
** 3.175 mm, or 1/8".
**
** PART D: Boundary Conditions (Global)
**
*BOUNDARY
FIXEDEND,1,6
** Sets all dof at support end to zero (fully fixed).
SYMEND,XYMM
** Sets appropriate dof such that the nodes move in a plane
** z=constant.
**
** Loading Definition
**
*STEP,NLGEOM,INC=200
** Defines large displacement analysis and the max.
** # of iterations as 200.
*STATIC,RIKS
0.1,1.0,,,,1531,3,-.052
** Defines a riks analysis (load-deflection curve).
** Parameters: time increment, total step time, min.
** time increment, max. increment, max. value of load

```

```

** proportionality factor, node # for displ. monitoring,
** dof being monitored, value of total displ. that ends
** step (here 52 mm, same as lab test).
*DLOAD
ELPATCH,P,-1
** Defines pressure acting on element set ELPATCH.
**
*EL PRINT, FREQ=0
S, MISES
E
IE,PEMAG,CEMAG
** suppresses printed output to the .dat file in order to
** reduce file sizes.
*NODE PRINT, FREQ=0
U
V
A
RF
NT
** suppresses printed output to the .dat file in order to
** reduce file sizes.
*NODE FILE,NSET=SYMEND
U
** outputs all displacement components for nodeset SYMEND to
** the results file.
*EL FILE,ELSET=ELPATCH
LOADS
** outputs distributed loads
** to the results file for element set ELPATCH.
*EL FILE,ELSET=ELSTRAIN
S,E
** outputs stresses and strains for element set ELSTRAIN.
** These elements are located at the same positions as the
** strain gauges on the test specimen.
*RESTART,WRITE,OVERLAY
** Writes job info. to a restart file for future processing.
** The OVERLAY parameter indicates that only the info. from
** the last increment completed is retained in the restart
** file. This greatly reduces disk space required to analyse
** structure.
*END STEP

```

CASE 2x: EIGENVALUE BUCKLING ANALYSIS

```
*HEADING
Sensitivity Analysis of Stiffened Plate Model
*PREPRINT,ECHO=YES,MODEL=NO,HISTORY=NO
*****
** This model represents the laboratory specimen, by using symmetry
** only half its length needs modelling.
**
** General Notes:
** 1. All dimensions and loads are in metric units.
** 2. Material is ASTM A36 steel.
** 3. Structure is modelled using S8R thick shell elements.
** 4. Stiffener thickness is doubled from original analysis.
**
** Comments related to this particular input file:
** 1. modelling lab test number 1, with a 125 x 125 mm patch load.
** 2. eigenvalue buckling analysis.
** 3. distributed load applied.
*****
**
** PART A: Stiffened Plate Modelling
**
** Plating Nodal Definition
**
**
** *NODE
1,0,0,0
31,.15,0,0
3001,0,.15,0
3031,.15,.15,0
** Defines the corner nodes of the 150x150 mm shell plate.
** *NGEN, NSET=EDGE1
1,31,1
** *NGEN, NSET=EDGE2
3001,3031,1
** Generates two plate edges lengthwise.
** *NFILL, NSET=PNODES
EDGE1,EDGE2,60,50
** Fills nodes in between EDGE1 and EDGE2.
**
** Plating Element Definition
**
** *ELEMENT, TYPE=S8R
1,1,3,103,101,2,53,102,51
** Defines element #1 with its 8 nodes.
** *ELGEN, ELSET=PLATE
1,15,2,1,30,100,50
** Generates all plate elements as per the following
** sequence:
** master elem. #, # of elems in row, inc. in node #'s between elems.,
** inc. in elem. #'s in row, # of rows, inc. in node #'s
** between rows, inc. in elem #'s between rows.
```

```

**
** Stiffener Nodal Definition
**
*NODE
3051,0,.025,-.0025
3081,.15,.025,-.0025
4001,0,.025,-.05
4031,.15,.025,-.05
4051,0,.075,-.0025
4081,.15,.075,-.0025
5001,0,.075,-.05
5031,.15,.075,-.05
5051,0,.125,-.0025
5081,.15,.125,-.0025
6001,0,.125,-.05
6031,.15,.125,-.05
** Defines the nodes for the first stiffener.
** Starts at an offset z-coordinate because the nodes on the
** line z=0 have already been generated with the plate nodes.
*NGEN, NSET=ALAYER
3051,3081,1
4051,4081,1
5051,5081,1
*NGEN, NSET=BLAYER
4001,4031,1
5001,5031,1
6001,6031,1
** Generates two lengthwise strings of nodes along top & bottom of
** first stiffener.
*NFILL, NSET=SNODES
ALAYER,BLAYER,19,50
** Fills nodes between LAYER's.
**
** Stiffener Element Definition
**
*ELEMENT, TYPE=S8R
1501,3101,3103,503,501,3102,3053,502,3051
1521,3201,3203,3103,3101,3202,3153,3102,3151
1701,4101,4103,1503,1501,4102,4053,1502,4051
1721,4201,4203,4103,4101,4202,4153,4102,4151
1901,5101,5103,2503,2501,5102,5053,2502,5051
1921,5201,5203,5103,5101,5202,5153,5102,5151
** Defines the first two elements in each stiffener (This is done
** because of the different increments in node #'s for the
** stiffener elements attached to the plating.)
*ELGEN, ELSET=FRAMES
1501,15,2,1
1521,15,2,1,9,100,20
1701,15,2,1
1721,15,2,1,9,100,20
1901,15,2,1

```

```

1921,15,2,1,9,100,20
** Generates the stiffener elements as follows:
** - the line with 01 element #'s generates only 1 row of elements
**   (refer to plating element generation for explanation of each #).
** - the line with 21 element #'s generates the remaining 3 rows
**   necessary to fully define the stiffener.
**
** PART B: Node and Element Definition for Boundary Conditions
**         and Load Application
**
*NGEN,NSET=FIXEDEND
1,3001,50
3051,4001,50
4051,5001,50
5051,6001,50
** Defines nodes as fully fixed.
*NGEN, NSET=SYMEND
31,3031,50
3081,4031,50
4081,5031,50
5081,6031,50
** Defines the nodes which will have a symmetric boundary condition.
*ELGEN, ELSET=ELPATCH
110,6,2,1,26,100,50
** Defines the element set that to which the patch load will be
** applied.
*ELSET,ELSET=ELSTRAIN
465,515,965,1015,1695,1895,2095
** Defines elements where axial strain is to be measured to compare with
** experimental data.
**
** Material Definition
**
*MATERIAL, NAME=ASTMA36
*ELASTIC
192E3,.3
** Sets the Young's Modulus to be 192E3 MPa and Poisson's ratio to 0.3
*PLASTIC
324
** Defines perfect plastic behaviour beyond a stress level of
** 0.5*(yield + ultimate).
**
** Plate and Stiffener Section Definition
**
*SHELL SECTION, ELSET=PLATE, MATERIAL=ASTMA36, POISSON=0.5
.003175
*SHELL SECTION, ELSET=FRAMES, MATERIAL=ASTMA36, POISSON=0.5
.00635
** Defines the plate as having a shell thickness of
** 3.175 mm, or 1/8" and the stiffener thickness is doubled.
**

```

```

** PART D: Boundary Conditions (Global)
**
*BOUNDARY
FIXEDEND,1,6
** Sets all dof at support end to zero (fully fixed).
SYMEND,XSYMM
** Sets appropriate dof such that the nodes move in a plane
** z=constant.
**
** Loading Definition
**
*STEP
*BUCKLE
1,1
** Defines the # of eigenvalues estimated (1), the max.
** eigenvalue (1) and the # of iterations is 30 (default).
**
*DLOAD
ELPATCH,P,-1
** Defines 1 MPa pressure acting on element set ELPATCH.
**
*EL PRINT, FREQ=0
S, MISES
E
IE,PEMAG,CEMAG
** suppresses printed output to the .dat file in order to
** reduce file sizes.
*NODE PRINT, FREQ=0
U
V
A
RF
NT
** suppresses printed output to the .dat file in order to
** reduce file sizes.
*NODE FILE
U
** Outputs all displacements for all nodes to a file.
*RESTART,WRITE,OVERLAY
** Writes job info to a restart file for future processing.
*END STEP

```

CASE 2x: POSTBUCKLING ANALYSIS

```
*HEADING
Sensitivity Analysis of Stiffened Plate Model
*PREPRINT,ECHO=YES,MODEL=NO,HISTORY=NO
*****
** This model represents the laboratory specimen, by using symmetry
** only half its length needs modelling.
**
** General Notes:
** 1. All dimensions and loads are in metric units.
** 2. Material is ASTM A36 steel.
** 3. Structure is modelled using S8R thick shell elements.
** 4. Stiffener thickness is doubled from original analysis.
**
** Comments related to this particular input file:
** 1. modelling lab test number 1, with a 125 x 125 mm patch load.
** 2. postbuckling analysis.
** 3. distributed load applied.
*****
**
** *NODE,INPUT=double.cds
** input of nodal coordinates from eigenvalue analysis.
** (max. imperfection = 50% plate thickness)
**
** PART A: Stiffened Plate Modelling
**
** Plating Nodal Definition
**
** *NGEN, NSET=EDGE1
** 1,31,1
** *NGEN, NSET=EDGE2
** 3001,3031,1
** Generates two plate edges lengthwise.
** *NFILL, NSET=PNODES
** EDGE1,EDGE2,60,50
** Fills nodes in between EDGE1 and EDGE2.
**
** Plating Element Definition
**
** *ELEMENT, TYPE=S8R
** 1,1,3,103,101,2,53,102,51
** Defines element #1 with its 8 nodes.
** *ELGEN, ELSET=PLATE
** 1,15,2,1,30,100,50
** Generates all plate elements as per the following
** sequence:
** master elem. #, # of elems in row, inc. in node #'s between elems.,
** inc. in elem. #'s in row, # of rows, inc. in node #'s
** between rows, inc. in elem #'s between rows.
**
** Stiffener Nodal Definition
```

```

**
*NGEN, NSET=ALAYER
3051,3081,1
4051,4081,1
5051,5081,1
*NGEN,NSET=BLAYER
4001,4031,1
5001,5031,1
6001,6031,1
** Generates two lengthwise strings of nodes along top & bottom of
** first stiffener.
*NFill, NSET=SNODES
ALAYER,BLAYER,19,50
** Fills nodes between LAYER's.
**
** Stiffener Element Definition
**
*ELEMENT, TYPE=S8R
1501,3101,3103,503,501,3102,3053,502,3051
1521,3201,3203,3103,3101,3202,3153,3102,3151
1701,4101,4103,1503,1501,4102,4053,1502,4051
1721,4201,4203,4103,4101,4202,4153,4102,4151
1901,5101,5103,2503,2501,5102,5053,2502,5051
1921,5201,5203,5103,5101,5202,5153,5102,5151
** Defines the first two elements in each stiffener (This is done
** because of the different increments in node #'s for the
** stiffener elements attached to the plating.)
*ELGEN, ELSET=FRAMES
1501,15,2,1
1521,15,2,1,9,100,20
1701,15,2,1
1721,15,2,1,9,100,20
1901,15,2,1
1921,15,2,1,9,100,20
** Generates the stiffener elements as follows:
** - the line with 01 element #'s generates only 1 row of elements
**   (refer to plating element generation for explanation of each #).
** - the line with 21 element #'s generates the remaining 3 rows
**   necessary to fully define the stiffener.
**
** PART B: Node and Element Definition for Boundary Conditions
**         and Load Application
**
*NGEN,NSET=FIXEDEND
1,3001,50
3051,4001,50
4051,5001,50
5051,6001,50
** Defines nodes as fully fixed.
*NGEN, NSET=SYMEND
31,3031,50

```

```

3081,4031,50
4081,5031,50
5081,6031,50
** Defines the nodes which will have a symmetric boundary condition.
*ELGEN, ELSET=ELPATCH
110,6,2,1,26,100,50
** Defines the element set that to which the patch load will be
** applied.
*ELSET,ELSET=ELSTRAIN
465,515,965,1015,1695,1895,2095
** Defines elements where axial strain is to be measured to compare with
** experimental data.
**
** Material Definition
**
*MATERIAL, NAME=ASTMA36
*ELASTIC
192E3,.3
** Sets the Young's Modulus to be 192E3 MPa and Poisson's ratio to 0.3
*PLASTIC
324
** Defines perfect plastic behaviour beyond a stress level of
** 0.5*(yield + ultimate).
**
** Plate and Stiffener Section Definition
**
*SHELL SECTION, ELSET=PLATE, MATERIAL=ASTMA36, POISSON=0.5
.003175
*SHELL SECTION, ELSET=FRAMES, MATERIAL=ASTMA36, POISSON=0.5
.00635
** Defines the plate as having a shell thickness of
** 3.175 mm, or 1/8" and the stiffener thickness is doubled.
**
** PART D: Boundary Conditions (Global)
**
*BOUNDARY
FIXEDEND,1,6
** Sets all dof at support end to zero (fully fixed).
SYMEND,XSYMM
** Sets appropriate dof such that the nodes move in a plane
** z=constant.
**
** Loading Definition
**
*STEP,NLGEOM,INC=200
** Defines large displacement analysis and the max.
** # of iterations as 200.
*STATIC,RIKS
0.1,1.0,,,,1531,3,-.052
** Defines a riks analysis (load-deflection curve).
** Parameters: time increment, total step time, min.

```

```

** time increment, max. increment, max. value of load
** proportionality factor, node # for displ. monitoring,
** dof being monitored, value of total displ. that ends
** step (here 52 mm, same as lab test).
*DLOAD
ELPATCH,P,-1
** Defines pressure acting on element set ELPATCH.
**
*EL PRINT, FREQ=0
S, MISES
E
IE,PEMAG,CEMAG
** suppresses printed output to the .dat file in order to
** reduce file sizes.
*NODE PRINT, FREQ=0
U
V
A
RF
NT
** suppresses printed output to the .dat file in order to
** reduce file sizes.
*NODE FILE,NSET=SYMEND
U
** outputs all displacement components for nodeset SYMEND to
** the results file.
*EL FILE,ELSET=ELPATCH
LOADS
** outputs distributed loads
** to the results file for element set ELPATCH.
*EL FILE,ELSET=ELSTRAIN
S,E
** outputs stresses and strains for element set ELSTRAIN.
** These elements are located at the same positions as the
** strain gauges on the test specimen.
*RESTART,WRITE,OVERLAY
** Writes job info. to a restart file for future processing.
** The OVERLAY parameter indicates that only the info. from
** the last increment completed is retained in the restart
** file. This greatly reduces disk space required to analyse
** structure.
*END STEP

```

CASE 3x: EIGENVALUE BUCKLING ANALYSIS

```
*HEADING
Sensitivity Analysis of Stiffened Plate Model
*PREPRINT,ECHO=YES,MODEL=NO,HISTORY=NO
*****
** This model represents the laboratory specimen, by using symmetry
** only half its length needs modelling.
**
** General Notes:
** 1. All dimensions and loads are in metric units.
** 2. Material is ASTM A36 steel.
** 3. Structure is modelled using S8R thick shell elements.
** 4. Stiffener thickness is tripled from original analysis.
**
** Comments related to this particular input file:
** 1. modelling lab test number 1, with a 125 x 125 mm patch load.
** 2. eigenvalue buckling analysis.
** 3. distributed load applied.
*****
**
** PART A: Stiffened Plate Modelling
**
** Plating Nodal Definition
**
**
** *NODE
1,0,0,0
31,.15,0,0
3001,0,.15,0
3031,.15,.15,0
** Defines the corner nodes of the 150x150 mm shell plate.
** *NGEN, NSET=EDGE1
1,31,1
** *NGEN, NSET=EDGE2
3001,3031,1
** Generates two plate edges lengthwise.
** *NFILL, NSET=PNODES
EDGE1,EDGE2,60,50
** Fills nodes in between EDGE1 and EDGE2.
**
** Plating Element Definition
**
** *ELEMENT, TYPE=S8R
1,1,3,103,101,2,53,102,51
** Defines element #1 with its 8 nodes.
** *ELGEN, ELSET=PLATE
1,15,2,1,30,100,50
** Generates all plate elements as per the following
** sequence:
** master elem. #, # of elems in row, inc. in node #'s between elems.,
** inc. in elem. #'s in row, # of rows, inc. in node #'s
** between rows, inc. in elem #'s between rows.
```

```

**
** Stiffener Nodal Definition
**
*NODE
3051,0,.025,-.0025
3081,.15,.025,-.0025
4001,0,.025,-.05
4031,.15,.025,-.05
4051,0,.075,-.0025
4081,.15,.075,-.0025
5001,0,.075,-.05
5031,.15,.075,-.05
5051,0,.125,-.0025
5081,.15,.125,-.0025
6001,0,.125,-.05
6031,.15,.125,-.05
** Defines the nodes for the first stiffener.
** Starts at an offset z-coordinate because the nodes on the
** line z=0 have already been generated with the plate nodes.
*NGEN, NSET=ALAYER
3051,3081,1
4051,4081,1
5051,5081,1
*NGEN, NSET=BLAYER
4001,4031,1
5001,5031,1
6001,6031,1
** Generates two lengthwise strings of nodes along top & bottom of
** first stiffener.
*NFILL, NSET=SNODES
ALAYER,BLAYER,19,50
** Fills nodes between LAYER's.
**
** Stiffener Element Definition
**
*ELEMENT, TYPE=S8R
1501,3101,3103,503,501,3102,3053,502,3051
1521,3201,3203,3103,3101,3202,3153,3102,3151
1701,4101,4103,1503,1501,4102,4053,1502,4051
1721,4201,4203,4103,4101,4202,4153,4102,4151
1901,5101,5103,2503,2501,5102,5053,2502,5051
1921,5201,5203,5103,5101,5202,5153,5102,5151
** Defines the first two elements in each stiffener (This is done
** because of the different increments in node #'s for the
** stiffener elements attached to the plating.)
*ELGEN, ELSET=FRAMES
1501,15,2,1
1521,15,2,1,9,100,20
1701,15,2,1
1721,15,2,1,9,100,20
1901,15,2,1

```

```

1921,15,2,1,9,100,20
** Generates the stiffener elements as follows:
** - the line with 01 element #'s generates only 1 row of elements
**   (refer to plating element generation for explanation of each #).
** - the line with 21 element #'s generates the remaining 3 rows
**   necessary to fully define the stiffener.
**
** PART B: Node and Element Definition for Boundary Conditions
**         and Load Application
**
*NGEN,NSET=FIXEDEND
1,3001,50
3051,4001,50
4051,5001,50
5051,6001,50
** Defines nodes as fully fixed.
*NGEN, NSET=SYMEND
31,3031,50
3081,4031,50
4081,5031,50
5081,6031,50
** Defines the nodes which will have a symmetric boundary condition.
*ELGEN, ELSET=ELPATCH
110,6,2,1,26,100,50
** Defines the element set that to which the patch load will be
** applied.
*ELSET,ELSET=ELSTRAIN
465,515,965,1015,1695,1895,2095
** Defines elements where axial strain is to be measured to compare with
** experimental data.
**
** Material Definition
**
*MATERIAL, NAME=ASTMA36
*ELASTIC
192E3,.3
** Sets the Young's Modulus to be 192E3 MPa and Poisson's ratio to 0.3
*PLASTIC
324
** Defines perfect plastic behaviour beyond a stress level of
** 0.5*(yield + ultimate).
**
** Plate and Stiffener Section Definition
**
*SHELL SECTION, ELSET=PLATE, MATERIAL=ASTMA36, POISSON=0.5
.003175
*SHELL SECTION, ELSET=FRAMES, MATERIAL=ASTMA36, POISSON=0.5
.009525
** Defines the plate as having a shell thickness of
** 3.175 mm, or 1/8" and the stiffener thickness is tripled.
**

```

```

** PART D: Boundary Conditions (Global)
**
*BOUNDARY
FIXEDEND,1,6
** Sets all dof at support end to zero (fully fixed).
SYMEND,XSYMM
** Sets appropriate dof such that the nodes move in a plane
** z=constant.
**
** Loading Definition
**
*STEP
*BUCKLE
1,1
** Defines the # of eigenvalues estimated (1), the max.
** eigenvalue (1) and the # of iterations is 30 (default).
**
*DLOAD
ELPATCH,P,-1
** Defines 1 MPa pressure acting on element set ELPATCH.
**
*EL PRINT, FREQ=0
S, MISES
E
IE,PEMAG,CEMAG
** suppresses printed output to the .dat file in order to
** reduce file sizes.
*NODE PRINT, FREQ=0
U
V
A
RF
NT
** suppresses printed output to the .dat file in order to
** reduce file sizes.
*NODE FILE
U
** Outputs all displacements for all nodes to a file.
*RESTART,WRITE,OVERLAY
** Writes job info to a restart file for future processing.
*END STEP

```

CASE 3x: POSTBUCKLING ANALYSIS

```
*HEADING
Sensitivity Analysis of Stiffened Plate Model
*PREPRINT,ECHO=YES,MODEL=NO,HISTORY=NO
*****
** This model represents the laboratory specimen, by using symmetry
** only half its length needs modelling.
**
** General Notes:
** 1. All dimensions and loads are in metric units.
** 2. Material is ASTM A36 steel.
** 3. Structure is modelled using S8R thick shell elements.
** 4. Stiffener thickness is tripled from original analysis.
**
** Comments related to this particular input file:
** 1. modelling lab test number 1, with a 125 x 125 mm patch load.
** 2. postbuckling analysis.
** 3. distributed load applied.
*****
**
** *NODE, INPUT=triple.cds
** input of nodal coordinates from eigenvalue analysis.
** (max. imperfection = 50% plate thickness)
**
** PART A: Stiffened Plate Modelling
**
** Plating Nodal Definition
**
** *NGEN, NSET=EDGE1
1,31,1
** *NGEN, NSET=EDGE2
3001,3031,1
** Generates two plate edges lengthwise.
** *NFILL, NSET=PNODES
EDGE1,EDGE2,60,50
** Fills nodes in between EDGE1 and EDGE2.
**
** Plating Element Definition
**
** *ELEMENT, TYPE=S8R
1,1,3,103,101,2,53,102,51
** Defines element #1 with its 8 nodes.
** *ELGEN, ELSET=PLATE
1,15,2,1,30,100,50
** Generates all plate elements as per the following
** sequence:
** master elem. #, # of elems in row, inc. in node #'s between elems.,
** inc. in elem. #'s in row, # of rows, inc. in node #'s
** between rows, inc. in elem #'s between rows.
**
** Stiffener Nodal Definition
```

```

**
*NGEN, NSET=ALAYER
3051,3081,1
4051,4081,1
5051,5081,1
*NGEN,NSET=BLAYER
4001,4031,1
5001,5031,1
6001,6031,1
** Generates two lengthwise strings of nodes along top & bottom of
** first stiffener.
*NFILL, NSET=SNODES
ALAYER,BLAYER,19,50
** Fills nodes between LAYER's.
**
** Stiffener Element Definition
**
*ELEMENT, TYPE=S8R
1501,3101,3103,503,501,3102,3053,502,3051
1521,3201,3203,3103,3101,3202,3153,3102,3151
1701,4101,4103,1503,1501,4102,4053,1502,4051
1721,4201,4203,4103,4101,4202,4153,4102,4151
1901,5101,5103,2503,2501,5102,5053,2502,5051
1921,5201,5203,5103,5101,5202,5153,5102,5151
** Defines the first two elements in each stiffener (This is done
** because of the different increments in node #'s for the
** stiffener elements attached to the plating.)
*ELGEN, ELSET=FRAMES
1501,15,2,1
1521,15,2,1,9,100,20
1701,15,2,1
1721,15,2,1,9,100,20
1901,15,2,1
1921,15,2,1,9,100,20
** Generates the stiffener elements as follows:
** - the line with 01 element #'s generates only 1 row of elements
**   (refer to plating element generation for explanation of each #).
** - the line with 21 element #'s generates the remaining 3 rows
**   necessary to fully define the stiffener.
**
** PART B: Node and Element Definition for Boundary Conditions
**         and Load Application
**
*NGEN,NSET=FIXEDEND
1,3001,50
3051,4001,50
4051,5001,50
5051,6001,50
** Defines nodes as fully fixed.
*NGEN, NSET=SYMEND
31,3031,50

```

```

3081,4031,50
4081,5031,50
5081,6031,50
** Defines the nodes which will have a symmetric boundary condition.
*ELGEN, ELSET=ELPATCH
110,6,2,1,26,100,50
** Defines the element set that to which the patch load will be
** applied.
*ELSET,ELSET=ELSTRAIN
465,515,965,1015,1695,1895,2095
** Defines elements where axial strain is to be measured to compare with
** experimental data.
**
** Material Definition
**
*MATERIAL, NAME=ASTMA36
*ELASTIC
192E3,.3
** Sets the Young's Modulus to be 192E3 MPa and Poisson's ratio to 0.3
*PLASTIC
324
** Defines perfect plastic behaviour beyond a stress level of
**  $0.5 \times (\text{yield} + \text{ultimate})$ .
**
** Plate and Stiffener Section Definition
**
*SHELL SECTION, ELSET=PLATE, MATERIAL=ASTMA36, POISSON=0.5
.003175
*SHELL SECTION, ELSET=FRAMES, MATERIAL=ASTMA36, POISSON=0.5
.009525
** Defines the plate as having a shell thickness of
** 3.175 mm, or 1/8" and the stiffener thickness is tripled.
**
** PART D: Boundary Conditions (Global)
**
*BOUNDARY
FIXEDEND,1,6
** Sets all dof at support end to zero (fully fixed).
SYMEND, XSYMM
** Sets appropriate dof such that the nodes move in a plane
**  $z = \text{constant}$ .
**
** Loading Definition
**
*STEP, NLGEOM, INC=200
** Defines large displacement analysis and the max.
** # of iterations as 200.
*STATIC, RIKS
0.1,1.0,,,,1531,3,-.052
** Defines a riks analysis (load-deflection curve).
** Parameters: time increment, total step time, min.

```

```

** time increment, max. increment, max. value of load
** proportionality factor, node # for displ. monitoring,
** dof being monitored, value of total displ. that ends
** step (here 52 mm, same as lab test).
*DLOAD
ELPATCH,P,-1
** Defines pressure acting on element set ELPATCH.
**
*EL PRINT, FREQ=0
S, MISES
E
IE,PEMAG,CEMAG
** suppresses printed output to the .dat file in order to
** reduce file sizes.
*NODE PRINT, FREQ=0
U
V
A
RF
NT
** suppresses printed output to the .dat file in order to
** reduce file sizes.
*NODE FILE,NSET=SYMEND
U
** outputs all displacement components for nodeset SYMEND to
** the results file.
*EL FILE,ELSET=ELPATCH
LOADS
** outputs distributed loads
** to the results file for element set ELPATCH.
*EL FILE,ELSET=ELSTRAIN
S,E
** outputs stresses and strains for element set ELSTRAIN.
** These elements are located at the same positions as the
** strain gauges on the test specimen.
*RESTART,WRITE,OVERLAY
** Writes job info. to a restart file for future processing.
** The OVERLAY parameter indicates that only the info. from
** the last increment completed is retained in the restart
** file. This greatly reduces disk space required to analyse
** structure.
*END STEP

```

Appendix D

Analytical Calculations

COMPARISON CALCULATIONS

The calculations presented here are based on the same equations used in Appendix A, but, from the observations from the experiment, the flatjack contact area has been modified.

Initial flatjack contact area [mm ²]	15236
Final flatjack contact area [mm ²]*	16900
Revised ice load breadth, b _{NEW} [mm]	130
Revised ultimate rupture coefficient, c _{NEW}	2.48538

*Derived from estimates of the dimensions of the loading ram imprint on the deformed flatjack.

Again, based on experimental observation, the increase in contact area is not really apparent until after yield, therefore the revised parameters above will be applied only to the ultimate rupture limit state.

Analytical Load-Deflection Response

Limit State	Load	Deflection
initial	0.00	0.00
first yield	41.53	0.11
three-hinge	89.38	5.00
rupture	163.18	45.06

Appendix E

Sample Reliability Analysis

Summary file for Run 14 (see description at end)

```

NN      NN  EEEEEEEE  SSSSSSS  SSSSSSS  UU      UU  SSSSSSS
NNN     NN  EE          SS          SS          UU      UU  SS
NN N    NN  EE          SS          SS          UU      UU  SS
NN  N   NN  EEEEEEE  SSSSSSS  SSSSSSS  UU      UU  SSSSSSS
NN     N NN  EE          SS          SS  UU      UU          SS
NN      NN  EE          SS          SS  UU      UU          SS
NN      NN  EEEEEEEE  SSSSSSS  SSSSSSS  UUUUUU  SSSSSSS
    
```

DATE: 12-30-2001 15:16 - LEVEL 2.40 - DATED DEC 31, 1998

THIS IS A PROPRIETARY PROGRAM. IT MAY ONLY BE USED UNDER THE TERMS OF THE LICENSE AGREEMENT BETWEEN SOUTHWEST RESEARCH INSTITUTE AND CLIENT.

SOUTHWEST RESEARCH INSTITUTE DOES NOT MAKE ANY WARRANTY OR REPRESENTATION WHATSOEVER, EXPRESSED OR IMPLIED, INCLUDING ANY WARRANTY OF MERCHANTABILITY OR FITNESS OF ANY PURPOSE WITH RESPECT TO THE PROGRAM; OR ASSUMES ANY LIABILITY WHATSOEVER WITH RESPECT TO ANY USE OF THE PROGRAM OR ANY PORTION THEREOF OR WITH RESPECT TO ANY DAMAGES WHICH MAY RESULT FROM SUCH USE.

```

          FFFFFFFF      PPPPPP      IIIIIIII
          FF           PP  PP      II
          FF           PP  PP      II
          FFFFFFFF      PPPPPP      II
          FF           PP           II
          FF           PP           II
          FF           PP           IIIIIIII
    
```

FAST PROBABILITY INTEGRATOR

SOUTHWEST RESEARCH INSTITUTE, COPYRIGHT 1989

THIS EDUCATIONAL VERSION OF FPI HAS THE FOLLOWING LIMITS:

1. TOTAL RANDOM VARIABLES NUMER LIMIT = 7
2. TOTAL LIMIT STATES NUMBER LIMIT = 6
3. NO FAST CONVOLUTION METHODS
4. NO RESPON OR USERES OPTION
5. NO CONFIDENCE INTERVAL OPTION

```

=====
***** INPUT ECHO *****
=====
    
```

LINE

```
1 *FPI
2 Run #14: t=15.8, w=10
3 *RVNUM      5
4 *METHOD     FORM
5 *GFUNCTION  UEQN
6 g1=(Sy+Su)*(t/870)*(250/w)**0.118*sin(2.2581)-P
7 *PRINTOPT   LONG
8 *ANALTYPE   ZLEV
9 *END
10 *ZLEVELS   1
11   0.0
12 *DEFRANVR
13 P
14 .4730000E+00 .4580000E+00 EVD1
15 Sy
16 .3150000E+03 .1575000E+02 LOGN
17 Su
18 .5150000E+03 .2575000E+02 LOGN
19 t
20 .1602100E+02 .1602100E+00 NORM
21 w
22 .1014000E+02 .1014000E+00 NORM
23 *END
```

=====

=====

***** PARAMETER INTERPRETATION *****

=====

Problem Title: Run #14: t=15.8, w=10

Number of Random Variables: 5

Type of Response (g) Function Approximation:

6 = User-defined response function

Response function defined by closed-form equation in FPI input deck

Number of Datasets: 0

Solution Technique:

0 = First order reliability method

Analysis Type:

1 = User-defined Response Function levels (Z-levels)
*ZLEVELS keyword is required in model input data

Confidence Interval Calculation on CDF:

0 = No

Print option:

1 = Long printout

Debugging Option:

0 = No

***** MODEL INTERPRETATION *****

Problem Title: Run #14: t=15.8, w=10

User-Defined Response Function Z-levels:

Number	Z-Level
1	0.0000

Random Variable Statistics:

Random Variable	Distribution	Mean	Standard Deviation
P	EVD	0.4730	0.4580
SY	LOGNORMAL	315.0	15.75
SU	LOGNORMAL	515.0	25.75
T	NORMAL	16.02	0.1602
W	NORMAL	10.14	0.1014

User-Defined Response Function Equation Parameters (Sub [RESPON]) :

Equation Number = 1

***** OUTPUT SUMMARY *****

PROBLEM TITLE: Run #14: t=15.8, w=10

RESPONSE FUNCTION (LIMIT STATE): USER-DEFINED FUNCTION
 IN SUBROUTINE [RESPON]

PROBABILISTIC ANALYSIS METHOD: FIRST-ORDER RELIABILITY METHOD

APPROXIMATE STATISTICS FOR Z:

MEDIAN = 16.82
 MEAN = 16.77
 STANDARD DEVIATION = 0.7957

NOTE: Standardized Normal Variates are used in the following analysis.
 This means that the random variable, u, represents a normal probability distribution with mean = 0 and standard deviation = 1. For example, u = -3 implies that the chance of observing a u value ≤ -3 is .00135 (cdf). Also, u = 3 implies that the chance of observing a u value ≤ 3 is 0.99875.

FIRST-ORDER PROBABILITY ANALYSIS

LIMIT STATE VALUE (Z=Z0) = 0.0000

RANDOM VARIABLES (X)

VARIABLE	DISTRIBUTION	MEAN	STD
P	EVD	0.4730	0.4580
SY	LOGNORMAL	315.0	15.75
SU	LOGNORMAL	515.0	25.75
T	NORMAL	16.02	0.1602
W	NORMAL	10.14	0.1014

MPP IN THE INDEPENDENT u SPACE AND THE CORRESPONDING X VALUES
 (FOR CORRELATED VARIABLES, THE u VALUES DO NOT CORRESPOND
 ONE-TO-ONE TO THE x VALUES)

VARIABLE	u VALUE	x VALUE
P	0.0000	14.85
SY	-2.0650	283.8
SU	-3.1911	438.5
T	-1.0632	15.85
W	0.1239	10.15

Standard normal variate (u) = -3.9488

Probability (Z<=Z0) = Probability u < -3.9488 = 0.3928542974E-04

Limit State Value (Z0) = 0.0000

Standard Normal Variate (u) = -3.9488

Probability (Z<=Z0) = Probability u < -3.9488 = 0.3928542974E-04

Probability (Z>Z0) = Probability u >= -3.9488 = 0.9999607146

 Probabilistic Sensitivity Results printed by level

NOTE: FOR CORRELATED VARIABLES, THE FOLLOWING Alpha VALUES DO NOT
 CORRESPOND ONE-TO-ONE TO THE ORIGINAL RANDOM VARIABLES

=====
 Level No. 1 Beta = 3.949

Random Variable	Alpha	d(beta)/d(mean)	d(beta)/d(std)	d(prob)/d(mean)	d(prob)/d(std)
1	0.1902E-31	0.000	0.5616E-03	0.000	-0.9212E-07
2	-0.5229	0.9351E-02	-0.1782E-01	-0.1534E-05	0.2923E-05
3	-0.8081	0.9288E-02	-0.2583E-01	-0.1523E-05	0.4236E-05
4	-0.2692	0.4278	-0.4528	-0.7017E-04	0.7427E-04
5	0.3138E-01	-0.7877E-01	-0.7214E-02	0.1292E-04	0.1183E-05

STOP DUE TO FPI ANALYSIS COMPLETE

ELAPSED CPU TIME: 5.66 seconds

RELIABILITY-BASED DESIGN EXAMPLE

Objective:

To determine the plate/web thickness combination that meets a target probability of failure of 1×10^{-6} for the ultimate limit state.

Plate/web thickness pairs:

As seen in results.

Constants:

Parameter	Value [mm]
stiffener depth, d	250
stiffener spacing, s	600
stiffener span, L	1490
ice load breadth, b	870

Random Variables:

Variable	Distribution	Mean, μ	Std. Dev., σ
Load, P	Gumbel(max)	0.473	0.458
Yield stress, σ_Y	Lognormal	315	15.75
Ultimate stress, σ_{ULT}	Lognormal	515	25.75
Plate thickness, t	Normal	1.014t	.01 μ
Web thickness, w	Normal	1.014w	.01 μ

Analysis Method:

FORM - First Order Reliability Method

Results:

Run #:	t [mm]	w [mm]	β	P_f
1	12.50	7.50	-0.740	2.30E-01
2	13.00	8.00	-1.560	5.92E-02
3	13.50	8.50	-1.901	2.87E-02
4	14.00	9.00	-1.219	1.12E-01
5	14.50	9.50	-3.734	9.41E-05
6	15.00	10.00	-3.805	7.09E-05
7	15.50	10.50	-3.878	5.27E-05
8	16.00	11.00	-10.011	6.82E-24
9	16.00	10.00	-10.104	2.64E-24
10	15.50	10.00	-3.894	4.93E-05
11	15.75	10.00	-3.940	4.08E-05
12	15.90	10.00	-10.052	4.49E-24
13	15.85	10.00	-10.026	5.85E-24
14	15.80	10.00	-3.949	3.93E-05
15	15.82	10.00	-10.011	6.84E-24
16	15.81	10.00	-10.005	7.25E-24
17	15.805	10.00	-10.002	7.44E-24
18	15.802	10.00	-10.001	7.55E-24
19	15.801	10.00	-10.000	7.59E-24

Conclusion:

A sharp drop in the probability of failure is seen just above a thickness of 15.8 mm. Within the accuracies of normal mill tolerances, we can use a plate thickness of 15.8 mm and a web thickness of 10 mm to satisfy the target probability.



